OPTICAL STIMULATION OF QUANTAL EXOCYTOSIS ON

TRANSPARENT MICROCHIPS

A Dissertation

presented to

the Faculty of the Graduate School

University of Missouri-Columbia

In Partial Fullfillment

of the Requirements for the Degree

Doctor of Philosophy

by

XIAOHUI CHEN

Dr. Kevin D. Gillis, Dissertation Supervisor

DECEMBER 2007

The undersigned, appointed by the dean of the Graduate School, have examined the [thesis or dissertation] entitled

OPTICAL STIMULATION OF QUANTAL EXOCYTOSIS

ON TRANSPARENT MICROCHIPS

presented by Xiaohui Chen,

a candidate for the degree of doctor of philosophy

and hereby certify that, in their opinion, it is worthy of acceptance.

Professor Kevin Gillis

Professor Shubhra Gangopadhyay

Professor Tzyh-Chang Hwang

Professor Jinglu Tan

Professor Liqun Gu

To Baba, Mama, Xiaokai and Xiaojian, I will not be

here without you.

ACKNOWLEDGEMENTS

My graduate school journey at Mizzou has been wonderful. It was challenging but at the same time, very rewarding. I would never have been able to make it and finish this dissertation were it not for the tremendous support from my mentors, colleagues, fellow students, friends and family. To all of them, I would like to say "Thank you!"

Great mentor makes a difference! I am extremely fortunate to have one of the very best, Dr. Kevin Gillis, to be my mentor. His scientific passion and insights, integrity and intellectual honesty, problem-solving attitude and high performance expectations have guided me to grow to be a better scientist and more importantly, a better person. His down-to-earth personality and good sense of humor has made him so approachable that I am not afraid of going to him even with the silliest questions. I am really grateful that he and his family have welcomed all of us in the lab with open arms and made us feel like having a big family together.

I would also like to thank Dr. Shubhra Gangopadhyay of Electrical Engineering for training me and letting me use the cutting-edge facilities at the center for micro/nano systems and nanotechnology. Her insightful critiques at our jointed biochip meetings have always been intriguing.

A huge thank you to my fellow graduate students, colleagues at Gillis lab, Dalton cardiovascular research center, Department of Biological Engineering and Department of Electrical and Computer Engineering, I am grateful to them for welcoming me into their lives and making this journey much more fun. I would like to especially acknowledge Dr. Peng Chen, James Dunning and Sangeetha Udayasankar for introducing me into Gillis

Most importantly, I am deeply indebt to my family, my father, my mother, my brother, my sister and her family for believing in me and helping me brave the storms not only during some of my most trying years at Mizzou but also throughout my life. Thank you for keeping me at bay and I hope I make you proud.

TABLE OF CONTENTS

LIST OF FIGURES

LIST OF TABLES

OPTICAL STIMULATION OF QUANTAL EXOCYTOSIS ON TRANSPARENT

MICROCHIPS

Xiaohui Chen

Dr. Kevin D. Gillis, Dissertation Supervisor

ABSTRACT

Photorelease of caged Ca^{2+} is a uniquely powerful tool to study the dynamics of Ca^{2+}-triggered exocytosis from individual cells. Using photolithography and other microfabrication techniques, we have developed transparent microchip devices to enable photorelease of caged Ca^{2+} together with electrochemical detection of quantal catecholamine secretion from individual cells or cell arrays as a step towards developing high-throughput experimental devices. A 110 nm – thick transparent Indium-Tin-Oxide (ITO) film was sputter-deposited onto glass coverslips, which were then patterned into 24 cell-sized working electrodes (~20 µm by 20 µm). We loaded bovine chromaffin cells with acetoxymethyl (AM) ester derivatives of the Ca^{2+} cage NP-EGTA and Ca^{2+} indicator dye Fura-4F, then transferred these cells onto the working ITO electrodes for amperometric recordings. Upon flash photorelease of caged Ca^{2+}, a uniform rise of $[Ca^{2+}]_i$ within the target cell leads to quantal release of oxidizable catecholamines measured amperometrically by the underlying ITO electrode. We observed a burst of amperometric spikes upon rapid elevation of $[Ca^{2+}]_i$ and a "priming" effect of sub-stimulatory $[Ca^{2+}]_i$ on the response of cells to subsequent $[Ca^{2+}]_i$ elevation, similar to previous reports using different techniques. We conclude that UV photolysis of caged Ca^{2+} is a suitable stimulation technique for higher-throughput studies of Ca^{2+}-dependent exocytosis on transparent electrochemical microelectrode arrays.

CHAPTER 1

INTRODUCTION

Exocytosis is an essential cellular trafficking process by which a cell directs membrane-bound vesicles to fuse with the plasma membrane and release their contents to the extracellular environment or send the contents to become components of the cell membrane. There are basically two types of exocytosis in eukaryotic cells. One is the non Ca^{2+} triggered constitutive exocytosis, the other is Ca^{2+} triggered non-constitutive exocytosis. Constitutive exocytosis, the process that delivers newly synthesized proteins to the cell membrane and extracellular environment, occurs in all eukaryotic cells (Palade, 1975; Schmoranzer and others, 2000). Most neurons and neuroendocrine cells secrete via Ca^{2+}-dependent exocytosis, a process in which discrete vesicles fuse with the cell membrane and release their contents of hormones and neurotransmitters into extracellular space in response to an increase in intracellular Ca^{2+} concentration ($[Ca^{2+}]_i$). In this research, I focused on Ca^{2+}-dependent exocytosis.

Ca^{2+}-dependent exocytosis is a fundamental mechanism in cellular signaling. The fusion of vesicles with plasma membrane leads to the release of hormone and neurotransmitter, which can trigger various responses in the target cell. Exocytosis-related problems within neurons can lead to different neurological disorders. Some exocytosis-related proteins

1

can help treat or alleviate pathologic symptoms. For example, Parkinson's disease is mainly caused by the loss of dopaminergic neurons of the substanitia nigra in the brain and the consequent loss of dopamine release from neurons. L-3,4-dihydroxyphenylalanine (a.k.a. L-dopa or Levodopa), the precursor of dopamine, remains the gold standard for treating Parkinson's disease by acting through increasing quantal size of dopamine release from dopaminergic neurons (Pothos and others, 1996; Pothos and others, 1998; Sulzer and Pothos, 2000; Pothos, 2002). Another well-known example is Botulinum Toxin type A (BOTOX), a neurotoxin protein, that temporarily improves the appearance of frown lines between the eyebrows and can be used to treat some neurological diseases too. The underlying working principle is that Botulinum Toxin A selectively blocks exocytosis of acetylcholine at a neuromuscular junction, inhibiting acetylcholine-contained vesicle fusion with cell membrane through cleavage of SNAP-25, one of the fusion proteins. By inhibiting acetylcholine release, the toxin causes flaccid paralysis of muscles, which can temporarily "relax" frown lines.(Song, 1998; Frampton and Easthope, 2003; Said and others, 2003) Beyond the most well-known cosmetic application, Botulinum Toxin type A is also used for treating excessive underarm sweating and certain neurological disorders such as spasticity and muscle pain disorders including cervical dystonia, eyelid spasms and crossed eyes (Kreyden and Burg, 2000; Connolly and de Berker, 2003; Blumenfeld and others, 2004; Boghen, 1996; McNeer and others, 2000).

 Although there has been extensive study of the biophysical and biochemical properties of exocytosis, it remains a challenge to fully understand its molecular mechanism and

kinetics. Nevertheless, several single-cell techniques with high signal-noise ratio and spatio-temporal resolution have emerged to help advance our understanding of this fundamental mode of intercellular communication. We mainly employed three techniques in this research, including patch-clamp techniques, amperometry and caged Ca^{2+} techniques.

1.1 Patch-clamp technique

Patch-clamp is a powerful technique that allows electrophysiological study of individual cells or even an individual ion channel within a patch of membrane. Erwin Neher and Bert Sakmann developed this technique in the late 1970s and early 1980s. They won the Nobel Price in Physiology and Medicine in 1991 for the development of this technique to discover "the function of single ion channels in cells"(1991).
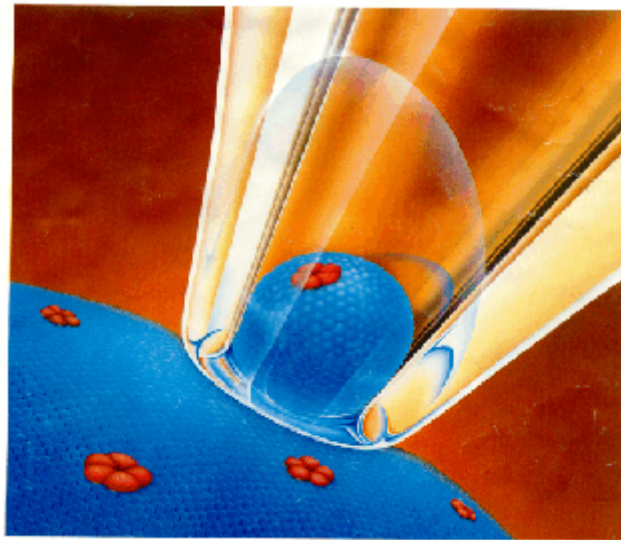
Fig. 1.1 A schematic showing a single ion channel being recorded within the patch pipette (Neher and Sakmann, 1992).

The basic working principle is shown in Fig. 1.1. A glass pipette electrode with a tip diameter of ~1 μm is pressed against a cell membrane and suction is applied to the inside of the glass pipette. A small patch of the cell membrane is consequently pulled into the pipette tip and a tight seal is formed, with an electrical resistance over 1 gigaohm. (So the seal is called a "gigaseal"). Since the little patch is electrically isolated from the rest of the cell, the incredibly small electrical current (picoampere-10^{-12} A) due to ion flow through individual ion channels in the patch can be measured. Upon rupturing the patch, access to exchange intracellular solution can be achieved by diffusion between the glass pipette and intracellular space, and current throughout the whole cell can be recorded, which is the so-called whole-cell recording configuration. When exocytosis occurs, vesicles fuse with the cell membrane, causing an increase of the plasma membrane area which causes a change in membrane capacitance. Thus whole-cell recording is a powerful tool to indirectly measure exocytosis by monitoring changes in membrane capacitance.

A variation of whole-cell recording is "perforated patch", in which pore-forming antibiotics are included in the pipette solution to permeabilize the membrane patch to allow low-resistance access to the inside of the cell. Another variation is called "inside-out" patch, which is made from pulling the patch quickly away from the cell so the inside of the patch is facing external media. Or the pipette in whole-cell mode can be withdrawn slowly from the cell, pulling a patch of membrane from the cell with the outside of the patch facing the bath solution. This is called an "outside-out" patch. The

different variations are suited for different applications. In this study, we mainly employed whole-cell recording to measure exocytosis-related changes in membrane area.

The capacitance of a cell membrane is proportional to its area. Increase in membrane capacitance is associated with exocytotic events. Patch-clamp techniques are well suited to measure membrane capacitance.The equivalent circuit of a patch-clamped cell is shown in Fig. 1.2. The lipid bilayer of a cell membrane can be simplified as a membrane resistor (R_m) and a membrane capacitor (C_m) together with a cell resting potential (E_{REV}) resulting from different ion concentrations between extracellular and intracellular space. The pipette electrode has series resistance (R_A). By applying a sinusoidal voltage (V_P) to the glass pipette electrode and measuring the current (I_P), membrane capacitance can be calculated using complex impedance analysis of the equivalent circuit (Marty and Neher, 1995).
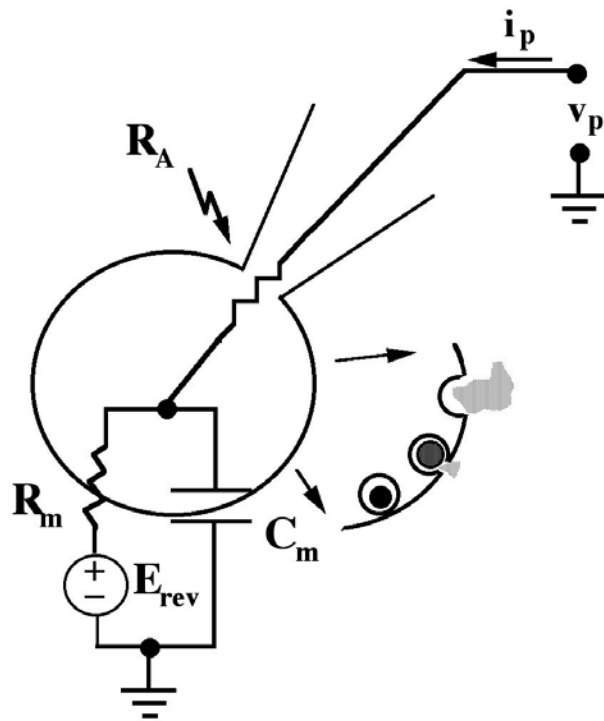
Fig. 1.2. The equivalent circuit of a cell in the whole-cell recording configuration.

1.2   Carbon fiber amperometry

In the 1950s, Sir Bernard Katz and colleagues pioneered the study of exocytosis by recording the miniature endplate potentials at neuromuscular junction of frogs generated by the release of acetylcholine molecules from individual vesicles (Fatt and Katz, 1950a; Fatt and Katz, 1950b; Fatt and Katz, 1952). These experiments led to the "quantal" hypothesis whereby transmitter is released in discrete packets, now understood to be vesicles. However, it was not until the development of amperometry 40 years later that quantal release of transmitter was directly measured.

Following the work by the Adams group on the basic principles of monoamine oxidation at the electrode surface (Kissinger and others, 1973; McCreery and others, 1974), Wightman's group (Leszczyszyn and others, 1990; Travis and Wightman, 1999) and others (Chow and others, 1992) employed carbon fiber electrodes to detect quantal secretion of catecholamine from single vesicles of chromaffin cells.

Catecholamines are readily oxidized, and therefore can be detected using electrochemical techniques. Voltammetry experiments measure the faradaic current that results upon scanning the potential of the working electrochemical electrode. The resulting current versus voltage curve is called a votammagram and can be used to identify and quantify analyte in a test solution. Amperometry refers to the measurement of faradaic current while the electrode potential is held at a constant value. This allows measurement of analyte with high time resolution although the identity and concentration of the analyte can not be resolved. Some neurons and neuroendocrine cells secrete hormones and neurotransmitters, such as the catecholamines and serotonin, that can be oxidized on electrochemical electrodes. Fig. 1.3. shows the redox reaction of norepinephrine, one kind of neurotransmitter that is oxidizable (Sakmann and Neher, 1995). The oxidation of one norepinephrine molecule leads to the generation of two electrons. Collectively the oxidation of many norepinephrine molecules generates an oxidative current on the surface of electrochemical electrodes. Other electroactive neurotransmitters include epinephrine, dopamine and serotonin.
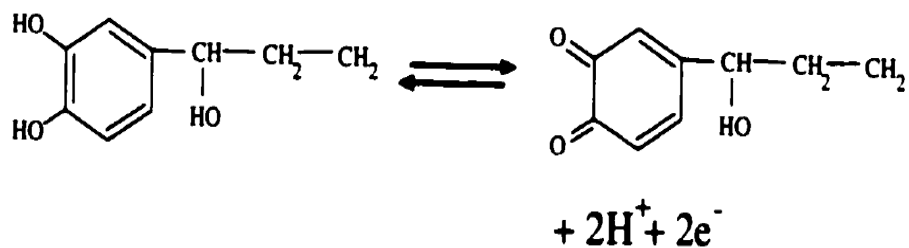
Fig. 1.3. The redox reaction of norepinephrine. The oxidation of norepinephrine (left) to its quinone product (right) leads to the loss of two protons and two electrons (Sakmann and Neher, 1995).

The most commonly used electrochemical electrode for measuring exocytosis is made from a carbon fiber. In brief, a carbon fiber electrode is positioned near a secretory cell and a constant positive voltage is applied to the carbon fiber to oxidize released neurotransmitters and thus generate an oxidative current flow through it shown as a spike in Fig. 1.4, with each spike representing a single-vesicle release event (Evanko, 2005). Parameters from these amperometric spikes contain a lot of important information regarding the exocytosis process. For example, integration of these amperometric currents indicates the amount of transmitter released from a single vesicle. The so-called "foot-signal", a little hump right before the big spike shown in Fig. 1.4, gives information on fusion pore formation before full fusion of vesicles with the plasma membrane occurs. The time course of the spike also provides important information about vesicle fusion and release kinetics. With amperometry, one can achieve millisecond time resolution and sensitivity of less than 1,000 molecules of released transmitters.
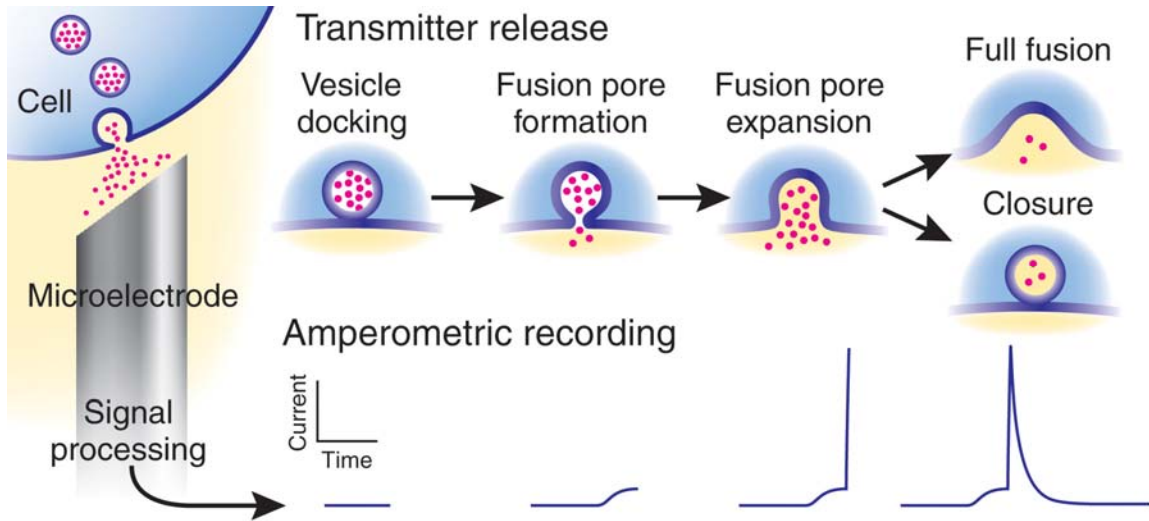
Fig. 1.4. Illustration of carbon fiber amperometry. (Reprinted by permission from Macmillan Publishers Ltd: Nature Methods, 2005, 2(9): P650, Katie Ris-Vicari, copyright 2005)

Compared to patch-clamp technique, amperometry is an electrochemical method that directly measures the amount and kinetics of neurotransmitter release from single cells. Carbon fiber amperometry can be combined with patch-clamp techniques so that the patch-clamp pipette can be used to stimulate exocytosis whereas a carbon fiber electrode is positioned on the other side of the cell to record amperometric spikes. Fig.1.5 shows a typical configuration of carbon fiber amperometry experiments (Sakmann and Neher, 1995). A glass pipette patch-clamps a chromaffin cell on the right while a carbon fiber detects cell secretion on the left.
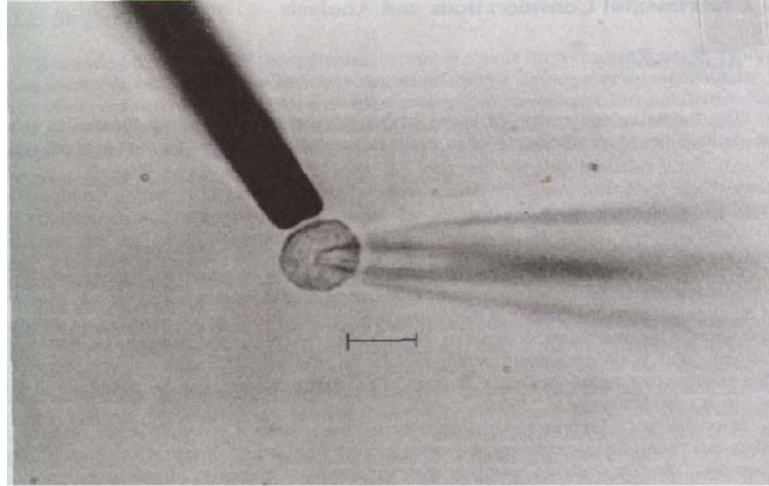
Fig. 1.5. Combination of patch clamp technique and carbon fiber amperometry. A chromaffin cell with a patch pipette sealed to it in the whole-cell configuration and a carbon fiber electrode approaching the cell from the upper left. (Scale bar, 10 μm) (Sakmann and Neher, 1995).

1.3   Caged Ca^{2+} technique

Another powerful tool for studying Ca^{2+}-dependent exocytosis is the caged Ca^{2+} technique, which was developed in the late 1980s (Tsien and Zucker, 1986; Kaplan and Ellis-Davies, 1988; Grell and others, 1989). Caged Ca^{2+} compound are organic molecules that bind Ca^{2+} with a high affinity but undergo a large decrease in affinity for Ca^{2+} upon UV photolysis. The release of Ca^{2+} after photoillumination is rapid and uniform, which gives experimenters better control of the intracellular Ca^{2+} concentration. When combined with a fluorescent Ca^{2+} indicator dye, it provides a very powerful tool for quantitative manipulation of intracellular Ca^{2+}. Before the development of caged Ca^{2+} technique, a high K^+ solution was often used for stimulation of Ca^{2+}-dependent exocytosis. High K^+ in the bath depolarized the cell, leading to opening of voltage-

10

dependent Ca^{2+} channel, Ca^{2+} influx and then triggering of Ca^{2+}-dependent exocytosis. One disadvantage of this stimulation method is that the intracellular Ca^{2+} concentration is higher near the Ca^{2+} channel, while it is lower further away from the Ca^{2+} channel. The Ca^{2+} concentration at the Ca^{2+} sensor for exocysois can not be easily resolved with Ca^{2+} indicator dyes, because the distance between the channel and sensor may be very small--- within the diffraction limit of light. The caged Ca^{2+} technique can overcome this problem by uniformly elevating $[Ca^{2+}]_i$ such that what is reported by fluorescent Ca^{2+} indicators reflects the concentration at the Ca^{2+} sensors for exocytosis. This Ca^{2+} gradient can not be accurately reported by Ca^{2+} indicator dyes since they only report the average Ca^{2+} concentration within a cell, which is typically lower than the local Ca^{2+} concentration near the Ca^{2+} channel. The caged Ca^{2+} technique can overcome this problem and give better control for intracellular Ca^{2+} concentration.

The caged Ca^{2+} technique is often used together with carbon fiber amperometry and/or patch clamp techniques (Hamill and others, 1981; Neher and Marty, 1982; Ashery and others, 2000; Yang and others, 2007; Yang and Gillis, 2004). Fig. 1.6 (top) shows a schematic of using a patch pipette to deliver caged Ca^{2+} into a cell. Upon UV photolysis of caged Ca^{2+}, a uniform rise in intracellular Ca^{2+} concentration leads to Ca^{2+}-dependent exocytosis. Fig. 1.6 (bottom) shows the chemical structure of Nitrophenyl-EGTA, a popular Ca cage. Upon UV photolysis, the photocleavage of the red N bond leads to the release of the trapped Ca^{2+} molecule.
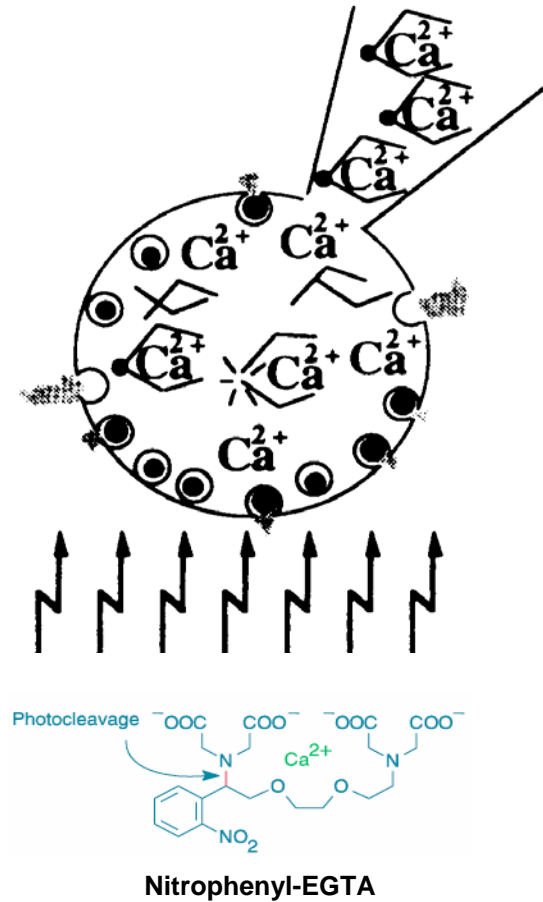
Nitrophenyl-EGTA

Fig. 1.6. Top: schematic of caged Ca^{2+} technique (Gillis and Chow, 1997); Bottom: chemical structure of Ca^{2+} cage Nitrophenyl-EGTA (Invitrogen).

The common drawback of these methods is low-throughput due to the fact that 1) Carbon fiber microelectrodes and/or patch clamp electrodes are manually positioned close to cells using micromanipulators which is labor-intensive and time-consuming; 2) Carbon fiber microelectrodes and patch clamp electrodes are made one by one in small lots; 3) Amperometric and/or patch clamp recordings can only be collected one cell at a time by trained experimenters.

Recently, Biomedical or Biological Micro-Electro-Mechanical Systems (BioMEMS) has become an actively researched area with a lot of miniaturized biomedical applications (Bashir, 2004; Di Carlo and Lee, 2006). The BioMEMS devices are also know as lab-on-a-chip devices or micro-total analysis systems (µTAS). Examples of bioassays and biological procedures that have been mininaturized into a chip format include DNA sequencing (Blazej and others, 2006), polymerase chain reaction (PCR) (Zhang and others, 2006), electrophoresis (Guttman and others, 2003), DNA separation (Obeid and others, 2004), enzymatic assays (Wilke and Buttgenbach, 2003), immunoassays (Li and others, 2005), cell sorting (Ho and others, 2005) and cell culture (Li and others, 2003). There are also a few biochip assays developed in recent years that detect exocytosis. For example, the Lindau group developed a glass microchip with plantinum electrodes to reveal the spatio-temporal dynamics of exocytosis in single cells (Dias and others, 2002). The Parpura group used carbon-based electrodes on silicon substrate to detect serotonin release from mast cell granules (Parpura, 2005). The Sheu group fabricated gold microelectrode arrays to detect dopamine exocytosis from PC12 cells (Cui and others, 2006). Our group designed and fabricated picolitersized-well electrodes of gold (Chen and others, 2003) and glass microchips with transparent ITO electrodes (Sun and Gillis, 2006) to detect quantal catecholamine release from single chromaffin cells. Around the same time, the Amatore group also demonstrated quantal release of catecholamines from chromaffin cells using transparent ITO electrodes patterned on a glass substrate to allow simultaneous optical and amperometric measurements of cells using conventional inverted microscopy (Amatore and others, 2006). In the majority of these biochip studies of neurosecretion, the most commonly used way to stimulate exocytosis is perfusion of

high-K$^+$ solution. Although high-K$^+$ stimulation is an effective way to trigger exocytosis, it lacks the control or information about local $[Ca^{2+}]_i$, which is crucial for studying the coupling of $[Ca^{2+}]_i$ increase and exocytosis. Here we report the development of ITO microelectrode arrays to integrate caged Ca^{2+} technique, the "gold standard" for rapid and uniform elevation of intracellular Ca^{2+} concentration, with amperometry and fluorescence microscopy to study Ca^{2+}-dependent exocytosis. To our advantage, $[Ca^{2+}]_i$ can be highly controlled and monitored throughout the cell using the caged Ca^{2+} technique and the Ca^{2+} indicator dye technique. Upon UV photolysis, an increase of $[Ca^{2+}]_i$ triggers exocytosis of readily oxidizable transmitters, which can be detected amperometrically by transparent ITO electrodes patterned on glass substrates.

In summary, we have employed three conventional techniques mentioned above (patch-clamp technique, carbon fiber amperometry and caged Ca^{2+} technique) to study Ca^{2+}-dependent exocytosis in single cells in the first part of this study. Whereas in the second part of this study, as a step further, we have borrowed the microfabrication technique from the semiconductor industry and innovatively integrated it with some of these conventional techniques to develop a higher-throughput assay for controlled stimulation and detection of single cell exocytosis.

CHAPTER 2

MATERIALS AND METHODS

2.1   Preparation of bovine adrenal chromaffin cells

Chromaffin cell preparation was modified from previously published protocols (Ashery and others, 1999; Smith, 1999) and was described in details in a recent paper from our group (Yang et al., 2007), more detailed information is included in Appendix 1. In brief, fresh bovine adrenal glands from a local slaughterhouse (Jennings Premium Meat, New Franklin, MO) were isolated from surrounding tissue/fat and kept in a Ca^{2+}- free and Mg^{2+}-free buffer solution (Buffer 1 solution) at room temperature while transporting to the lab. Residue fat was trimmed off from the glands using sterile scissors under a sterile culture hood. Blood inside each gland was washed out by injecting Buffer 1 solution into the opening of adrenal vein with a 60 ml sterile syringe and then gently messaged the gland to let the solution out. This step was repeated several times until the solution coming out of the gland was no longer reddish. Collagenase P was dissolved into Buffer 1 solution at a concentration of 1 mg/ml and injected into each gland through the opening of the adrenal vein. The glands were placed into a sterile beaker and put in a 37°C shaking water bath for 8 min. Then the glands were taken out, injected again with collagenase P and shaken for another 8 min. This collagenase digestion step allows

isolation the medulla from the outer cortex tissue. In another sterile Petri dish, the gland was cut open along the circumference of the cortex, within which the white gel-like medulla was peeled off and put into Buffer 1 solution in another Petri dish. The medullae were then thoroughly minced into small pieces using scissors. The medullae-containing Buffer 1 solution was filtered to through a nylon mesh (70 μm opening). After filtration, the filtered solution within the tube was centrifuged at 140 g/1000 rpm for 10 min at room temperature. The supernatant was aspirated and the pellet was resuspended in 20 ml Buffer 1 solution. In another tube, percoll gradient solution was mixed with a 10-fold concentration Buffer 1 solution at a ration of 9:1 to make a solution with physiological tonicity and a pH of 7.2. The percoll solution was mixed with the cell solution at a 1:1 ratio and then centrifuged at 15,000 rpm for 30 min at 18°C. Following centrifugation, the percoll gradient resulted in 4 layers: dead tissue in the top layer, norepinephrine and epinephrine secreting chromaffin cells in the middle two layers, and red blood cells in the bottom layer. The middle two layers were gently pipetted out and transferred to a tube. Buffer 1 solution was added in to fill the tube and the cell mixture was centrifuged at 1000 rpm for 10 min. The supernatant was removed and the cell pellet was resuspended in Buffer 1 solution. Chromaffin cell culture media was added at a 1:3 ratio into the cell suspension to help cells to adapt to normal Ca^{2+}-containing media. The suspension was centrifuged again at 1000 rpm for another 10 min and the supernatant was removed. The cell pellet was resuspended in chromaffin cell culture media. Cell density was calculated by adding a drop of cell solution onto a hemacytometer. The cell solution was then diluted into appropriate density for plating either in 25 mm cell culture dishes or in T 25

cell culture flasks. Cells were then stored in a humidified incubator (37°C and 5% CO_2) and used for 1-5 days after the preparation.

2.2 $[Ca^{2+}]_i$ calibration

$[Ca^{2+}]_i$ was measured by dual-excitation wavelength spectrofluorimetry using either an equimolar combination of the indicators fura-2FF (K_d=35 µM) and bisfura-2 (K_d=370 nM) or a single ratiometric dye fura-4F(AM) (K_d=770 nM). We used the Ca^{2+} indicator combination of two ratiometric dyes, fura-2FF and bisfura-2 to report $[Ca^{2+}]_i$ for most experiments in the first part of this study and part of the experiments (digitonin permeabilization experiments) in the second part of this study. $[Ca^{2+}]_i$ was calibrated in vivo or in vitro as in Yang and Gillis (Yang and Gillis, 2004). Eight solutions (Table 2.1) with known free $[Ca^{2+}]$ of 0, 0.31, 1.2, 3.6, 7.2, 28, 127 µM and 10 mM were prepared using Ca^{2+} buffers EGTA (Ethylene lycol-bis(2-aminoethyl-ether)-N, N, N', N'-tetraacetic acid, Kd=150 nM at pH=7.2),   HEDTA   (N-(2-Hydroxyethyl)-ethylenediamine-triacetic acid, Kd=3.6 µM at pH=7.2) and DPTA (1,3-Diaminopropan-2-ol-tetraacetic acid, Kd=81 µM at pH= 7.2). NMG-GL solution without Mg^{2+} consists of: 120 mM NMG(N-Methyl-D-Glucamine),120mM L-Glutamic Acid, 8 mM NaCl and 40 mM HEPES, titrate the pH to 7.2 using NMG. To make 100 mM free buffer and Ca^{2+}-saturated Ca-buffer stock (Ca-EGTA, Ca-HEDTA, Ca-DPTA), we use the pH-metric approach to make free and Ca^{2+} saturated buffer solutions side by side. Take Ca-EGTA as an example. If we want to make 100 ml of 100mM EGTA and 100 ml of 100 mM Ca-EGTA, we start with making 100 ml of 200 mM K_2EGTA by titrating with KOH. Then

we split this 100 ml into two 50 ml, dilute one part to 100 ml with DD water, which is 100 mM free EGTA. For the other 50 ml of 200 mM EGTA, we add small amount of 1M $CaCl_2$ and 1N KOH alternatively into it, monitoring pH oscillation above and below 7.2. We always added small amount of one of the solutions ($CaCl_2$ or KOH) to bring the pH back to 7.2. At the end of the titration, we reached a point where when we added 1 unit of $CaCl_2$, we only needed 1 unit of KOH to bring the pH back to 7.2, which shows that EGTA molecules are saturated with Ca^{2+}. We then brought the volume to 100 ml and 100 mM Ca-EGTA was made.

Table 2.1. Ingredients of 8 calibration solutions for $[Ca^{2+}]_i$ calibration without Ca^{2+} indicator dyes
(Bisfura-2 and Fura-2FF)

[Ca](μM)	Ca-buffer (100 mM stock)	Buffer (100mM stock)	NMG-GL
0		10 mM EGTA	90%
0.311	6.65 mM Ca-EGTA	3.35 mM EGTA	90%
1.2	2.5 mM Ca-HEDTA	7.5 mM HEDTA	90%
3.6	5 mM Ca-HEDTA	5 mM HEDTA	90%
7.2	6.67 mM Ca-HEDTA	3.33 mM HEDTA	90%
28	7.5 mM Ca-DPTA	22.5 mM DPTA	70%
127	18 mM Ca-DPTA	12 mM DPTA	70%
10000	10 mM CaCl2		90%

Whole-cell recording was used to deliver calibration solution into the cells and the ratio of fluorescence emission (535±25 nm) from 340 nm and 365 nm excitation was recorded. The measured values of the eight solutions (R) were fit to equation (2.1) to get the five parameters (R_0, R_1, R_2, K_1, K_2) (Voets, 2000). Inversion of equation (2.1) was used to calculate $[Ca^{2+}]_i$ from measured ratio recordings from single cells. For the digitonin

18

permeabilization experiments (Chapter 5), we used in vitro drops of solution on ITO chips to perform the calibration.

$$R = R_0 + R_1 \frac{[Ca^{2+}]_i}{[Ca^{2+}]_i + K_1} + R_2 \frac{[Ca^{2+}]_i}{[Ca^{2+}]_i + K_2}.$$

(2.1)

For the AM ester experiments, we used the Ca^{2+} indicator dye Fura-4F(AM). Since Fura-4F(AM) was esterasized into Fura-4F inside the cell, we used the Fura-4F salt in 4 calibration solutions (0 μM, 311 nM, 1.2 μM and 10 mM) to do whole-cell recording in chromaffin cells to obtain $[Ca^{2+}]_i$ calibration for Fura-4F(AM). We could fit the ratio recordings to equation (2.2) from Grynkiewicz., et.al. (Grynkiewicz and others, 1985) to get $[Ca^{2+}]_i$ calibration for Fura-4F(AM).

$$[Ca^{2+}]_i = K_{eff} * \frac{R - R\min}{R\max - R}$$

(2.2)

2.3   HCSP project

In this project (Chapter 3), we used an EPC-9 double amplifier with two headstages and two sets of Burleigh micromanipulators to do whole-cell recording and carbon fiber amperometry simultaneously (The experiment configuration is just like that in Fig. 1.5). A protocol was designed to deplete the "Highly Calcium Sensitive Pool (HCSP)" first with UV flash, then 10 consecutive depolarization pulses were applied to release "Readily Releasable Pool (RRP)". Carbon fiber electrodes measured catecholamine secretion from both the HCSP and RRP. Then amperometric spikes from both pools

within the same cell were analyzed to confirm their similar vesicle identity (See Chapter 3 for more detailed information).

2.3.1 Electrophysiology

All electrophysiological experiments were conducted using the standard whole-cell recording configuration. Patch pipettes werefabricated from Kimax glass (Kimax-51, Kimble Glass Inc., Vineland, NJ) using a Flaming/Brown micropipette puller (Model P-97, Sutter instrument Co., Novato, CA). The pipette resistance typically ranged from 2 $M\Omega$ to 5 $M\Omega$ when filled with intracellular solution. The series resistance ranged from 5 $M\Omega$ to 10 $M\Omega$ and the membrane conductance was below 700 pS. The pipette holding potential was -70 mV in all whole-cell recordings. Capacitance measurements were conducted using the "sine+dc" method implemented in PULSE software (Pusch and Neher, 1988; Gillis, 2000). The lock-in sinusoid had an amplitude of 25 mV and a frequency of 1.5 KHz. Using a micromanipulator, a patch pipette can be positioned close to a single cell. Immediately after the pipette touched the cell, suction was applied inside the patch pipette to form a "gigaseal" (membrane resistance$>10^9\Omega$). An abrupt pulse at suction was applied to rupture the patch inside the pipette tip and make it possible to exchange pipette solution with the intracellular solution. In most electrophysiological experiments, caged Ca^{2+} and Ca^{2+} indicator dyes are delivered into the cells by dialysis. Upon photorelease of caged Ca^{2+}, the capacitance increase immediately thereafter indicating vesicle fusion with the plasma membrane.

2.3.2 Photometry

A monochromator (Polychrome II, TILL Photonics, Munich BioRegio, Germany) was coupled to the epifluorecence port of an inverted Olympus IX50 microscope (Olympus America, Center Valley, PA, USA) with an optical fiber. A 40X 1.15 NA water immersion lens (U-APO, Olympus America) focused the excitation light and collected fluorescent light. The fluorescent light (535 nm ± 25 nm) was measured using a photodiode mounted in a viewfinder (TILL Photonics). A two-port condenser (TILL Photonics) combined the monochromator excitation path with that of the UV flash lamp. We alternated the excitation wavelength for Ca^{2+} indicator dyes at 340 nm and 365 nm each for 5 ms. Fluorescent signals from Ca^{2+} indicator dyes within the cells were collected by the photodiode (TILL Photonics). Then we calculated the ratio of the signals from these two wavelengths and used previously described Ca^{2+} calibration equations to calculate $[Ca^{2+}]_i$.

2.3.3 Carbon fiber amperometry

Carbon fiber electrodes (diameter 8 μm) were purchased from ALA scientific Inc. (Westbury, NY). A micromanipulator (PCS-5000, Burleigh, EXFO, Quebec, Canada) was used to position a carbon fiber electrode to touch the surface of the cell. A constant

potential of 700 mV was applied to the carbon fiber electrode to oxidize catecholamine that contact the working electrode surface. The amperometric current was measured using a patch-clamp amplifier (EPC-9 double, HEKA, Lambrecht, Germany). Using an upright microscope (MGC-10), each carbon fiber electrode was cut diagonally at a 45° angle after recording from 1 to 2 cells (#10 carbon steel blade, BD, Franklin Lakes, NJ). The signal was filtered at 2.9 kHz and sampled at 17.5 KHz. Samples were averaged in groups of 12 to give a final temporal resolution of 0.7 ms per point. Analysis of amperometric spikes was performed using software from the Borges lab (Segura and others, 2000) and the Sulzer lab (Mosharov and Sulzer, 2005) (written by Eugene Mosharov).

2.3.4. Statistical analysis of amperometric recordings

The Mann-Whitney rank sum test (Mann and Whitney, 1947) is a suitable statistical analyzing method for data analysis when " 1.) You want to find out if the median of two different samples are significantly different; 2.) The samples are not drawn from normally distributed populations with the same variances, or you do not know if they were drawn from normal populations. As a nonparametric procedure, the Mann-Whitney rank sum test works by ranking all the observations from smallest to largest without regard to which group each observation comes from. The smallest number gets a rank of 1 and the largest number gets a rank of N, where N is the total number of observations in these two groups. The ranks for each group are summed and the rank sums are compared. If the samples are large, or if there are identical values, it assumes a Gaussian distribution

for the rank sums (control limit theorem). A P value is then calculated from an ordinary two-sample t test. If the P value is small, we can conclude that the two populations have different medians. If the P value is large, the data do not give us any reason to conclude that the overall medians differ. This is different from saying that the medians are the same. Instead we just have no compelling evidence that they differ.

Since the parameters for the amperometric spikes from the HCSP and RRP are not normally distributed, it is more appropriate to compare the median than the mean in order to find out if there is statistically significant difference between the two populations of vesicles. The Mann-Whitney rank sum test is a valid method for this type of analysis.

We used SigmaStat 3.1 (Systat Sofware Inc., San Jose, CA, USA) to do the Mann-Whitney rank sum test for our amperometric recordings.

2.3.5 Solutions

The typical bath solution for chromaffin cells consisted of (in mM): 150 NaCl, 5 KCl, 2 MgCl$_2$, 10 HEPES, 2.5 CaCl$_2$, 2.6 Glucose, pH 7.2. For whole-cell recording, the base pipette solution consisted of (in mM): 120 N-methylglucamine, 120 L-glutamic acid, 8 NaCl and 40 HEPES titrated to pH 7.2 with N-Methylglucamine. In the HCSP project, 0.5 mM NP-EGTA, 0.2 mM CaCl$_2$, 1 mM MgCl$_2$, 2 mM Na$_2$-ATP, 0.1 mM bisfura-2 and 0.1 mM fura-2FF were added into the base pipette solution to make the final pipette

solution. The backfilling solution for patch pipette consisted of (in mM): 140 L-Glutamic acid, 40 HEPES, and titrated with CsOH to pH 7.2.

2.4   Action potential project

2.4.1   Electrical stimulation and detection of action potentials using the same carbon fiber electrode

A VA-10 amplifier, an EPC-9 amplifier and two Burleigh micromanipulators were used for simultaneous patch-clamp and carbon fiber recording. Whole-cell patch-clamp recording in current-clamp mode was used to monitor the membrane potential of a cell. A carbon fiber electrode was positioned adjacent to the cell. Brief voltage pulses (0.3 ms duration) were applied to the carbon fiber electrode and the resulting membrane voltage change was monitored by a patch pipette electrode sealed on the same cell. We found that the ±1 V stimulus range of the VA-10 amplifier was not sufficient to stimulate an action potential. Therefore we bypassed the 0.1-gain resistor-divider in the stimulus pathway to allow a stimulus range of $\sim \pm 10V$. We also found that we needed to reduce the value of the feedback resistor from 500 MΩ to 100 MΩ (R_f in Fig. 2.1) so that the amplifier would not be saturated from the current elicited by the voltage pulses. After the circuit modification, we were able to elicit action potentials in chromaffin cells using a 0.3 ms voltage pulse from 0.7 V to 6 V. (See Chapter 4 for more detailed information).
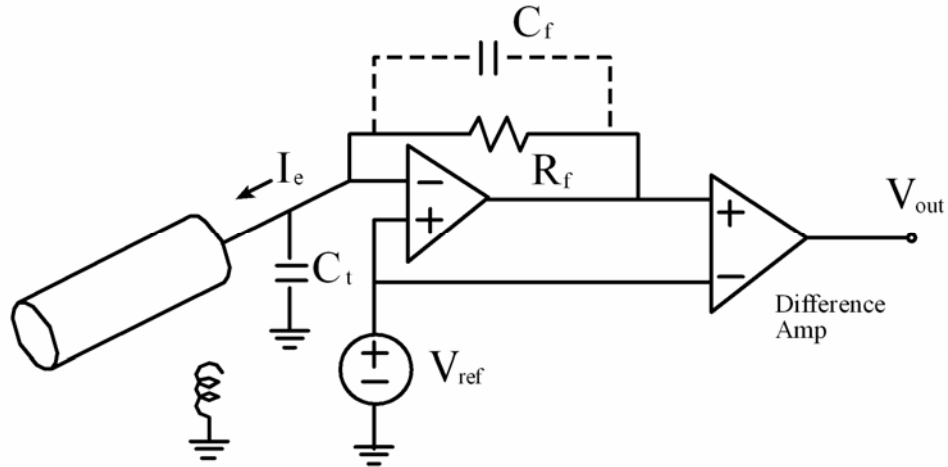
Fig. 2.1. Resistor feedback I-V converter used in patch-clamp amplifiers

2.4.2 Solutions

For the action potential project, the pipette solution consisted of (in mM): 140 mM L-Glutamic acid, 10 HEPES, 1 mM $MgCl_2$, 2 mM Na_2-ATP and 0.1 mM bisfura-2, 0.1 mM fura-2FF and 20 Sucrose, titrated by KOH to pH 7.2.

2.5 Caged Ca^{2+} experiment with permeabilized cells project

2.5.1 Carbon fiber amperometry to verify permeabilization effect of digitonin or α-hemolysin on chromaffin cells

In order to verify that digitonin can effectively permeabilze chromaffin cells, we first immersed chromaffin cells in bath solution without Ca^{2+}. Then we positioned a patch pipette with digitonin and Ca^{2+} near the cell. We broke the tip of the patch pipette a little bit by touching on the bottom of the coverslip. Then the broken tip was brought close to

the cell and small pressure was added to blow the pipette solution onto the cell surface. To verify that Ca^{2+} could get into the cell with the help of digitonin-permeabilized holes on plasma membrane, we used a carbon fiber electrode to record Ca^{2+}-induced exocytosis simultaneously and therefore confirm the permeabilization effect of digitonin. For the effect of α-hemolysin, we used the same experiment configuration except replacing digitonin with α-hemolysin.

2.5.2 Trypan blue assay to verify permeabilization effect of α-hemolysin on chromaffin cells

Trypan blue is commonly used as a cell or tissue viability stain because it is membrane impermeant, but it can stain the nucleus if the membrane becomes compromised during cell death. In this case, since we permeabilized the surface membrane, Trypan blue got into the cell and stained the nuclei even if the cells were still alive. In order to verify the permeabilization effect of α-hemolysin, we used Trypan blue to incubate cells together with α-hemolysin for 15 min, and then exchanged the bath solution to Trypan blue-free solution and tracked the color change of the cells over time by taking digital pictures every 5 minutes using an inverted microscope (Olympus IX50, Olympus America, Center Valley, PA), a 20X objective lens (Olympus Ach 20X/0.40) and an digital camera (Olympus Camedia C-3040ZOOM).

2.5.3 Propidium iodide to verify permeabilization effect of α-hemolysin on chromaffin cells

Propidium iodide is another vital stain we used to test for plasma membrane permeabilization. We incubated chromaffin cells with 4 µg/ml propidium iodide for 15 min, then exchanged the extracellular solution with propidium iodide-free bath solution and took fluorescent pictures of the cells. If the cells turned orange, the permeabilization was effective.

2.5.4 Fabrication of monolithic polydimethylsiloxane (PDMS) microvalves to stop solution flow in microfluidic channels

PDMS microvalves consist of two layers as shown in Fig. 2.2 (Unger and others, 2000). The microfabrication process consisted of three parts: fabrication of the control layer master, fabrication of the flow layer master and microvalve fabrication and assembly.
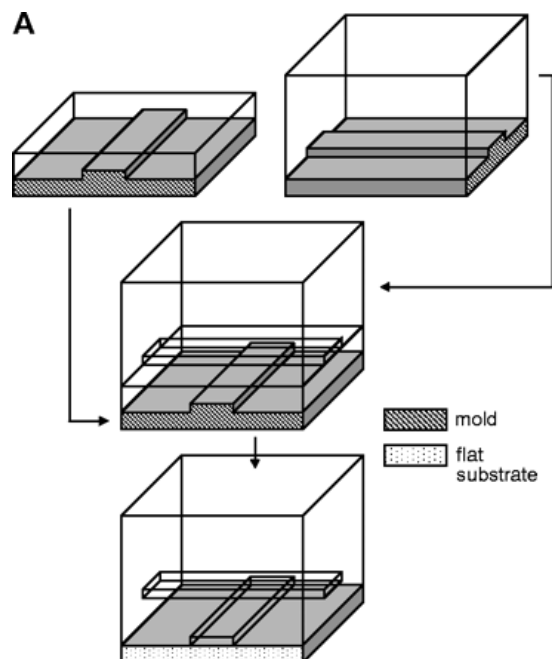
Fig. 2.2. Process flow for microfabrication of PDMS microvalve (From Science 288(5463): 113-116. Reprint with permission from AAAS.) PDMS flow layer (top left) and control layer (top right) are partially cured separately. Then the control layer is peeled off and sealed onto the flow layer followed by complete curing together (middle). The combining piece is peeled off the master and sealed onto the substrate to form a PDMS microvalve. By applying pressure into the control layer, the thin membrane at the cross section of the two layers will pinch off and serve as a valve to stop solution flow within the underlying flow channel.

2.5.4.1 Control layer master

A 6" silicon wafer (MEMC, St. Peters, MO) was dehydrated on a hotplate at 200°C for 5 min. Negative photoresist SU-8 2025 (Microchem Corp. Newton, MA) was spincoated onto the wafer at 1000 rpm for 60 s (photoresist thickness ~ 75 μm) using a single wafer spin processor (Laurell Technology Corp., North Wales, PA). The coated silicon wafer was then soft baked at 65°C on a hotplate for 3 min, followed by another bake at 95°C on

another hotplate for 9 min. the photoresist-covered control channel pattern was obtained by exposing the coated silicon wafer to UV light for 90 s (Kinsten KVB-30D exposure box, Taiwan) through a 5080 dpi transparent mask (UIUC printing service, UIUC, Champaign, IL), which was designed using software Freehand 9 (Adobe Systems Inc.). The exposed silicon wafer underwent post exposure bake at 65°C for 1 min and then 95°C for 7 min. It was then developed in SU-8 developer (Microchem Corp.) for ~6 min or until no white residue was observed coming off while washing with 2-propanol. The patterned wafer was cleaned with 2-propanol or acetone and then air dried.

2.5.4.2 Flow layer master

A 6" silicon wafer (MEMC) was dehydrated on a hotplate at 200°C for 5 min. An adhesion layer of HMDS (1,1,1,3,3,3-Hexamethyldsilazane, Sigma) was spincoated onto the surface of the wafer at 1000 rpm for 60 s, followed by a 3 min bake on a hotplate at 150°C. Positive photoresist AZ P4620 (AZ Electronic Materials USA Corp., Branchburg, NJ) was spincoated onto the wafer at 600 rpm for 60 s (photoresist thickness ~ 16 μm). The coated wafer was then baked on a hotplate at 110°C for 5 min followed by an exposure under UV light for 700 s using a 5080 dpi transparency mask (UIUC printing service). The exposed wafer was left in darkness for 1 hr before being developed in AZ 400K developer (AZ Electronic Materials) until the pattern was clearly resolved. The patterned wafer was washed with DD water and air dried. Then it was baked in a conventional oven (Economy vacuum oven 1400E, VWR International, West Chester,

PA) at 200°C for 30 min to reflow the rectangular cross-section of the photoresist into a more rounded cross section for better actuation of the microvalve.

2.5.4.3 Microvalve fabrication and assembly

Sylgard 184 elastomer kit (A: monomer, B: cross-linking agent, Dow Corning, Midland, MI) was used to make the microvalve. For the flow layer, the mixing ratio of the two components was 20 A:1 B (6 g:0.3 g). For the control layer, the mixing ratio is 5 A:1 B (40 g:8 g). We first treated the flow layer master with HMDS vapor in a desiccator by adding several drops of HMDS in a small beaker beside the flow layer master. Vacuum was applied to the desiccator to generate HMDS vapor treatment for 5 min. The flow layer elastomer mixture was degassed in another desiccator and spincoated onto the HMDS treated flow layer master at 3000 rpm for 60 s. (3000 rpm for 20 μm targeted flow layer height, 2500 rpm for 25 μm targeted flow layer height). The control layer elastomer mixture was degassed in a desiccator for ~30 min and then it was poured onto the control layer master with a plastic ring on top of it to confine the gel-like mixture. Both masters with elastomer mixture were partially baked in a conventional oven (VWR) at 80°C for 16 min. Then the partially cured control layer was peeled off. Inlet and outlet holes were punched at both ends of the control channels using homemade blunt 16G needles (Ref#305198, Becton Dickinson and Company). Tygon microbore tubings (ID 0.02", OD 0.06", EW-06418-01, Cole-parmer Instrument Company, Vernon Hills, IL) were inserted into the holes for connection to a pressure injector (MPPI-2, Applied Scientific Instrumentation Inc., Eugene, OR) for microvalve actuation. Then the control

layer was aligned and sealed onto the flow layer master and put back into the conventional oven (VWR) at 80°C for 3 hr to allow the complete curing and merging of the two layers (Fig. 2.3 bottom). After the complete curing, microvalve slabs of PDMS was cut out of the flow layer master and inlet/outlet holes for flow channels were punched using the previously mentioned 16G blunt needle. For irreversible bonding, the bottom of PDMS slabs and glass substrates were both treated with air plasma on medium RF level for 60 s (Plasma cleaner/sterilizer, PDC-32G, Harrick Scientific Corp., Pleasantville, NY). For reversible bonding between the PDMS and glass substrate, the two were sealed together by pressure and baked at 80°C in the conventional oven (VWR) overnight.

2.5.5   Design, microfabrication and testing of ITO microchip

2.5.5.1 ITO deposition

No. 2 borosilicate cover glass (thickness: 170 μm - 250 μm, Fisher Scientific, Pittsburgh, PA, USA) was used as the substrate for the biochip devices. A 110 nm-thick ITO film was sputtered onto the glass substrate using a magnetron sputtering system (ATC 2000-V, AJA International Inc. North Scituate, MA, USA) with an ITO target (90 wt% In_2O_3 and 10 wt% SnO_2, Williams Advanced Materials Inc, Buellton, CA, USA). The parameters for the sputtering process were adapted from Deng. et al., (Deng and others, 2001). We used DC mode deposition at a power of 100 W, a working pressure of 2 mTorr, and a substrate temperature of 325°C. Ar gas was introduced at a flow rate of 20

sccm, and O_2 was introduced at 0.2 sccm. The deposition time was 600 s. The transmittance spectrum for ITO-coated cover glass was measured using a UV-VIS recording spectrophotometer (UV-2401PC, Shimadzu, Kyoto, Japan). The conductance of the deposited ITO film was measured using a 4-point probe (S302, Lucas Labs, Gilory, CA, USA).

2.5.5.2 ITO electrode patterning and insulation

Transparent ITO electrodes were patterned on the ITO-coated cover glasses using photolithography and wet-etching techniques adapted from Sun and Gillis (Sun and Gillis, 2006). A schematic of the procedure is depicted in Fig. 2.3.
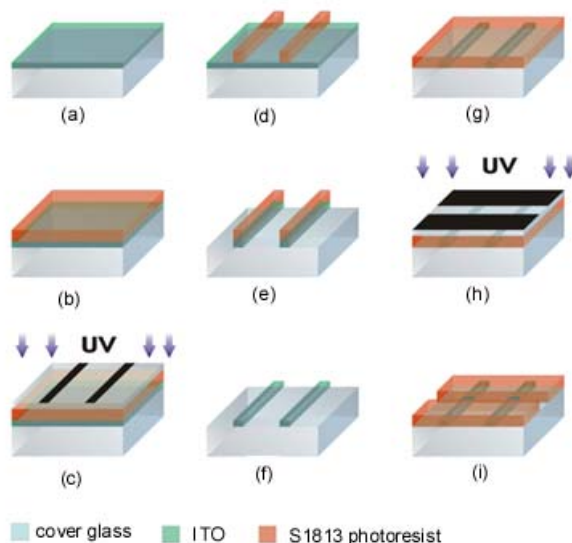
Fig. 2.3. Process flow for fabrication of ITO electrochemical microelectrode array.

Briefly, we first rinsed the ITO-coated cover glass (Fig. 2.3(a)) with 2-propanol, then sonicated for 20 min in acetone (Ultrasonic cleaner 1510, Branson, Danbury, CT, USA),

then cleaned using air plasma (Plasma cleaner/sterilizer, PDC-32G, Harrick Scientific Corp., Pleasentville, NY, USA) for 1 min at the medium RF power level. Shipley S1813 positive photoresist (Rohm and Haas Electronic Materials, Philadelphia, PA, USA) was then spincoated (single-wafer spin processor, Laurell Technologies Corp., North Wales, PA) onto the ITO-coated cover glass at 2500 rpm for 60 s to give a thickness of ~2 μm (Fig. 2.3(b)). The coated cover glass was baked on a hot plate at 115°C for 2 min. Photoresist-covered cover glass was exposed to UV light through a high-resolution (20,000 dpi) transparency mask (CAD Art Services, Bandon, OR) (Fig. 2.3(c)) and then developed in M351 (Rohm and Haas Electronic Materials) for ~1 min (Fig. 2.3(d)). It was then baked at 200°C on the hot plate for 10 min. An acidic solution composed of 6 M HCl and 0.2 M $FeCl_3$ was used to wet etch the portion of the ITO film that was not protected by photoresist for 30 min, leaving 20 μm-wide ITO stripes (Fig. 2.3(e)), also shown as vertical stripes in Fig. 2.4(b) that widened to form connecting pads on the edge of the chip (Fig. 2.4(a)).
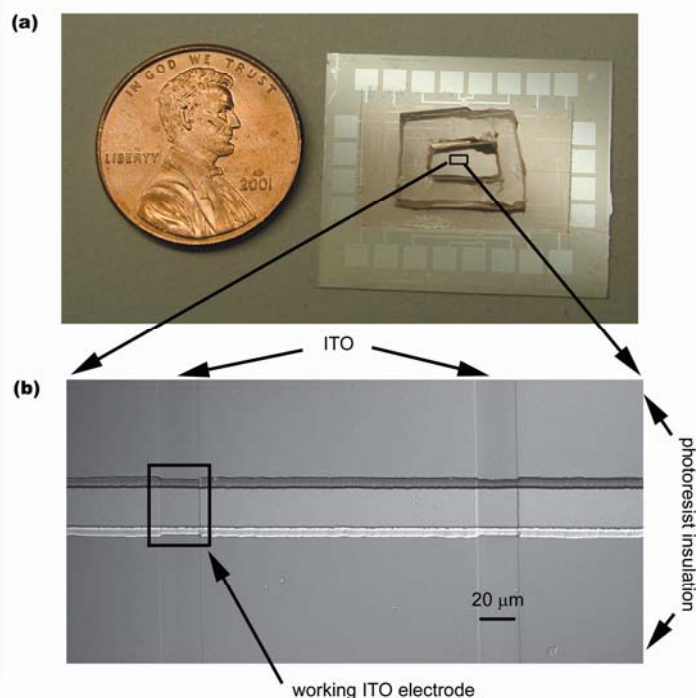
Fig. 2.4. A microfabricated biochip device. (a). Photo of microchip with 24 electrochemical ITO electrodes.(b). A DIC micrograph of two working ITO electrodes with dimensions of 20 x 20 μm.

The photoresist protection layer was then removed with an acetone wash (Fig. 2.3(f)). The cover glass with patterned ITO electrodes was rinsed with DD water and air-dried. Using similar photolithographic methods, we insulated the bulk of the ITO stripes with photoresist, leaving a 20 μm-wide opening orthogonal to the ITO stripes to result in an array of 24 working electrodes with dimensions of 20 μm by 20 μm (Fig. 2.3(g-i)), also shown as the horizontal stripe in Fig.2.4(b)). In some of our earlier experiments we used AZ P4620 positive photoresist (AZ Electronic Materials) to pattern ITO electrodes following a similar procedure.

2.5.5.3 ITO microchip assembly

A 10:1 ratio of PDMS (Sylgard 184, Dow Corning) monomer and cross-linking agent was used to make the PDMS gaskets for holding the cell-containing solution on the chip. The monomer and curing agent mixture was degassed in a vacuumed desiccator and poured into a plastic ring on a silicon wafer. After curing for 1 hr in a conventional oven at 80°C, the PDMS was cut into 10 mm by 8 mm slabs with a 6 mm by 3 mm opening in the middle serving as the PDMS gasket (Fig. 10(a)). It was then peeled off the wafer and sealed in the middle of the ITO microchip so that the 24 working ITO electrodes were within the opening of the PDMS gasket. A custom-built chamber was used to hold the ITO microchip device and provide electrical connection from the amplifier connection pin to the ITO connection pads at the edge of the chip.

2.5.5.4 Solutions

For the experiments of carbon fiber amperometry from digitonin permeabilized cells, the bath solution for chromaffin cells consisted of (in mM):160 K-Glutamate, 20 HEPES, 0.2 K-EGTA, 1 $MgCl_2$, 10 Glucose titrated with HCl to pH 7.2. Application pipette solution consisted of (in mM or otherwise labeled): 152 K-Glutamate, 20 HEPES, 10 DPTA, 2 Na_2-ATP, 3 $MgCl_2$, 2 $CaCl_2$, and 20 μM digitonin dissolved in DMSO, titrated with KOH to pH 7.2.

For the Trypan blue experiments, wild type recombinant α-hemolysin monomer was prepared following the previously described protocol (Cheley and others, 1999). Briefly, the protein was synthesized using the coupled in vitro transcription and translation kit (IVTT, Promega). Wild type α-hemolysin stock (0.93 mg/ml) was first diluted 10 times to 93 μg/ml in Ca^{2+}-free bath solution. Then 150 μl α-hemolysin was taken out and diluted again with Ca^{2+}-free bath solution at a 1:5 ratio (150 μl α-hemolysin solution mixed with 600 μl Ca^{2+}-free bath solution). A coverslip with chromaffin cell was taken out from a 25 mm Petri dish and mounted onto a microscope chamber, 750 μl α-hemolysin solution was added onto the coverslip followed by a 15 min incubation in a 37°C incubator (Model 3326, Forma Scientific Inc., Marietta, OH, USA). Then another 750 μl 0.4% Trypan blue solution was added into the chamber and digital pictures were taken at different times to verify the permeabilization effect.

For the propidium iodide experiments, 4 μg/ml propidium iodide was added into the incubation solution together with α-hemolysin. The rest of the procedure was similar to the previous Trypan blue experiments.

For the caged Ca^{2+} experiments with digitonin-permeablized cells on ITO electrodes, the "intracellular mimicking solution" consisted of (in mM): 100 K-glutamate, 20 DPTA, 6.49 $CaCl_2$, 10 NP-EGTA, 30 HEPES (titrated to pH 7.2 with KOH), 2 Na_2ATP, 50 μM bisfura-2 and 50 μM fura-2FF. Cells were initially permeabilized in culture media

containing 20 μM digitonin. The usual cell bathing solution consisted of (in mM): 150 NaCl, 5 KCl, 1.2 $MgCl_2$, 2 $CaCl_2$, 10 HEPES, 11 Glucose, titrated to pH 7.2 with NaOH.

For experiments of caged Ca^{2+} photolysis in microchannels, the intracellular mimicking solution consisted of (in mM or otherwise labeled):100 K-Glutamate, 30 K-DPTA, 5 NP-EGTA, 4.2 $CaCl_2$, 30 mM HEPES, 50 μM bisfura-2 and 50 μM fura-2FF titrated with KOH to pH 7.2.

For electrochemical testing of the ITO electrodes, ferricyanide or epinephrine solution was used to do cyclic voltammetry. Ferricyanide solution consisted of 1 mM $K_3Fe(CN)_6$ in 0.5 mM KCl, titrated to pH 3 using HCl. Epinephrine solution consisted of 100 μM epinephrine in 5 mM standard Ca^{2+} bath solution which consists of (in mM): 140 NaCl, 5 KCl, 2 $MgCl_2$, 5 $CaCl_2$, 10 HEPES and 10 Glucose titrated with NaOH to pH 7.2.

2.6 Caged Ca^{2+} experiments with AM ester cell loading project

2.6.1 On-chip amperometry and fluorescence microscopy

To load adrenal chromaffin cells with caged Ca^{2+} and Ca^{2+} indicator dye, we washed ~3 X 10^6 chromaffin cells off from a T25 flask with 2ml DMEM and transferred the solution into a 15 ml conical tube. After adding 10 μM NP-EGTA (AM) and 4 μM Fura-4F (AM) and mixing gently, the cell suspension was incubated in a humidified incubator (37ºC, 5% CO_2) for 45 min. Then the cell suspension was centrifuged at 100 g for 4 min. The

supernatant was removed with a Pasteur pipette and vacuum, and the pellet was resuspended with 5 ml Ca^{2+} bath solution containing 2 mM Ca^{2+}. The cell suspension was again centrifuged at 100 g for 4 min and the supernatant was removed with Pasteur pipette and vacuum. 500 μl Ca^{2+} bath solution was added in and the pellet was resuspended and ready for use. About 30 μl bovine adrenal chromaffin cells loaded with Ca^{2+} cage NP-EGTA (AM) and Ca^{2+} indicator dye Fura-4F (AM) were added into the cell reservoir on the ITO microchip. After 10 to 20 min, cells would settle onto the ITO microchip surface with some randomly settling directly on top of the working electrodes. An inverted fluorescence microscope (IX50, Olympus America) with a 40X 1.15 NA water immersion lens (U-APO, Olympus America) was used to observe cells and the transparent ITO electrodes. A monochromator (Poly II, TLL photonics) and a photodiode (TILL Photonics) were used together with the inverted fluorescence microscope to measure the fluorescent signal from the Ca^{2+} indicator dye to report $[Ca^{2+}]_i$ during the whole experiment. An EPC-9 amplifier (HEKA) and the corresponding software Pulse (HEKA) were used to record the amperometric and fluorescence data. The headstage of the EPC-9 amplifier was connected to an ITO connection pad on the edge of the chip to activate one of the working electrodes. A Ag/AgCl wire inserted in the cell reservoir on the ITO microchip was used as the ground electrode and connected to the ground port on the headstage of EPC-9 amplifer. A 700 mV constant potential was applied to a working ITO electrode during experiments. We used two methods to photorelease caged Ca^{2+}. One was using a monochromator, the other was using a UV flash lamp. In order to be able to use the monochromator to photorelease caged Ca^{2+}, we moved the optical fiber of the monochromator to the direct-illumination port of the combining condenser so that

38

~90% of the light can pass through and photolyze caged Ca^{2+}. In contrast, usually the monochromator is directed to the side port of the combining condenser such that only ~10% of the light is reflected into the illumination pathway. To photorelease caged Ca^{2+}, the excitation light from the monochromator was maintained at 360 nm with an occasional 5 ms interval of 380 nm to allow ratiometric measurements of $[Ca^{2+}]_i$ at the same time. The monochromator was off when the underlying ITO electrode was recording the amperometric spikes from the cell above the activated working electrode.

The other method to more rapidly photorelease caged Ca^{2+} is through use of a UV "flash" lamp to deliver impulses of intense illumination with millisecond duration. Next I will describe a feedback control system to control firing of the flash lamp to maintain $[Ca^{2+}]_i$ near a desired level.

2.6.2 Ca^{2+} clamping

We used a feedback-control program (Appendix 2) written in Igor (Wavemetrics, Portland, OR, USA), an ITC-16 computer interface (Instrutech Co., Long Island, NY) together with an EPC-9 patch-clamp amplifier (HEKA, Lambrecht, Germany) to control the firing frequency of a UV flash lamp. A monochromator (Polychrome II, TILL Photonics, Munich BioRegio, Germany) coupled to the epifluorecence port of an Olympus IX50 microscope (Olympus America, Center Valley, PA) with a fiber-optic cable excited the Ca^{2+} indicators at 360 nm and 380 nm. A 40X 1.15 NA water immersion lens (U-APO, Olympus) focused the excitation light and collected fluorescent

light. The fluorescent light (535 nm±25 nm) was measured using a photodiode (TILL Photnoics) mounted in a viewfinder (TILL Photonics). A two-port condenser (TILL Photonics) combined the monochromator excitation path with that of the UV flash lamp. Fluorescent signals from Ca^{2+} indicator dyes within the cells were collected by the photodiode. These signals were sent to the ITC-16 computer interface and converted into $[Ca^{2+}]_i$ using previously described Ca^{2+} calibration equation. The detected $[Ca^{2+}]_i$ was then compared with a targeted $[Ca^{2+}]_i$ level to decide if photorelease of caged Ca^{2+} was necessary or not. If $[Ca^{2+}]_i$ was below the targeted level, the ITC-16 computer interface would send a TTL signal to trigger the UV flash lamp, therefore photoreleasing Ca^{2+}.

2.6.3 Solutions

For the experiments using AM ester cell loading, the "incubation solution" for loading cells consisted of 25 μM NP-EGTA (AM) and 5 μM fura-4F (AM) in Dulbecco's Modified Eagles Medium (DMEM). Stock solutions of NP-EGTA (AM) and fura-4F (AM) were dissolved in DMSO at a concentration of 5 mM with 10% w/v Pluronic F-127 to facilitate loading.

For the "Ca^{2+} priming effect" experiments, the bath solution was either the standard cell bathing solution or a solution with lower Ca^{2+} (1 mM). NP-EGTA (AM) and fura-4F (AM) were obtained from Invitrogen (Carlsbad, CA, USA). All other reagents were obtained from Sigma (St. Louis, MO, USA) unless otherwise stated.

For the "Phorbol Myristate Acetate (PMA) enhancement" experiments, 1 µM PMA was added to the final cell suspension solution.

CHAPTER 3

VERIFICATION OF THE SIMILAR IDENTITY OF VESICLES WITH LOWER OR HIGHER SENSITIVITY TO $[CA^{2+}]_I$ USING SIMULTANEOUS WHOLE-CELL RECORDING AND CARBON FIBER AMPEROMETRY

3.1   Introduction to the different pools of vesicles involved in exocytosis

Ca^{2+}-triggered exocytosis of hormones or neurotransmitters is an important mechanism for cell-to-cell communication between neurons and neuroendocrine cells.   Upon repetitive or sustained stimulation, neurons or neuroendocrine cells usually initially secrete hormones or neurotransmitters at a very high rate, but the rate of exocytosis declines with continued stimulation over different time scales (Gillis and Chow, 1997). The complex kinetics of exocytosis are modeled as resulting from the successive depletion of several pools of vesicles that may represent different vesicle states or populations. The concept of different functional pools of vesicles emerged soon after the formulation of the quantal release hypothesis by Katz and colleagues (Del Castillo and Katz, 1954; Neher, 1998) The concept of equating release rates with vesicle pools has been useful, and different vesicle pools were defined on the basis of different release rates under different stimulation conditions. As shown in the cartoon model in Fig. 3.1,

the fastest component of exocytosis, upon strong stimulation of a chromaffin cell (e.g. upon photelevation of $[Ca^{2+}]_i$ to > 20μM), is called the Readily Releasable Pool (RRP) and consists of vesicles fully primed and located in the immediate vicinity of the plasma membrane. Vesicles that are in the next fastest release phase are defined as the "Slowly Releasable Pool" (SRP) which will refill RRP when it is depleted (Heinemann and others, 1994; Voets and others, 1999). The Reserve Pool is composed of vesicles that replenish the SRP and RRP when they are depleted (Sudhof, 2004). Depolarization protocols also define an "Immediately Releasable Pool" (IRP) that is believed to be a subset of the RRP located very close to Ca^{2+} channels (Voets et al., 1999; Mennerick and Matthews, 1996).
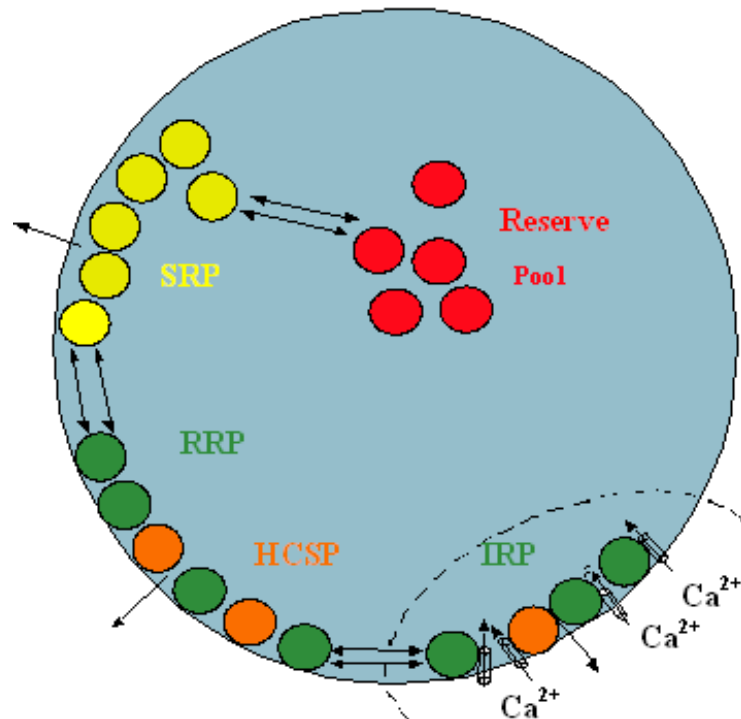
Fig. 3.1. Schematic of the model for different pools of vesicles within a cell.

Our group has discovered and defined a "Highly Ca^{2+}-Sensitive Pool" (HCSP) of vesicles (Fig. 3.1) in chromaffin cells that is released even faster than the RRP at lower concentration of intracellular Ca^{2+} ($[Ca^{2+}]_i$ < 10 µM) (Yang and others, 2002). Upon activation of Protein Kinase C (PKC) by Phorbol Myristate Acetate (PMA), the HCSP is enhanced in size to a greater extent than the RRP, indicating that PKC increases the percentage of vesicles in a highly Ca^{2+}-sensitive state (Yang et al., 2002). The HCSP is abolished upon expression of a c-terminal deletion mutant ($\Delta 9$) of Synaptosome-Associated Protein of 25 kDa (SNAP-25), one of the proteins of the SNARE complex that is essential for Ca^{2+}-triggered exocytosis, indicating the participation of HCSP in genuine SNARE-protein-mediated exocytosis (Yang et al., 2002). Further research in our group also shows that mimicking PKC phosphorylation with expression of a phosphomimetic mutation of SNAP-25 at Ser-187 increase the size of the HCSP by threefold, whereas the RRP only increase 1.5 fold (Yang et al., 2007). Thus Ca^{2+}-triggered exocytosis from the HCSP appears to have different molecular mechanisms than exocytosis from the RRP triggered by higher $[Ca^{2+}]_i$ (>10 µM) (Yang et al., 2007). One important question to answer is whether the vesicles in the RRP are different from those in the HCSP in terms of their catecholamine content and fusion kinetics (Yang et al., 2007).

3.2   Simultaneous measurements of capacitance change due to exocytosis and amperometric spikes to compare the identities of the HCSP and RRP

Our hypothesis was that the vesicles in the HCSP are morphologically similar as those in the RRP. Thus our hypothesis predicts that vesicles in the two pools have the same size, catecholamine content, and single-vesicle fusion kinetics. To test this hypothesis, we used capacitance measurement and carbon fiber amperometry simultaneously to compare the two vesicle populations. Then we can characterize and compare the contents and kinetics of single vesicles from the HCSP and RRP within the same cell.

We designed a protocol to measure both pools in a single stimulus train. A patch clamp pipette was used to deliver caged Ca and Ca^{2+} indicator dyes into a chromaffin cell and measure membrane capacitance change due to Ca^{2+}-triggered exocytosis. A carbon fiber electrode was positioned adjacent to the same cell and recorded amperometric spikes. A UV flash was used to photorelease cage Ca^{2+} in order to elevate $[Ca^{2+}]_i$ to several μM within the cell, leading to release of the HCSP. It was then followed by 10 brief depolarizing pulses (30 ms in duration) to deplete the RRP. The patch clamp electrode recorded the capacitance jumps corresponding to vesicles fusing, while the carbon fiber electrode reported amperometric spikes of individual vesicles (see Chapter 2 for more details). Fig. 3.2 shows a sample trace of this type of experiment. Fig. 3.2A shows the amperometric spikes detected by a carbon fiber. Right after the UV flash, there is a cluster of spikes detected from the release of the HCSP. The same carbon fiber detected another cluster of spikes from the release of the RRP upon membrane depolarization. A

patch pipette simultaneously monitored the small capacitance jump from the fusion of the

HCSP and the bigger increase of capacitance from the release of the RRP (Fig. 3.2B).

Ca^{2+} indicator dyes within the cell reported $[Ca^{2+}]_i$ increasing from a basal level of ~500

nM to 2.3 μM right after the UV flash, then the subsequent elevation to ~15 μM after 10

depolarizing pulses (Fig. 3.2C). At the same time, the inward Ca^{2+} current induced by the

depolarizing train was recorded by the patch clamp pipette (Fig. 3.2D).
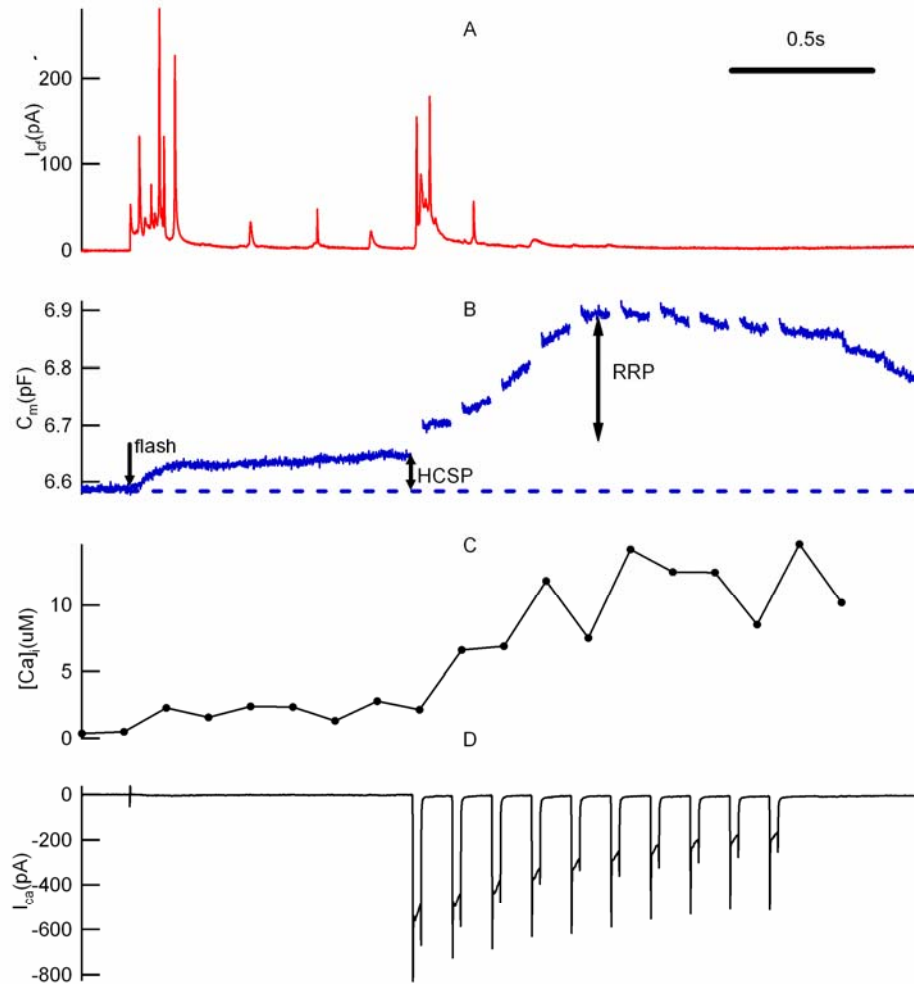
Fig. 3.2. Sample experiment comparing the vesicles released from the HCSP and RRP. A. Amperometric spikes from the HCSP and RRP; B. Membrane capacitance changes from the HCSP and RRP.; C. $[Ca^{2+}]_i$ throughout the experiment; D. Inward Ca^{2+} current induced by depolarization pulses.

Fig. 3.3 depicts the average of 44 traces obtained from 16 cells. Fig. 3.3A depicts the average amperometric recording showing the quantal secretion events from the HCSP and RRP. Fig. 3.3C shows the average $[Ca^{2+}]_i$ and Fig. 3.3D shows the average Ca^{2+}

47

current in 16 cells. In Fig. 3.3B, we compared the integral of the average amperometric trace in Fig. 3.3A (Q, red line) with the average capacitance trace (blue line). The scaled Q follows the ΔC trace with a delay resulting from the time it takes for catecholamine molecules to be released and oxidized on the surface of carbon fiber electrode following membrane fusion.
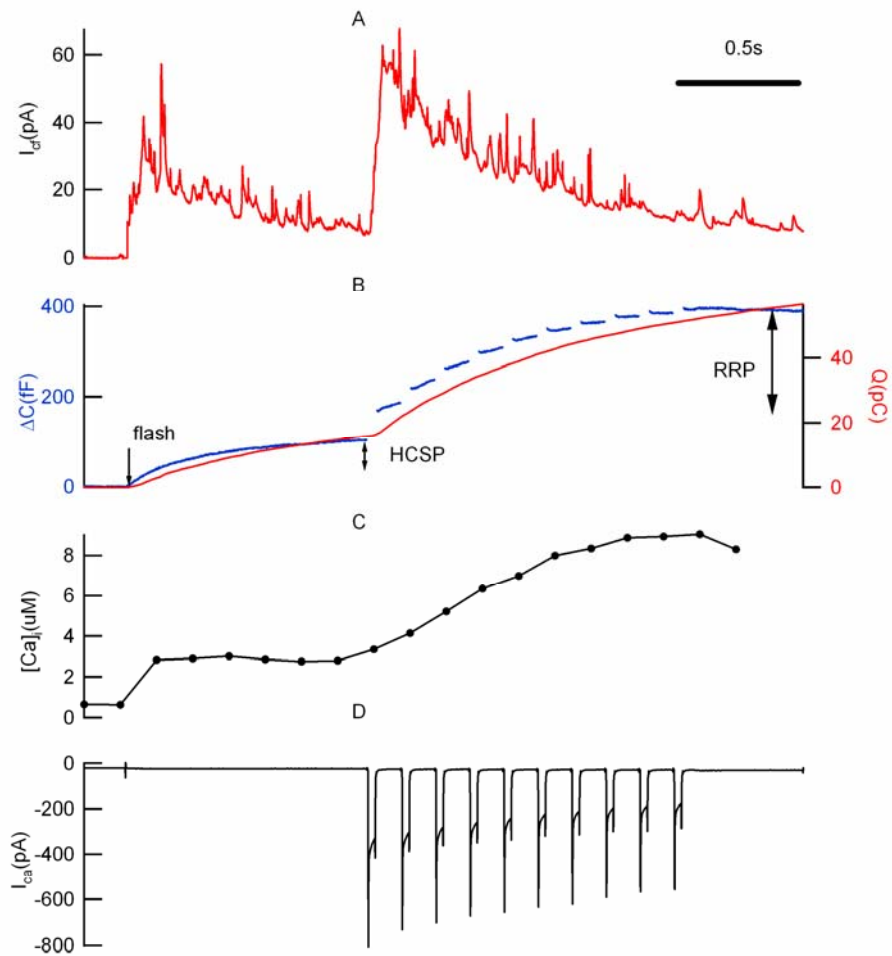
Fig. 3.3. Average of responses of 44 traces within 16 cells. A. Average amperometric recording with distinctive spikes for both the HCSP and RRP; B. Scaled integration of average amperometric spike (red) in A follows the membrane change (blue) with a delay; C. Average

48

[Ca^{2+}]$_i$ before and after flash (the first two points are measurements of [Ca^{2+}]$_i$ before the UV flash while the rest are measurements after UV flash. The average [Ca^{2+}]$_i$ before UV flash is 640 nM, the average [Ca^{2+}]$_i$ after UV flash is 2.86 µM); D. Average Ca^{2+} current during the depolarizing train.

We calculated the ratio of total charge (Q) generated from the oxidation of catecholamine for the HCSP and RRP to membrane capacitance change (ΔC) for the HCSP and RRP. For the HCSP, Q is 15.8 pC and ΔC is 103.6 fF; For the RRP, Q is 40.7 pC and ΔC is 298.6 fF. The ratio of Q to ΔC is therefore 153 C/F for the HCSP and 136 for the RRP, which differ by only 12.5%. Since Q scales with the vesicle volume (assuming vesicle catecholamine concentration is nearly constant (Albillos and others, 1997)) while ΔC scales with the total vesicle surface area which fuses with the plasma membrane, the similar ratio between (Q/ ΔC)$_{HCSP}$ and (Q/ ΔC)$_{RRP}$ indicates that the vesicles in these two phases of release have a similar volume to surface area ratio and are therefore likely to be of similar size.

We then studied single vesicles by analyzing individual amperometric spikes to see if quantal release differs between the HCSP and the RRP. We used software from the Borges lab to characterize single amperometric spike parameters (Segura et al., 2000). A group of kinetic parameters were generated from the program (Fig. 3.4).
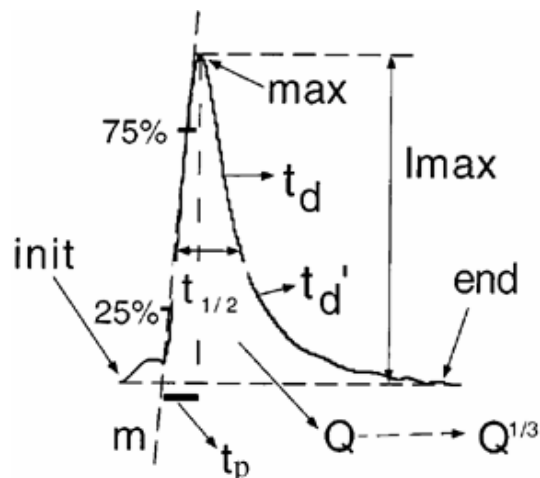
Fig. 3.4. Amperometric spike parameters (Segura et al., 2000).

These includes current peak (I_{max}), width at half-height of the amperometric spike ($t_{1/2}$), integration of the current/total charge from released contents (Q), index for the diameter of the vesicle ($Q^{1/3}$), rate of release calculated from 25% to 75% amplitude of the rising part of the spike (slope 25%-75%) and time from the end of foot signal to the peak of the spike (Time to peak t_p) (Segura et al., 2000; Jankowski and others, 1993). Figs.3.5 and 3.6 depict the histograms of the vesicular parameters for the HCSP and RRP.
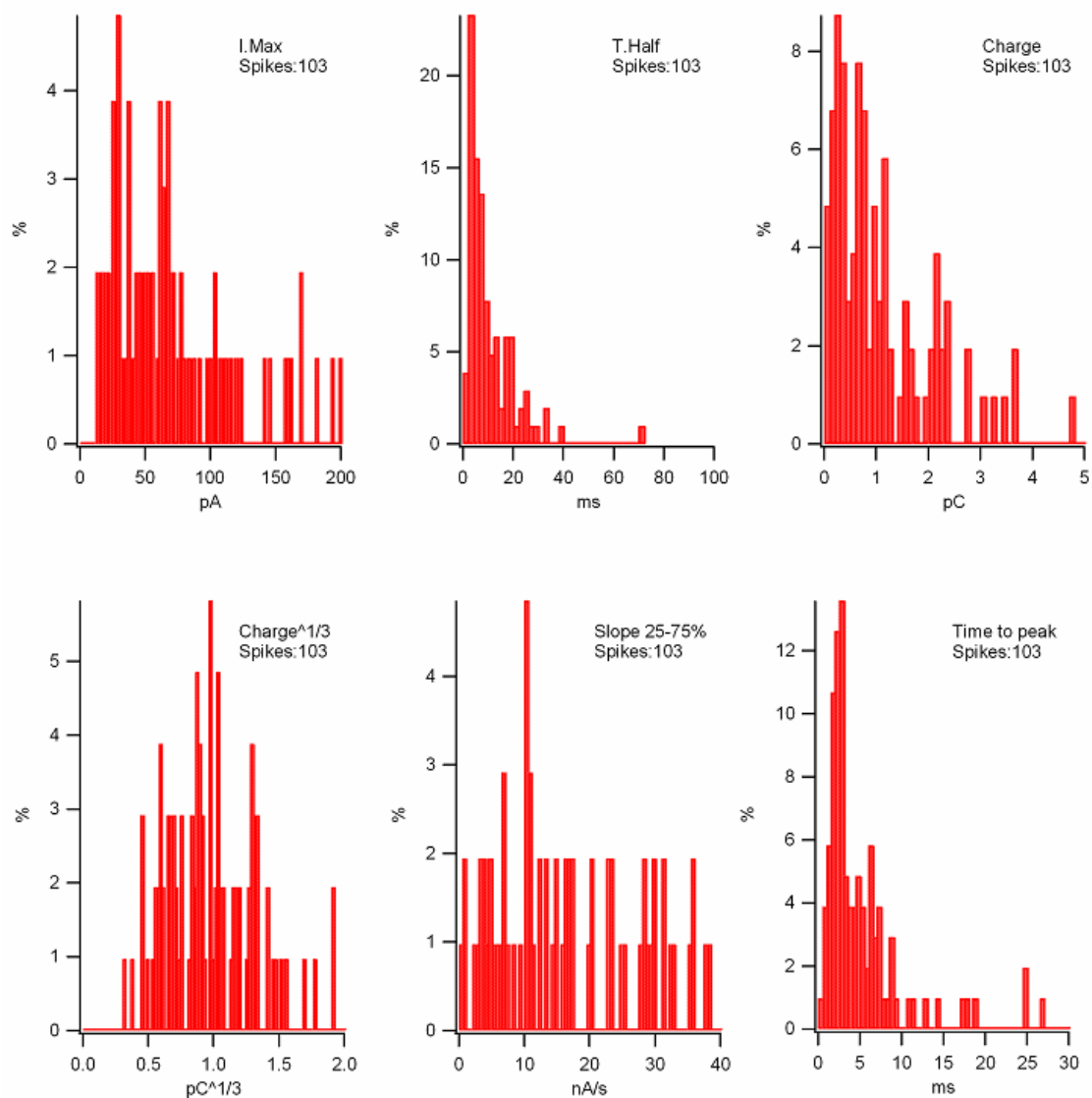
Fig. 3.5. Kinetic parameters of released vesicles from the HCSP. 103 amperometric spikes released from the HCSP (44 recordings from 16 cells) were analyzed using sofeware from the Borges lab (Segura et al., 2000).

51
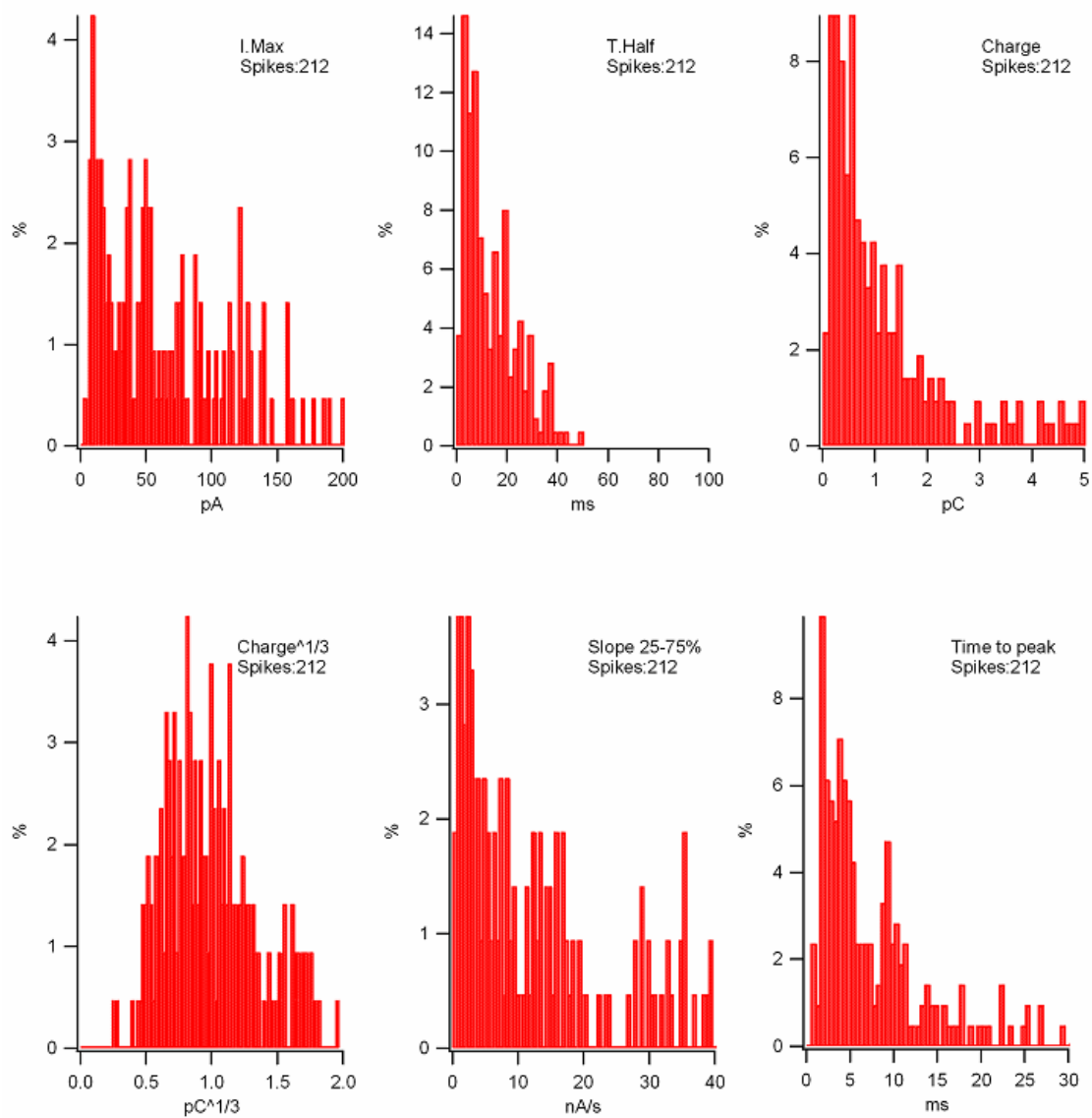
Fig. 3.6. Kinetic parameters of released vesicles from the RRP. 212 amperometric spikes released from the RRP (44 recordings from 16 cells) were analyzed using the program from Borges lab (Segura et al., 2000).

A

Q

B

Q^1/3

53
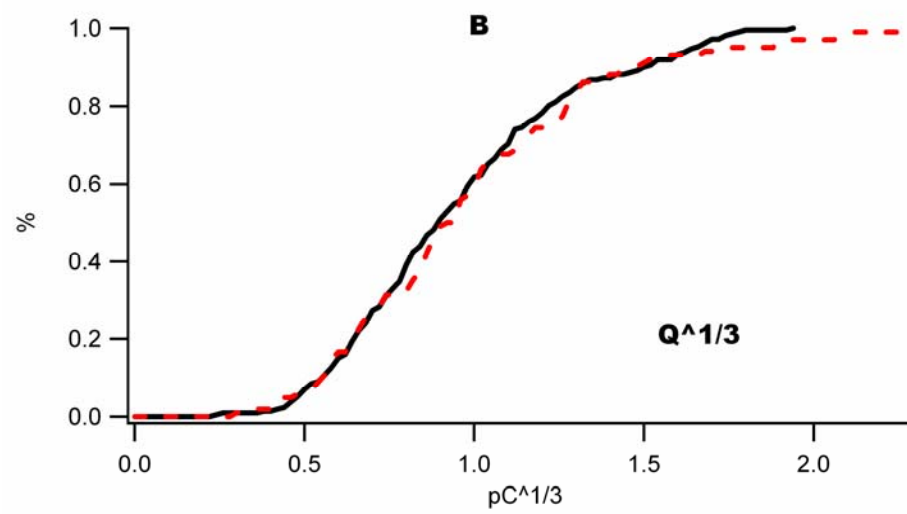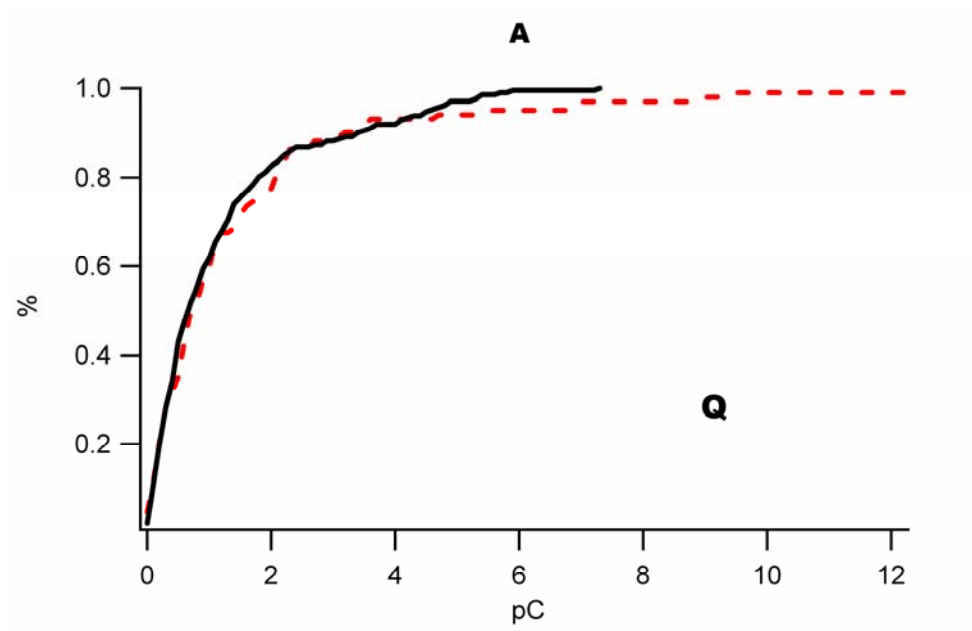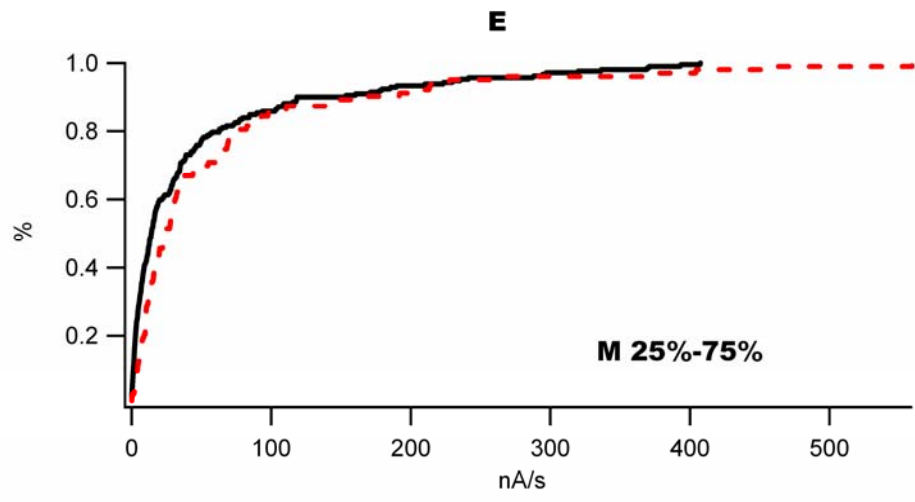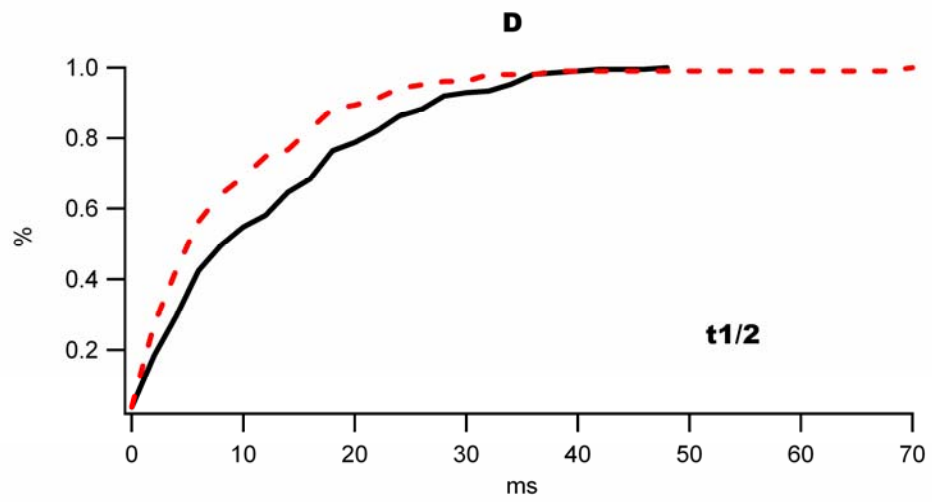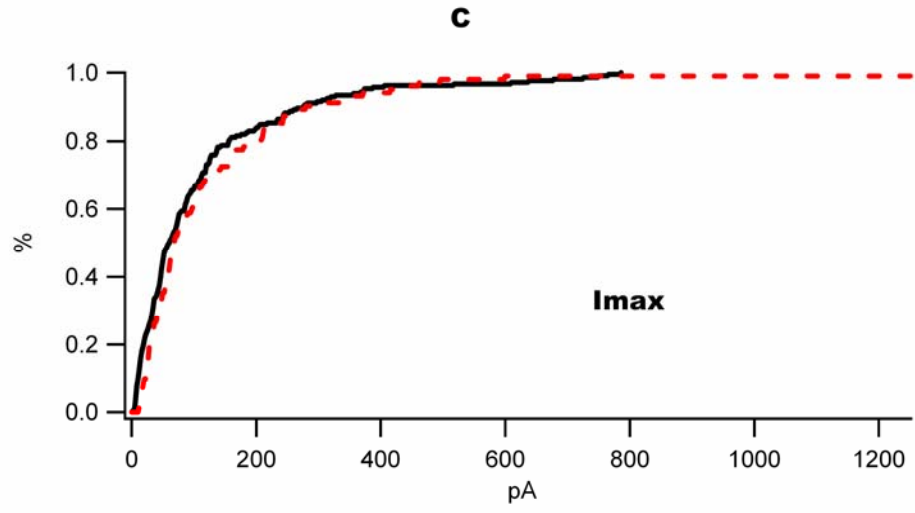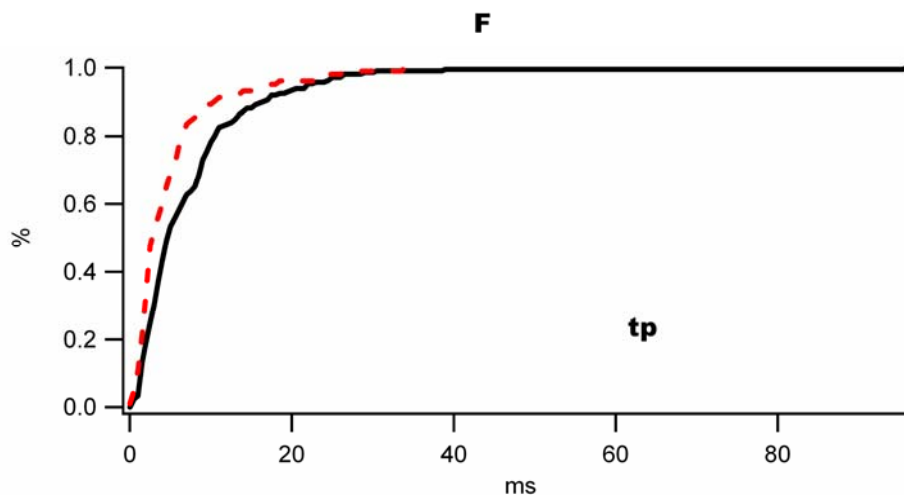
Fig. 3.7. The cumulative histograms of six vesicular parameters for the HCSP and RRP. A. integration of the current/total charge from released contents (Q); B. Index for the diameter of the vesicle ($Q^{1/3}$); C. current peak (I_{max}); D. Width at half-height of the amperometric spike ($t_{1/2}$); E. Rate of release calculated from 25% to 75% amplitude of the rising part of the spike (M25%-75%); F. Time to peak (tp); (HCSP: red dotted line, RRP: black solid line).

We then did the Mann-Whitney Rank Sum Test for this group of data to statistically analyze the difference between the amperometric parameters from the HCSP and those from the RRP (Table 3.1).

Table 3.1. Comparison of the parameters from the HCSP and RRP.

		Q	Q^1/3	Imax	t_half	M25-75%	tp
HCSP	Mean	1.51±0.20	1.00±0.04	128.87±16.13	10.38±0.99	60.30±9.52	5.39±0.57
HCSP	Median	0.84	0.94	69.9	7.1	24.8	3.22
RRP	Mean	1.28±0.10	0.97±0.02	113.75±9.96	13.57±0.71	46.95±5.48	7.92±0.61
RRP	Median	0.75	0.91	61.99	10.13	14.48	5.05
P		0.65	0.65	0.1	0.0035*	0.005*	0.001**

It is shown that there is no statistically significant difference between the HCSP and RRP for Q, $Q^{1/3}$ and I_{max}, indicating the vesicles in the HCSP and RRP are of similar size with similar transmitter content. However there is statistically significant difference between the HCSP and RRP for $t_{1/2}$, M25%-75% and t_p, indicating that there might be different transmitter release mechanisms involved in the exocytosis at these two $[Ca^{2+}]_i$ levels. More data may be needed to confirm this trend.

To further analyze the HCSP data, we fit an exponential to the membrane capacitance trace for ~200 ms following the UV flash. The fitted exponential gives the amplitude of the HCSP (A_m), the rate constant of release (k) and the delay time (t_d) between the onset of the UV flash and the beginning of the exponential rise in capacitance response (Fig. 3.8).

Fig. 3.8. Sample exponential fit to ΔC_m elicited by photorelease of caged Ca^{2+}. The black trace represents a capacitance trace corresponding to the release of the HCSP. The red trace illustrates an exponential fit for the first 200 ms of capacitance change corresponding to the release of HCSP. For this sample trace, the fitted parameters are Am = 46.6 fF, k = 8.35 s^{-1}, Td = 19.8 ms. (td: delay time between flash and exponential response).

For the capacitance trace (black trace in Fig. 3.8), the exponential fit is of the form in equation (3.1),

$$C_m = C_i + A_m(1-e^{-kt}) \qquad\qquad (3.1)$$

Fig. 3.9 depicts the histogram of the amplitude of the HCSP for 44 traces, the mean value of the HCSP is 78.3 fF; the histogram of the delay time t_d, the mean value of the delay time t_d is 39.9 ms (Fig. 3.10) and the histogram of the mean rate constant k, the mean value is 10.5 s^{-1} (i.e. time constant is 95 ms) (Fig. 3.11)
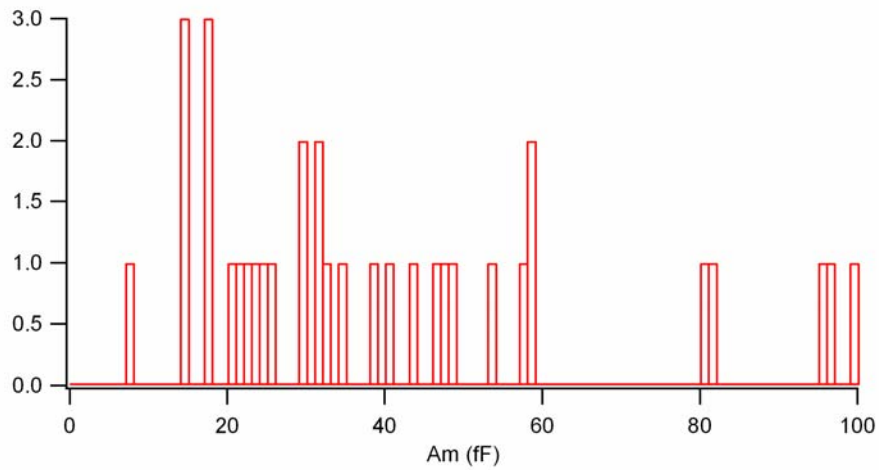
Fig. 3.9. The histogram of the amplitude of the HCSP of the 44 traces calculated from an exponential curve fit. Mean value of the amplitude of the HCSP is 78.3 fF.
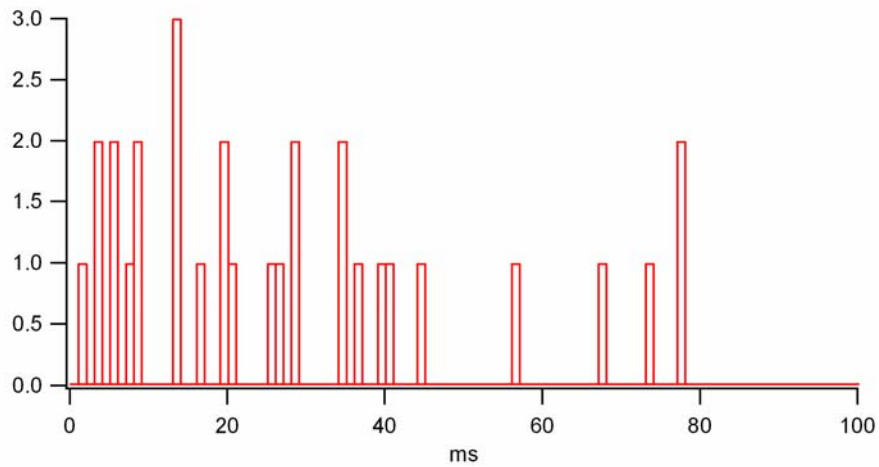
Fig. 3.10. The histogram of the delay time from the onset of UV flash and the starting point of capacitance change from 44 traces (8 negative values not included). The mean value is 39.9 ms.
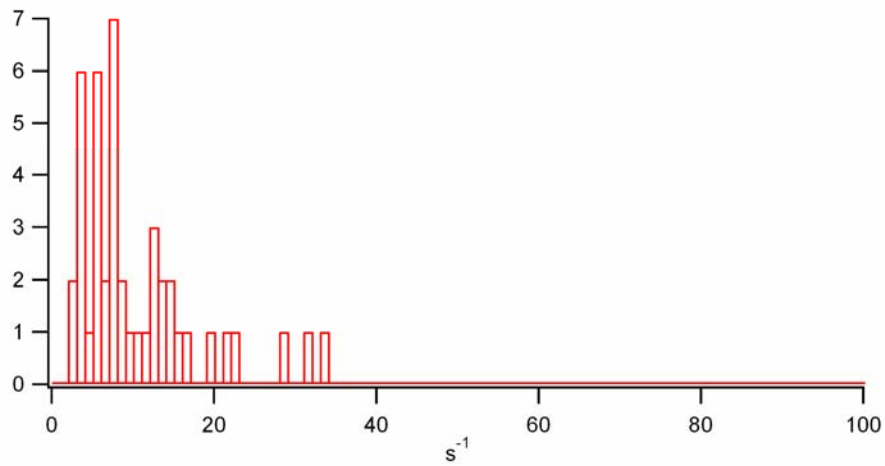
Fig. 3.11. The histogram of the rate constant for the release of HCSP from 44 traces. The mean value is 10.5 s^{-1}.

3.3 Conclusion and discussion

Our experiments confirm that the vesicles in the HCSP are likely to have a similar morphology as those in the RRP because $\Delta C/Q$ is similar for the two pools. The vesicles from these two pools also have similar catecholamine content. Therefore the difference between the pools may be differences in the composition of Ca^{2+}-sensing protein complexes in the vesicle membrane rather than large differences in vesicle size.

In this set of experiments, we have measured the mean value of HCSP to be 78.3 fF, which is larger than our previous report (Yang et al., 2002). One possible reason is that primary cell culture of adrenal glands from cows is somewhat seasonal. The level of secretion seems not to be uniform throughout the year. This set of experiments was done in spring and the secretion level seemed to be on the higher level. Although the average size of the HCSP is higher than our previous report, the rate constant of vesicle fusion is consistent with our previous report (Yang et al., 2002).

The complexity of analyzing spikes resulting from quantal exocytosis was thoroughly reviewed by Mosharov and Sulzer (Mosharov and Sulzer, 2005). In order to extract high information of transmitter release kinetics and content from single vesicles, we have to employ appropriate data acquisition and filtering methods. At the same time, it is equally important to use the appropriate spike detection criteria to identify spikes and to calculate fusion parameters with robust algorithms. We used the automatic analysis program from Borges lab (Segura et al., 2000) to analyze our data. The main challenges we encountered

while doing data analysis for amperometric spikes are 1.) Identification and rejection of spikes using appropriate cutoff criteria; 2.) Difficulties to analyze overlapping spikes.

To effectively identify valid amperometric spikes and reject noise artifacts, we mainly used trial-and-error method to find the right filter for optimal identification of spikes and to define the cutoff threshold for ruling out noise artifacts. Since the program made it possible to manually add or delete a spike, it is possible for us to correct spike identification errors. The more troubling problem for data analysis comes from overlapping spikes as shown in Fig. 3.12.
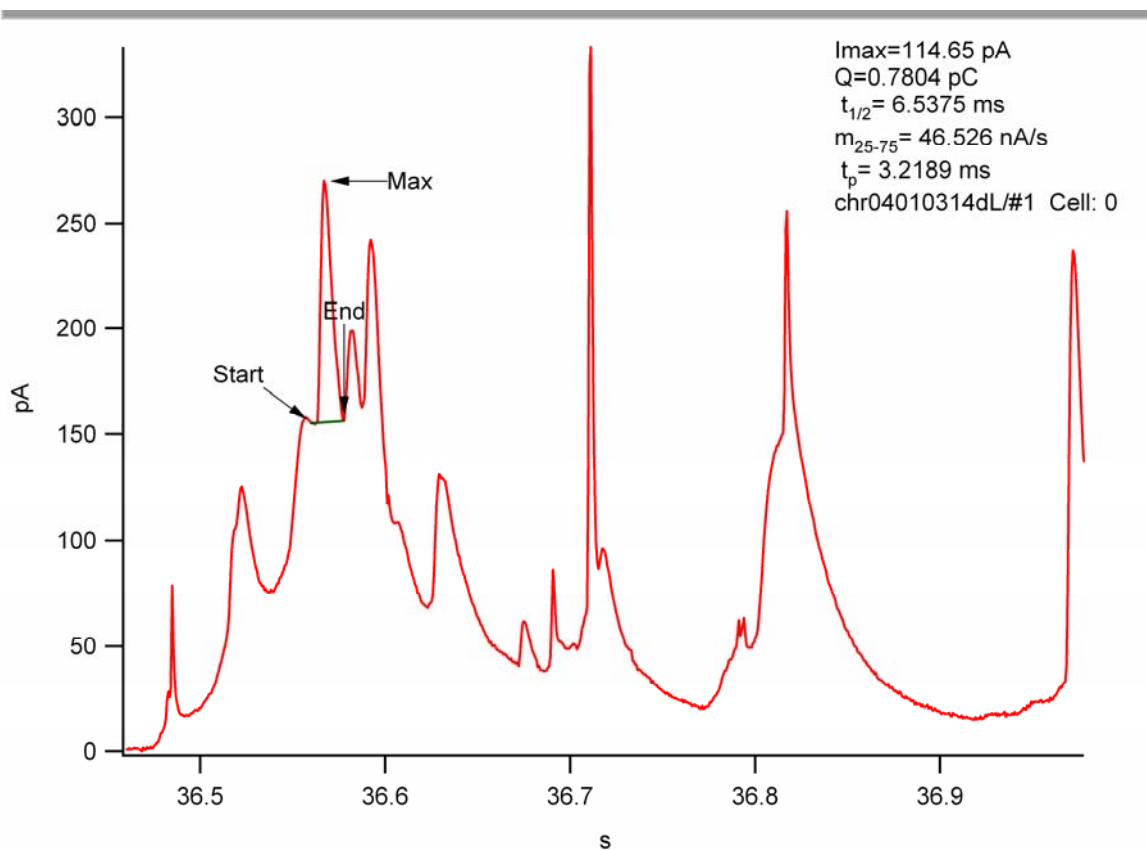
Fig. 3.12. The problem for data analysis of overlapping spikes. The amperometric spike analysis program identifies one spike (with arrows pointing to start point and end point) from a group of many overlapping spikes.

Apparently, the identified spike can not represent a full spike and therefore, if included in the data analysis, it can affect the accuracy of data interpretation. We therefore excluded the overlapping spikes while analyzing spike kinetics. However, deleting overlaps can also potentially bias our data. One possible solution to resolve this problem is to control experimental conditions so that there are less exocytotic events and therefore less overlapping spikes.

The complication involved in spike analysis, together with our small sample size, limit the strength of the conclusions we can draw from the comparisons between the HCSP and RRP made in Fig. 3.7 and Table 3.1, Whereas it is clear that 'Q' does not differ greatly between the two vesicle populations, we are not certain if the vesicle release kinetics differ. The trend, is for the vesicle kinetics to be ~50% slower for the RRP compared to the HCSP and this difference was shown to be statistically significant by the Mann-Whitney Rank Sum Test. Further experiments with larger sample sizes under conditions where the two release phases have fewer overlapping spikes would further support this finding.

CHAPTER 4

ELECTRICAL STIMUATION AND DETECTION OF ACTION POTENTIALS USING A CARBON FIBER ELECTRODE

4.1   Introduction

Action potentials are the physiological stimuli for secretion of hormones and neurotransmitters from most neurons and neuroendocrine cells. Typically an action potentional leads to opening of voltage-dependent Ca^{2+} channels, influx of Ca^{2+} and then Ca^{2+}-triggered exocytosis. A widely used approach employed in neuroscience is to trigger an action potential using a transient electrical field. Studies on the relationship between action potential stimuli and the resultant exocytosis have provided in-depth biological information about cell secretion. For example, the Misler group discovered that chromaffin cell secretion has a steeper dependence on the action potential frequency than many nerve terminals (Zhou and Misler, 1995). The Artalejo group showed that latencies between the onset of action potential stimuli and amperometric detection of quantal release of transmitters could be used to infer the distance between the L-type Ca^{2+} channel and the vesicle release sites (Elhamdani and others, 1998).

Several groups have demonstrated stimulation of action potential from cells on microchips using voltage pulses from patterned electrodes. The Stett group fabricated a silicon chip for capacitive stimulation of action potential (Fromherz and Stett, 1995). The Fromherz group developed a semiconductor chip to apply voltage pulses to a neuron that was immobilized on the surface of the chip to elicit action potential in the neighboring neuron whereas the action potential was monitored by the underlying chip (Zeck and Fromherz, 2001).

4.2 Stimulating action potential using capacitive coupling from a carbon fiber electrode

For our miniaturized biochip device, since the electrochemical electrode needs to be within several micrometers from the cell to detect quantal exocytosis, it is very desirable if we can simply use the same electrode to stimulate action potentials to trigger transmitter release. To test this idea, we conducted patch-clamp and carbon fiber amperometry experiments simultaneously on the same cell. The carbon fiber electrode served as both the stimulating electrode for eliciting action potential and the recording electrode for measuring quantal catecholamine release from single chromaffin cells. The experiment configuration is similar as that in the previous chapter, except that we used whole-cell recording in current-clamp mode, in order to monitor membrane potential changes generated by applying brief voltage pulses to the carbon fiber electrode.

An equivalent circuit (Fig. 4.1) illustrates the capacitive coupling (C_c) between a carbon fiber electrode and the membrane of a cell.
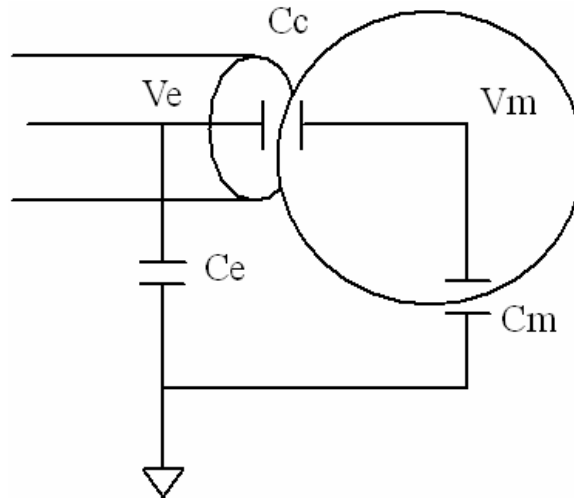
Fig. 4.1. Equivalent circuit showing capacitive coupling between a carbon-fiber electrode and the inner surface of the cell membrane. V_m is the voltage across the cell membrane and C_m is the membrane capacitance of the cell; V_e is the carbon fiber electrode voltage and C_e is the carbon fiber electrode capacitance; C_c is the coupling capacitance between the carbon fiber and the inner surface of the cell membrane.

A brief voltage pulse (V_e) is applied to the cell resulting in a capacitive current through which, in turn, leads to a change in membrane potential (V_m). If the evoked change in V_m exceeds a threshold value, an action potential is elicited. C_e denotes the capacitance between the carbon fiber electrode and the grounded bath solution, whereas C_m denotes the capacitance for the cell membrane. A brief voltage step in V_e leads to a much smaller voltage change in V_m due to the voltage divider that is formed from the series

combination of the coupling capacitance (C_c) and cell membrane capacitance (C_m). The relationship between ΔC_c and ΔC_m can be calculated (Equation 4.1).

$$\Delta V_m / \Delta V_e = C_c / (C_m + C_c) \qquad\qquad (4.1)$$

This can be rearranged to calculate C_c from experimental measurement of ΔV_m:

$$C_c = \Delta V_m C_m / (\Delta V_e - \Delta V_m) \qquad\qquad (4.2)$$

Thus, we can calculate the coupling capacitance from the measured ΔV_m in response to ΔV_e if C_m is known (Equation 4.2)

We found that brief voltage pulses (V_e) applied to the carbon fiber that are within the ± 1 V stimulus range of the VA-10 amplifier were not strong enough to elicit an action potential. We then modified the VA-10 amplifier to allow ± 10 V stimuli and increased the maximum current that can be delivered by the amplifier by replacing the feedback resistor (R_f in Fig. 2.1) from 500 MΩ to 100 MΩ. After the circuit modification, we were able to elicit action potentials in chromaffin cells with 0.3 ms pulses from 0.7 V to either 6 V or 10 V. A "holding" value of 0.7 V for the electrode potential was chosen to promote oxidation of released catecholamine from chromaffin cells. Through capacitive coupling between the carbon fiber electrode and the cell membrane, action potentials were triggered and monitored by the patch pipette electrode with a coupling transient preceding the action potential. In principle, we should be able to measure action

potential-triggered catecholamine release from cells using the same electrode. Fig. 4.2 depicts a sample trace of a carbon fiber-elicited action potential. A 0.3 ms voltage pulse from 0.7 V to 4 V failed to elicit an action potential (Fig. 4.2A) while a 0.3 ms voltage pulse from 0.7 V to 6 V succeeded in triggering an action potential as measured by the whole-cell recording in current-clamp mode (Fig. 4.2B).
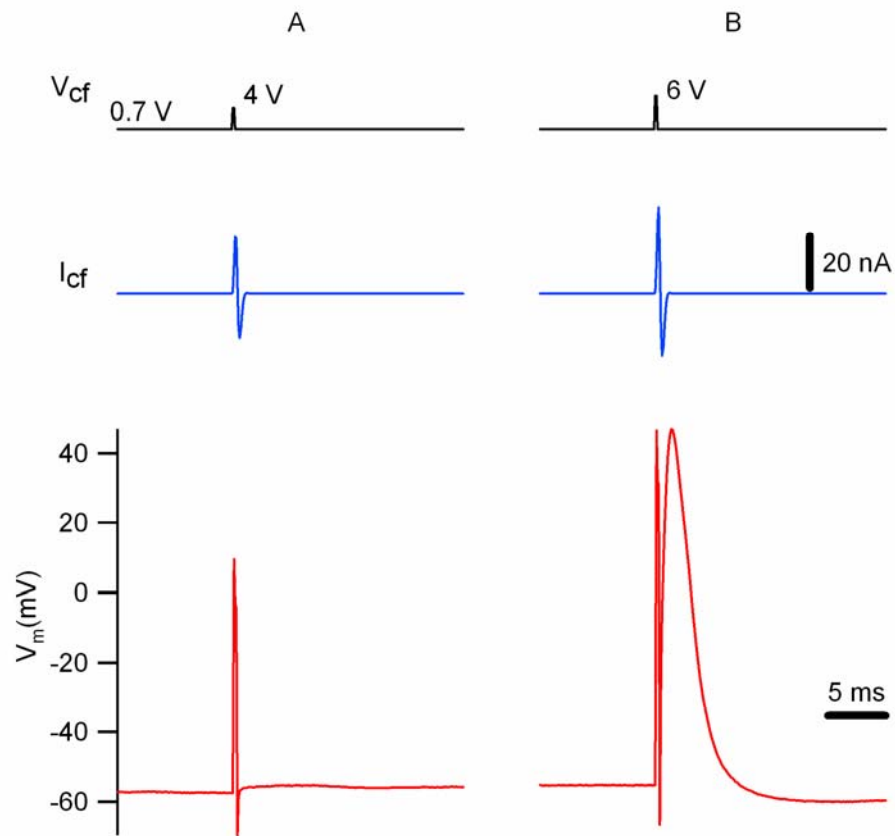
Fig. 4.2. A 0.3 ms pulse from 0.7 V to 4V fails to elicit an action potential (A), whereas a 0.3 ms pulse to 6V triggers an action potential in the cell (B). V_{cf} denotes the voltage applied on the carbon fiber; I_{cf} denotes the transient current generated in the carbon fiber; V_m denotes the membrane potential recorded by the patch pipette.

We calculated the mean coupling capacitance in several cells with successful action potential stimulation (Equation 4.2). The mean value is 83 fF. (SD = 16 fF, n = 4 cells, Table 4.1)

Table 4.1. Coupling capacitance for cells with elicited action potentials.

cell#	ΔVe(V)	ΔVm(mV)	Cm(pF)	Cc(fF)
1	9.3	126.7	6.69	92.4
2	9.3	122.3	5.99	79.82
3	9.3	115.3	4.98	62.52
4	5.3	86	5.95	98.14

4.3   Anode break stimulation of an action potential using a carbon fiber electrode

As described by Hodgkin and Huxley (Hodgkin and Huxley, 1952), a hyperpolarizing pulse can counter-intuitively trigger an action potential under certain conditions. This phenomenon is called anode break excitation or sometimes referred to as rebound excitation. The hyperpolarizing pulse removes Na^+ inactivation and decreases the K^+ conductance, thus lowering the threshold to trigger an action potential.

We tested anode break excitation to trigger an action potential and it worked in some cells. Fig. 4.3 shows a sample trace of anode break excitation of an action potential in a chromaffin cell.
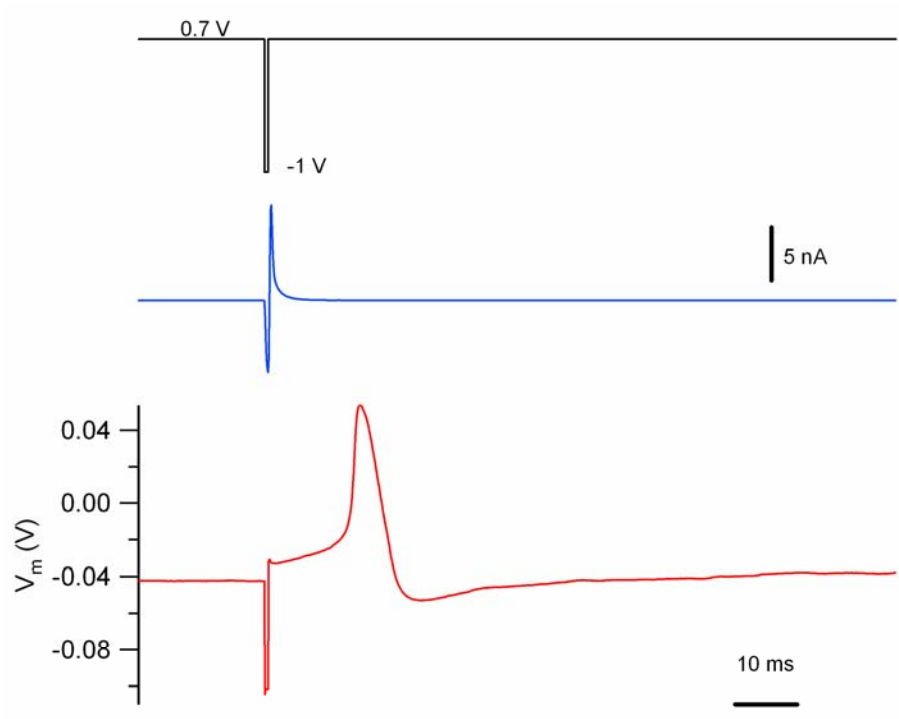
Fig. 4.3. Anode break excitation of action potential using a carbon fiber electrode. Hyperpolarization pulse of 0.3 ms (a voltage step from 0.7 V to -1 V and then back to 0.7 V) was applied to the cell through a carbon fiber electrode adjacent to the cell; The current in the carbon fiber electrode is shown in the blue trace; An action potential (red trace) was detected by a patch pipette electrode using a whole-cell recording at current-clamp mode. Note that there was a downward capacitive transient from the coupling of the carbon fiber and the inner surface of cell membrane.

4.4 Using a carbon fiber electrode to monitor when an action potential occurs in an adjacent cell

As shown in the equivalent circuit of Fig. 4.1, the carbon fiber electrode is capacitively coupled to the membrane potential when the carbon fiber electrode is placed near the cell.

Thus transient changes in V_m such as during an action potential should produce a transient current in the carbon fiber (I_{cf}). In this case I_{cf} can be monitored to tell when an action potential occurs. To elicit an action potential, we used a patch pipette to inject current into a cell with whole-cell recording in the current-clamp mode. Simultaneously we used a carbon fiber electrode to touch the same cell and record the current transient associated with the action potential. As shown in the sample trace (Fig. 4.4), an injection of 10.9 pA current to the cell triggered an action potential (top), and a simultaneous downward current transient was picked up by the carbon fiber. Here the capacitive coupling (C_c) between the cell membrane and the carbon fiber can generate a current within the carbon fiber at an amplitude of

$$I_c = C_c * dV_m / dt \tag{4.3}$$

Since our calculated C_c is at the order of 100 fF (Table 4.1), and the typical rate for the rising phase of an action potential is around 100 mV/ms, the calculated magnitude of the current transient will be at the order of 10 pA, consistent with Fig. 4.4. Since the amplitude of this current is very small, microchip devices have to be designed with small electrode area ($\sim$100 μm^2) in order to resolve this small signal from background noise. Recordings such as Fig. 4.4 support our hypothesis that carbon fiber electrodes can also be used to verify the occurrence of action potentials. Since the current transient is downward, it is feasible to use the same carbon fiber to detect upward amperometric spikes of catecholamine release triggered by action potentials. The bonus from this kind of recording is that we can get additional information including latencies between the onset of action potential and the transmitter release. The relationship between action

potential stimuli and quantal release of transmitters is subject to dynamic regulation by other secretagogues and second messengers and thus is important for the overall appreciation of the kinetics and regulatory mechanisms of transmitter release.
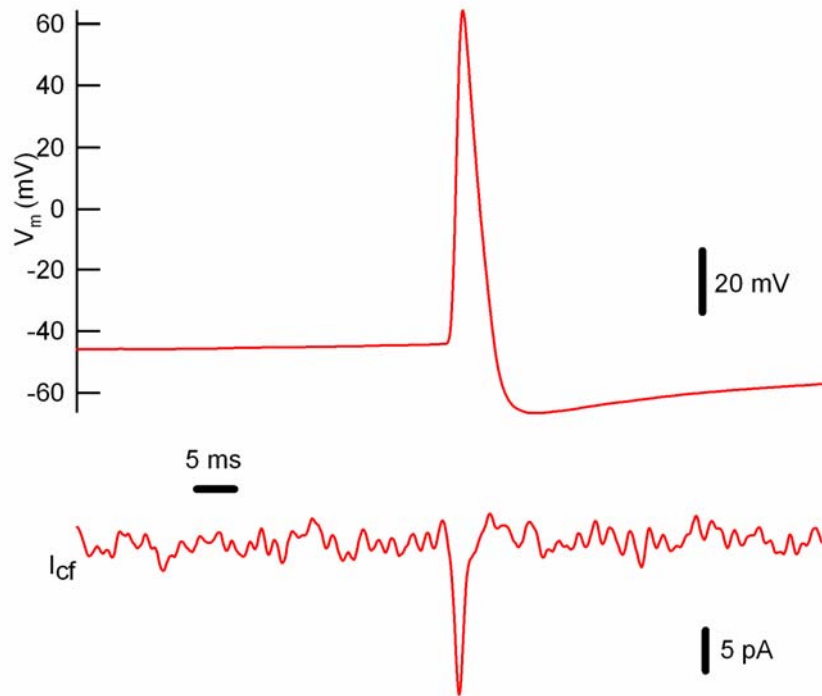
Fig. 4.4. An action potential induced by injecting 10.9 pA into the cell through a patch-clamp pipette induces a small transient current in the carbon-fiber electrode.

4.5 Conclusion and discussion

Our "proof-of-concept" experiments showed that it is feasible to use a carbon fiber electrode to electrically stimulate action potentials (Fig. 4.2), the physiological stimuli for Ca^{2+}-triggered exocytosis. Alternatively, a carbon fiber electrode can also be used to monitor the occurrence of an action potential as shown in Fig. 4.4. Since the capacitive

coupling current transient is downward, it is possible to use the same carbon fiber to record upward amperometric spikes from exocytotic events.

However, we found that the reproducibility of this electrical stimulation method is not as satisfactory as we desired. Our speculation is that the electric field generated at the tip of a carbon fiber electrode rapidly diverges from this point-like source so that the capacitive coupling is variable. A better approach may be to use an additional pair of electrodes (i.e., a "bipolar" electrode) to stimulate cells rather than attempt to both stimulate and record with the individual electrochemical electrode. The bipolar electrodes could be patterned on the surface of the microchip devices to focus the electric field for better capacitive coupling. Numerical modeling of the electric field distribution could help to optimize the layout of the patterned electrodes to achieve more efficient and reliable capacitive coupling.

We next tested an alternative approach using an optical stimulation method for stimulating exocytosis using caged Ca^{2+} technique, a method we used routinely in the lab. It turned out to be a very reproducible method to faithfully stimulate exocytosis through photorelease of cage Ca^{2+} on the chip. For the next two chapters, we mainly used this on-chip optical stimulation method to trigger exocytosis in single living cells.

CHAPTER 5

CONTROLLED ON-CHIP STIMULATION AND DETECTION OF QUANTAL CATECHOLAMINE RELEASE USING PHOTOLYSIS OF CAGED CA^{2+} IN PERMEABILIZED CELLS ON TRANSPARENT ITO MICROCHIP ELECTRODES

Recent years have seen significant growth and rapid progress of applying micro/nano fabrication and other bioMEMS techniques to revolutionize the study both in basic biological research as well as in translational research (Whitesides and others, 2001; Di Carlo and Lee, 2006). A handful of groups pioneered the research of applying bioMEMS techniques to study Ca^{2+}-dependent exocytosis. Our group developed the first generation of microchip device to detect single cell secretion from a large area of the cell using gold electrodes patterned in cell-sized wells which is etched in silicon substrate (Chen et al., 2003). We then developed a second generation of microchip device using transparent Indium-Tin-Oxide (ITO) as the electrochemical electrodes patterned on glass substrate (Sun and Gillis, 2006). The Amatore group has also manufactured a glass microchip with patterned transparent ITO electrodes for simultaneous optical and amperometric detection of exocytosis (Amatore et al., 2006). The Lindau group has developed a glass microchip with 4 platinum electrodes surrounding a single cell to identify the site of release from a

single cell (Dias et al., 2002; Hafez and others, 2005). All these efforts represent advancements towards the goal of high-throughput assays for the study of single-cell exocytosis.

A commonly used method to stimulate exocytosis is perfusion of high K^+ solution, which results in depolarization of cell membrane, opening of voltage-dependent Ca^{2+} channel, influx of Ca^{2+} and then Ca^{2+}-triggered exocytosis. A problem with this type of stimulation is that it is not easy to figure out which step in this stimulus-secretion cascade is affected by an experimented perturbation such as application of a drug, instead, it is desirable to more directly control the immediate trigger for exocytosis, a rise in $[Ca^{2+}]_i$. One way to do this is through photolysis of "caged" Ca^{2+}. Therefore we proposed to integrate the caged Ca^{2+} technique with ITO amperometry for better control and monitoring of the stimulation of exocytosis.

5.1 Permeabilize cells in order to introduce caged Ca^{2+} into them without using traditional dialysis from patch pipettes

To aim at developing high-throughput assay of exocytosis, we need to use an alternative method to load caged Ca^{2+} into cells instead of using the traditional dialysis from patch pipettes. Our initial approach to stimulate cell secretion through photorelease of caged Ca^{2+} was to pemeabilize cell membranes to allow loading of the cage and Ca^{2+} indicators into cells.

One commonly used detergent for cell membrane permeabilization is digitonin (TerBush and others, 1988; Holz and others, 1989; Tengholm and others, 2000). We employed carbon fiber amperometry to verify the permeabilizing ability of digitonin on chromaffin cells. We first positioned a carbon fiber electrode adjacent to a chromaffin cell in our standard cell bath solution lacking Ca^{2+}. A pipette containing 20 μM digitonin and ~20 μM free Ca^{2+} was brought close to the cell and the pipette solution was perfused onto the cell. Free Ca^{2+} diffused into the cell through the permeabilized cell membrane and triggered quantal catecholamine release, which was detected by the carbon fiber electrode. (Fig. 5.1)
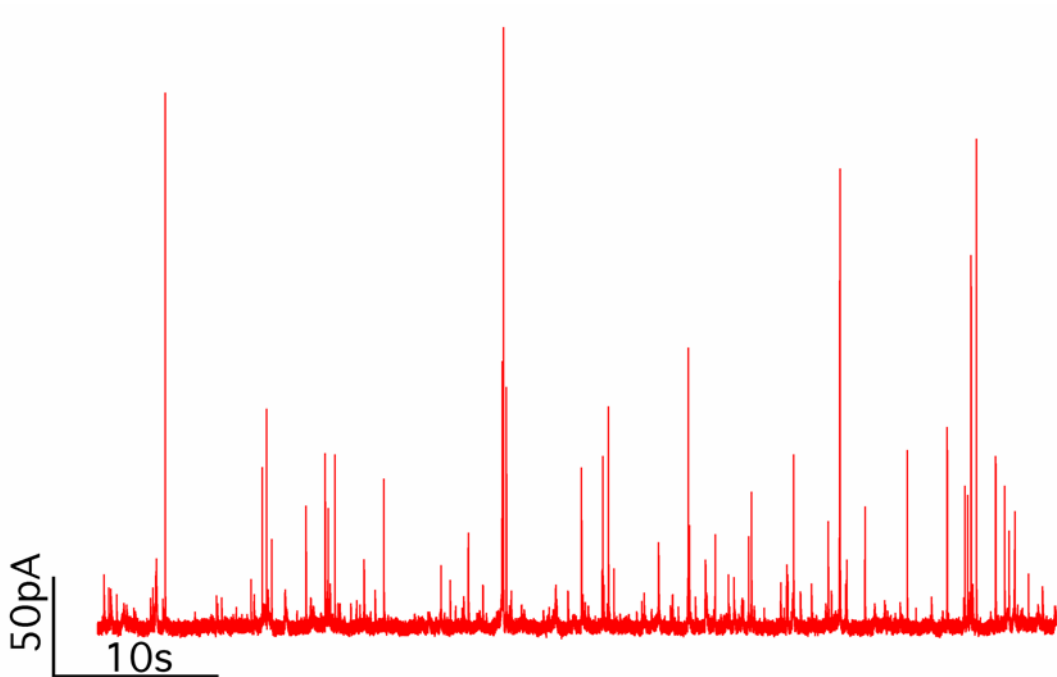
Fig. 5.1. Catecholamine release from digitonin-permeabilized chromaffin cells detected by a carbon fiber electrode.

Another method to permeabilize cell membrane is to use α-hemolysin, (α-hemolysin, also known as α-toxin), a pore-forming protein secreted by the bacterium Staphylococcus aureus, to insert transmembrane channels into the cell membrane (Gouaux, 1998). Since the heptameric pore is 10 nm in diameter, it only allows small molecules up to 3 kD to pass through the cell membrane, thus effectively prevent the releasing of macromolecules and organelles from the cell (Chang and others, 1995). Thus this method is likely to be less damaging to the cell than digitonin permeabilization. We employed three methods to confirm the efficacy of cell permeabilization by α-toxin: carbon fiber amperometry, a Trypan blue assay, and a propidium iodide assay.

Similar to the digitonin method, we performed carbon fiber amperometry on α-toxin permeabilized chromaffin cells and detected Ca^{2+}-triggered exocytosis (Fig. 5.2).
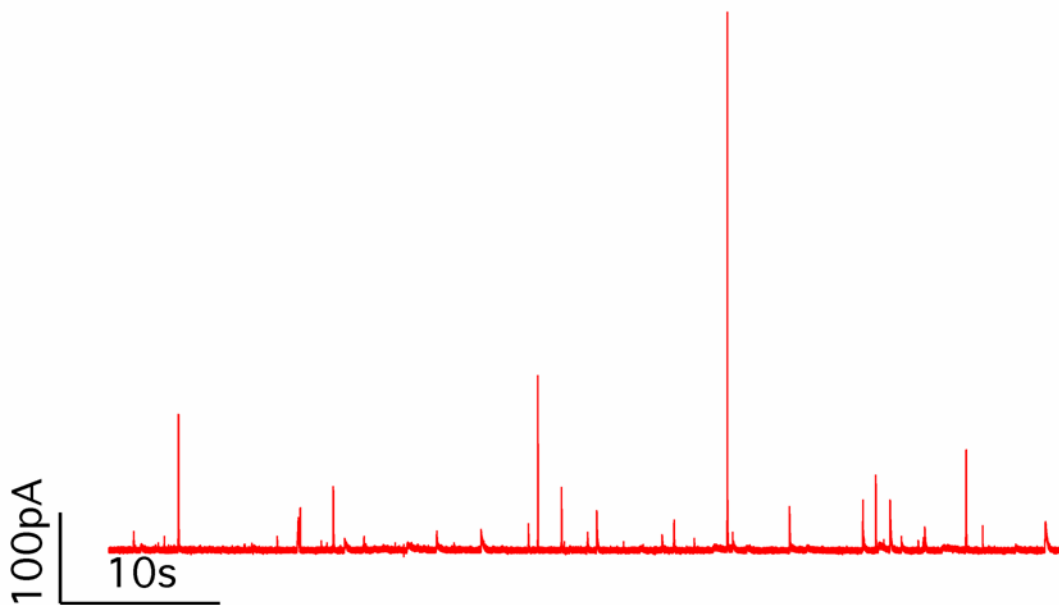
Fig. 5.2. Carbon fiber electrode detecting catecholamine release from α-toxin permeabilized chromaffin cells ([α-toxin] = 200 μg/ml)

We then used both Trypan blue assay and propidium iodide assay to further confirm the pore-forming function of α-toxin. As explained in Chapter 2, although Trypan blue is a common viability assay, it can stain the nucleus of a living cell if the cell membrane is permeabilized. As shown in Fig. 5.3, after co-incubation of α-toxin and Trypan blue, cell nuclei of chromaffin cells were stained by Trypan blue as a function of time indicating membrane permeabilization.
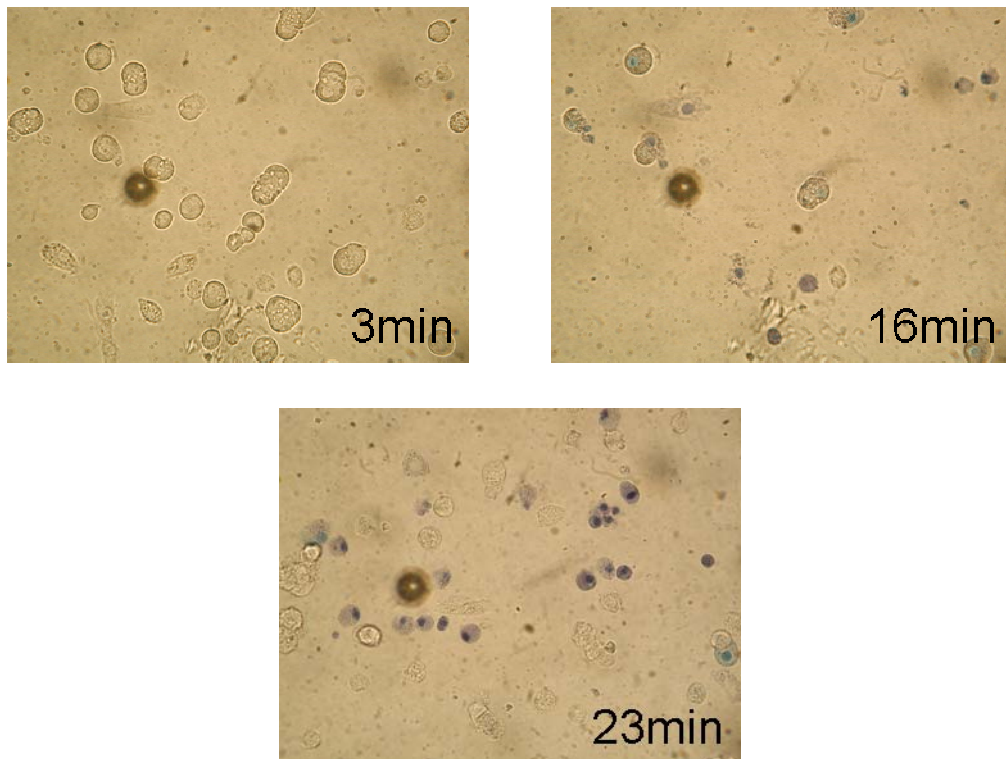
Fig. 5.3. Trypan blue assay to verify α-toxin-permeabilization of chromaffin cells. Trypan blue assay to verify permeability of chromaffin cells after 15 min incubation of 200 μg/ml α-toxin and 0.4% Trypan blue solution in Ca^{2+}-free bath solution. Digital pictures were each taken at 3 min, 16 min and 23 min after incubation.

Fluorescence detection of propidium iodide within cells (Fig. 5.4) also showed that α-toxin was forming pores to facilitate transmembrane delivery of small molecules.
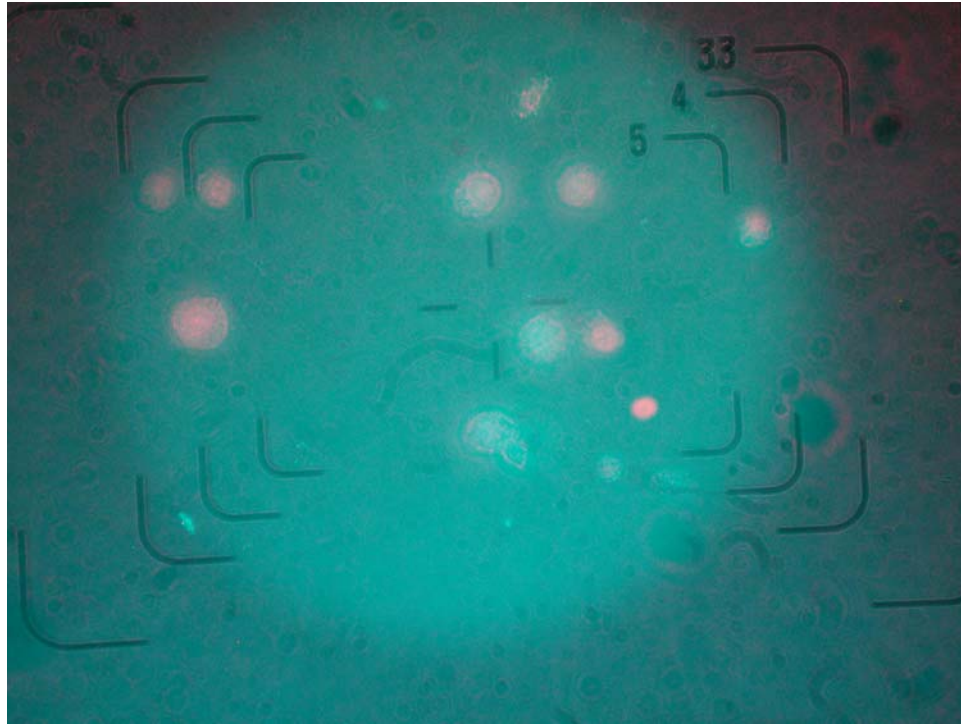
Fig. 5.4. Propidium iodide assay to verify the permeability of α-toxin on chromaffin cells. Chromaffin cells fluoresce orange following incubation with 4 μg/ml of propidium iodide for 15 min).

We found that it was more reproducible to permeabilize cells with digitonin. So we used digitonin for the first set of experiments to do amperometric recording on ITO electrodes.

5.2 Design a high Ca^{2+} buffer capacity solution to mimic the intracellular environment

Ideally, following permeabilization of the cell membrane, the intracellular and extracellular Ca^{2+} concentrations rapidly equilibrate so that $[Ca^{2+}]_i$ can be easily measured

with fura-type fluorescent indicators. However, endogenous Ca^{2+} buffers in cells will tend to make free $[Ca^{2+}]_i$ in the cell lower than in the surrounding solution. As shown in the schematic of Fig. 5.5, there would be a $[Ca^{2+}]_i$ gradient between the inside and outside of the cell after UV photolysis if using a low Ca^{2+} buffer capacity solution. However, we could avoid this problem by designing an extracellular solution with Ca^{2+} buffer capacity greater than that of the cell. In this case, following UV photolysis, the $[Ca^{2+}]$ outside and inside the cell would be the same.
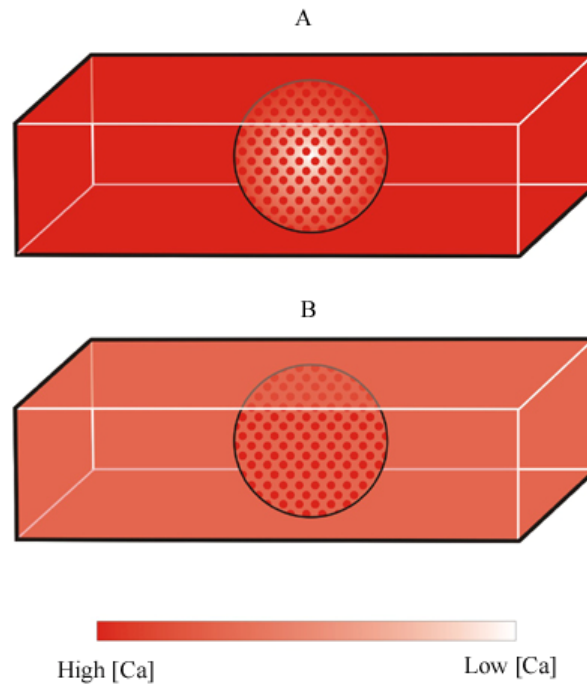
Fig. 5.5. Schematic of the difference of $[Ca^{2+}]$ after UV photolysis in different Ca^{2+} buffer capacity solutions. A: $[Ca^{2+}]$ gradient within a permeabilized cell after UV photolysis of low Ca^{2+} buffer solution in the microchannel; B. $[Ca^{2+}]$ is uniform inside and outside of a permeabilized cell after UV photolysis of high Ca buffer capacity solution in the microchannel.

To maintain the elevated $[Ca^{2+}]_i$ in cells within a microfluidic channel, we not only need a high Ca^{2+} buffer capacity solution, but also need to stop the solution flow in the microfluidic channel. Otherwise, the solution flow and diffusion exchange will rapidly

wash away the photolyzed cage. We first tried to balance the solution height in the inlet and outlet tubing connected to the PDMS channel so as to get zero flow in the microchannel. Then we realized that the elasticity from PDMS and plastic tubing made it very slow (hours) to reach a nearly zero-flow condition of a microscale level. However, if we waited long enough until the flow was insignificant, we recorded the elevation of $[Ca^{2+}]_i$ upon UV flash photolysis, followed by the drop of $[Ca^{2+}]_i$ to the basal level following diffusion of the photolyzed cage and free Ca^{2+} away from the illumination area.. We used a flash lamp to photolyze the cage over ~200 μm length of the channel and measured an elevation of free Ca^{2+} to several μM. The time course of the decline in free Ca^{2+} concentration was well described by the solution of the one-dimensional diffusion (Equation 5.1) when N(x, t) is the concentration of Ca^{2+} in the microfluidic channel.

$$\frac{\partial N}{\partial t} = D \frac{\partial^2 N}{\partial x^2}$$
(5.1)

If the initial Ca^{2+} concentration following the flash at t = 0 is normalized to a value of 1 and is assumed to be uniform throughout the light excitation area (-l/2 < x < l/2), then the solution of the diffusion equation in one dimension is:

$$N(x,t) = \frac{1}{2} [erf(\frac{x+l}{\sqrt{4Dt}}) - erf(\frac{x+l}{\sqrt{4Dt}})]$$
(5.2)

At the middle of the excitation area (x = 0), the Ca^{2+} concentration decays with time according to:

$$N(0,t) = erf(\frac{l}{\sqrt{4Dt}}) \qquad\qquad (5.3)$$

If we generalize the solution for the case where $[Ca^{2+}]_i$ decays from an initial value $(a+b)$ to a final equilibrium value of b, the $[Ca^{2+}]_i$ time course is given by:

$$f(t) = a * erf(\frac{l}{\sqrt{4Dt}}) + b \qquad\qquad (5.4)$$

Where L is the width of the excitation aperture, t_0 is the staring time of the recording. L and t_0 are known for specific experiments. We experimentally measured the $[Ca^{2+}]_i$ time course and fit the measurement with equation 5.X to obtain estimates of the diffusion coefficient for Ca^{2+} (D). The fitted diffusion coefficient was 0.21 $\mu m^2/ms$, very close to the expected diffusion coefficient of Ca^{2+} (0.22 $\mu m^2/ms$) (Fig. 5.6).
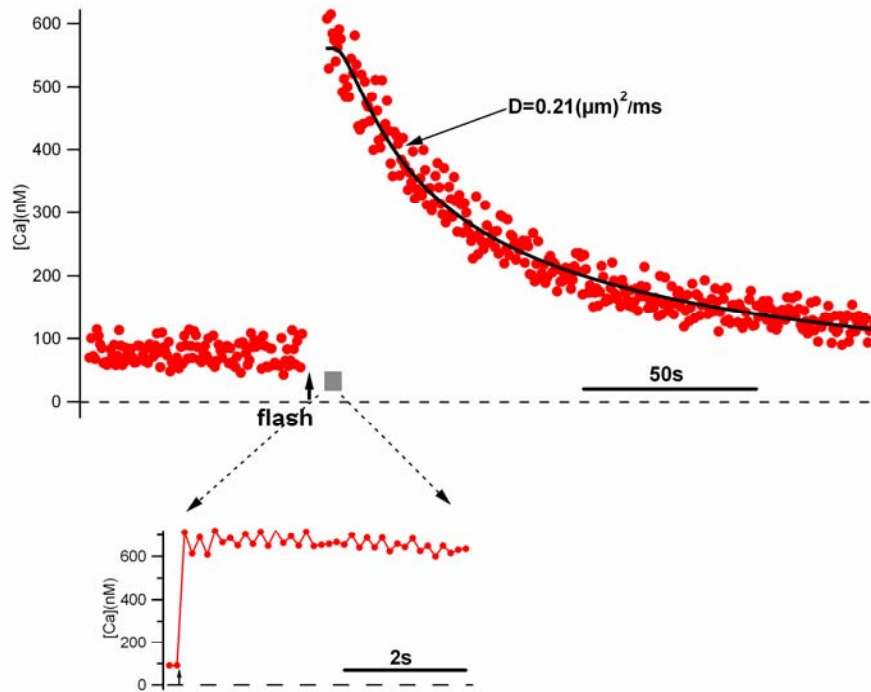
Fig. 5.6. Photorelease of caged Ca^{2+} in intracellular mimicking solution within a microfluidic channel. The time course of the decline in free Ca^{2+} concentration was well described by the solution of the one-dimensional diffusion equation (solid line, diffusion coefficient $D=0.21\mu m^2/ms$).

To more efficiently stop the flow within microfluidic channels, we tested monolithic multilayer PDMS microvalves (Unger et al., 2000; Anderson and others, 2000).

5.3   Microfluidic microvalves to maintain elevated [Ca^{2+}] after UV photolysis of caged Ca^{2+} within microchannels

As described in Chapter 2, we used soft lithography (Whitesides et al., 2001) to fabricate microfluidic channels with microvalves originally described by the Quake group (Unger et al., 2000) and the Whitesides group (Anderson et al., 2000). Fig. 5.7 depicts the actuation of a monolithic microvalve that stops the flow of beads in a solution containing green dye.
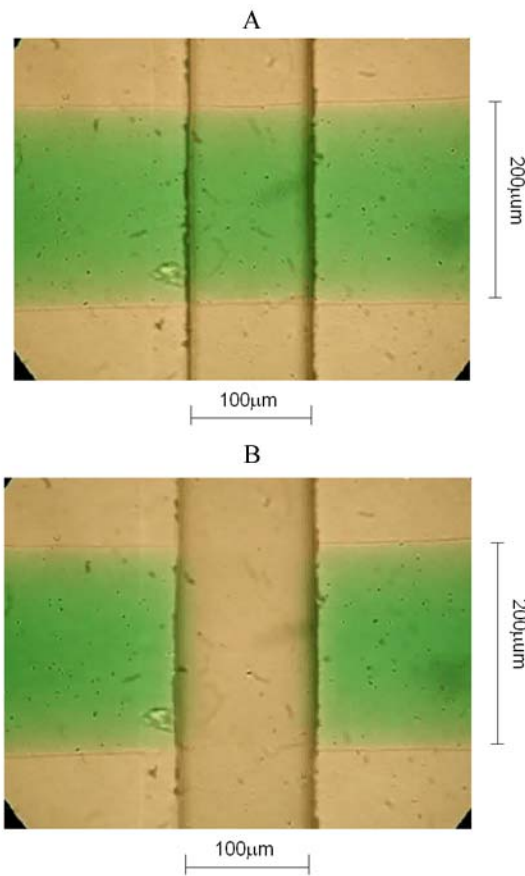
Fig. 5.7. Monolithic multilayer PDMS microvalve actuation. A. Before actuation of the microvalve; B. After actuation of the microvalve.

We measured the resistance of the channel following microvalve actuation to be about 6 GΩ (Fig. 5.8), indicating the PDMS valve completely closed the microchannel.
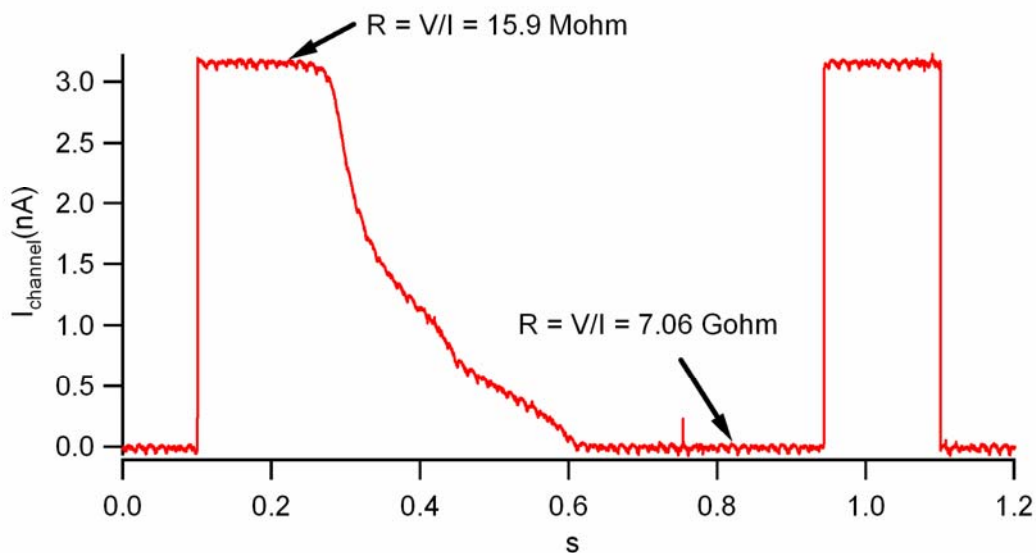
Fig. 5.8. Measurement of current through microfluidic channel during a push-up microvalve actuation. A 50 mV was added to the channel filled with standard bath solution containing 5 mM Ca^{2+}. The resistance before the microvalve actuation is 15.9 MΩ. After actuating the microvalve, the resistance increased dramatically to 7.06 GΩ indicating the microvalve was completely closed.

Our initial attempt to do amperometric experiments was to use digitonin to permeabilize cells sitting on top of ITO electrodes within microfluidic PDMS channels. However, we realized that targeting cells to ITO electrodes within a microfluidic channel and keeping them there was too challenging. So we turned to our next design of cell-sized electrodes with photoresist insulation.

5.4   Design and fabrication of a biochip device with multiple cell-sized ITO electrodes

Effective use of caged Ca^{2+} requires use of a high-numerical-aperture lens both to focus the excitation light and to collect fluorescent light emitted by the Ca^{2+} indicator dye with high efficiency. The distance between the lens surface and the sample (working distance) is typically ~0.3 mm for common high numerical apertures objective lenses, therefore fluorescent microcopy is often carried out using an inverted microscope with cells visualized from below through a thin glass coverslip. Thus fluorescence measurement of cells on microchips is most conveniently carried out using a thin transparent substrate. Another important design principle for our application is that the working electrochemical electrodes should be small to minimize background noise so that ~ pA-scale currents due to quantal exocytosis can be resolved. Finally, electrochemical electrodes need to be directly adjacent to cells (within several μm) so that released catecholamines diffuse to the electrode over a brief enough interval so that a recognizable "spike" of oxidative current is produced to indicate the time course of release from an individual vesicle.

Our solution to these design constraints is depicted in schematic fashion in Fig. 5.9A.
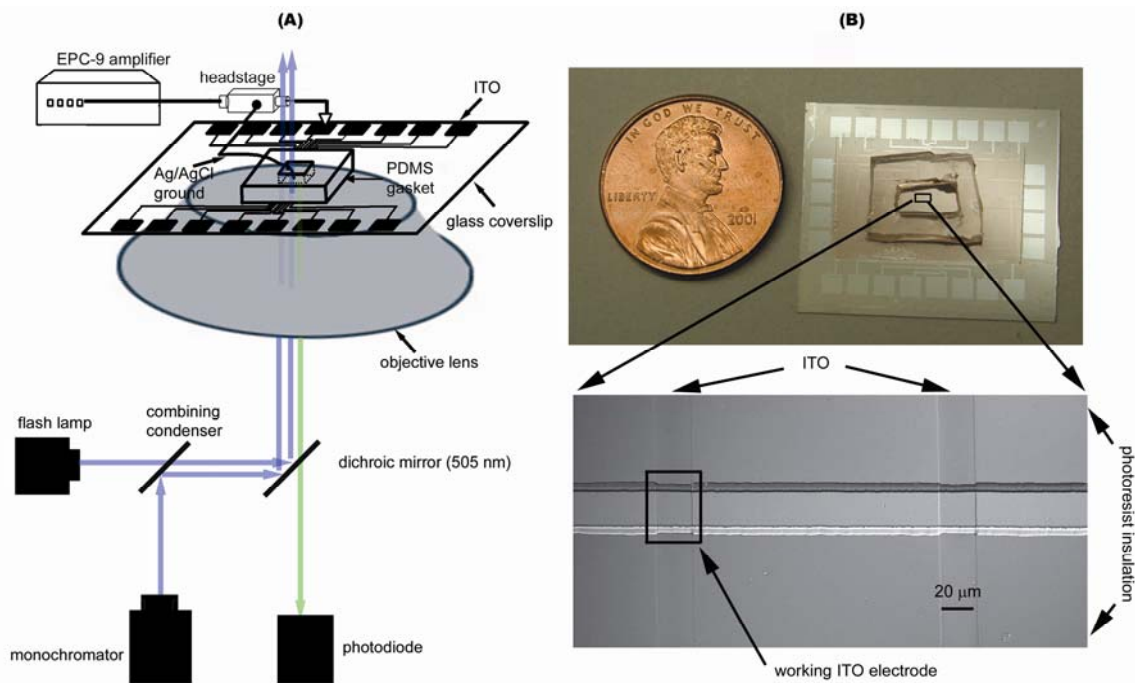
Fig. 5.9. Design of the instrument for on-chip photolysis of caged Ca^{2+} and electrochemical measurement of quantal exocytosis using transparent ITO microelectrodes. (A). Schematic of the experimental system. The flash lamp is used for rapid (~1 ms) photolysis of the cage whereas the monochromator excites Ca^{2+} indicator dyes to measure $[Ca^{2+}]_i$. (B). Top: Photo of microchip with 24 electrochemical ITO electrodes. Bottom: A DIC micrograph of 2 working ITO electrodes with dimensions of 20 x 20 μm.

Use of transparent ITO electrodes allows us to visualize cells sitting directly on top of electrochemical electrodes, therefore we sputter-deposited a thin (~110 nm) ITO film on size 2 glass coverslips (nominal thickness ~220 μm). We used photolithography and wet etching to pattern the ITO into 24 cell-sized working electrodes (see Methods section for details). During experiments, one of the electrodes is connected to the headstage of the amplifier to serve as the working electrode. A Ag/AgCl wire is immersed in the drop containing the cell suspension to serve as the ground electrode. A computer controls the firing of a UV flash lamp to photolyze caged Ca^{2+} within cells. A monochromator is

85

used to excite the Ca^{2+} indicator dye at a pair of wavelength (360/380 nm) and is also under computer control. A high numerical aperture objective lens on an inverted microscope is used to both focus the flash and monochromator excitation light on the cell and collect the emitted fluorescent light. A photodiode is used to measure the fluorescent light emitted by the Ca^{2+} indicator dye.

A photograph of our microchip device is shown in the upper panel of Fig.5.9(B). The 24 ITO squares around the edge of the microchip serve as the connection pads to facilitate connection to the amplifier headstage. A PDMS gasket sealed around the 24 ITO working electrodes functions as a reservoir for the drop of solution containing the cell suspension. The lower panel of Fig. 5.9(B) is a photomicrograph showing 2 of the 24 working electrodes. The vertical stripes are 20 µm-wide ITO stripes patterned by wet etching whereas the 20 µm-wide horizontal stripe is the opening of the photoresist that serves to insulate portions of the ITO film that are not electrochemically active. Therefore the working electrodes are at the intersection of the vertical and horizontal stripes.

5.5   Characterization of ITO working electrodes

It is important for our deposited ITO film to pass both visible and near-UV light in order to photolyze the Ca^{2+} cage (<~400 nm), excite the Ca^{2+} indicators (360 nm, 380 nm) and pass the fluorescent light (~500 nm). We optimized the fabrication parameters for ITO sputter-deposition on cover glass, so that 80% of light is transmitted for wavelengths longer than 360 nm (Fig. 5.10, see Methods section for deposition parameters). The

transmittance spectrum of our ITO-coated cover glasses (ITO thickness: 110 nm) is comparable to commercially available ITO-coated glass slides with a thinner ITO coating (15-30 nm). The electrical conductance of the ITO electrodes was also optimized. The measured sheet resistance of ITO-coated cover glass is 5.38 Ω/square, with a resistivity of 0.59×10^{-4} Ωcm.
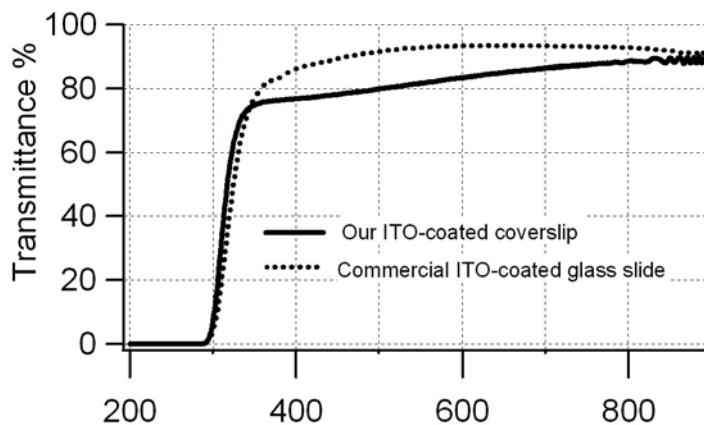
Fig. 5.10. Optical characterization of ITO microelectrodes. The optical transmittance of our sputtered ITO film is comparable to a commercially available ITO film (solid line: our ITO-coated coverslip with a 110 nm-thick ITO coating; dotted line: commercial ITO-coated glass slide with a 15-30 nm-thick ITO coating).

We next characterized the electrochemical response of our patterned ITO electrodes using a standard reversible analyte: 1 mM $K_3Fe(CN)_6$ in 0.5 M KCl, pH 3.0. Fig.5.11 shows a sample voltammogram (scan rate: 1V/s) that exhibits a sharp transition and flat diffusion-limited reduction current for potentials more negative than ~ -0.2 V versus Ag/AgCl, indicative of an appropriately low series resistance.
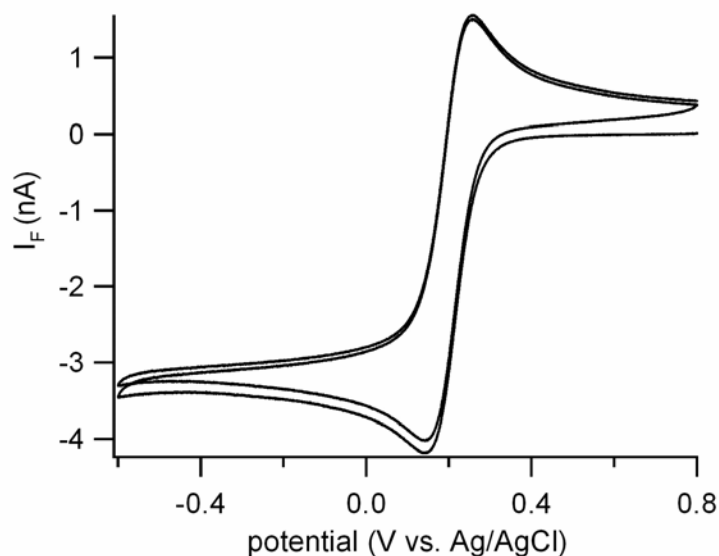
Fig. 5.11. Electrochemical characterization of ITO microelectrodes. Voltammogram with test analyte (1 mM $K_3Fe(CN)_6$ in 0.5 M KCl, pH 3, scan rate 1V/s). The ITO microelectrode had dimensions of 17.5 µm by 25 µm.

The theoretical value of a diffusion limited current (i_{lim}) for a univalent reaction on a disk electrode in an infinite plane is given by:

$$i_{lim} = 4FDCr \qquad (5.3)$$

where D is the diffusion coefficient, C is the analyte concentration, F is Faraday's constant and r is the radius of the electrode. For this experiment the working ITO electrode was rectangular with dimensions of 17.5 x 25 µm. If we assume the "effective radius" of our rectangular electrode is ~12 µm, (the radius of a circle with the same area), and a diffusion coefficient of 7.2×10^{-6} cm²/s for $Fe(CN)_6$, then the theoretical value of i_{lim} is 3.3 nA. Since the measured value in Fig. 5.11 is close to this theoretical value, we conclude that the working ITO electrode has the expected active area.

We also measured the specific capacitance of our deposited ITO film electrodes using sinusoidal voltage stimulation (frequency 1 kHz, peak amplitude 1 mV). The measured specific capacitance of a typical 20 μm by 20 μm ITO working electrode is ~0.1 pF/μm^2, comparable to the value we measured from commercially available ITO slides (Sun and Gillis, 2006) and carbon fiber microelectrodes (Kawagoe and others, 1991).

5.6   Photorelease of caged Ca^{2+} in digitonin-permeabilized cells

We next loaded digitonin permeabilized chromaffin cells with the Ca^{2+} cage NP-EGTA and Ca^{2+} indicator dyes (an equimolar combination of bisfura-2 and fura-2FF). To minimize the impact of endogenous Ca^{2+} buffers, we designed an "intracellular mimicking solution" with very high Ca^{2+} buffer capacity. This solution was intended to confound the ability of intracellular Ca^{2+} buffers to reduce [Ca^{2+}]$_i$ within the cell (e.g., see (Xu and others, 1997)) in order to minimize the gradient of [Ca^{2+}]$_i$ between the inside and outside of the cells after photolysis of caged Ca^{2+}. Loaded cells were transferred to the microchip device. Those cells settling on top of the ITO microelectrodes were used for amperometric recordings. Upon UV photolysis of caged Ca^{2+}, we detected oxidative current spikes as released catecholamine molecules were oxidized on the surface of ITO microelectrodes (Fig. 5.12).
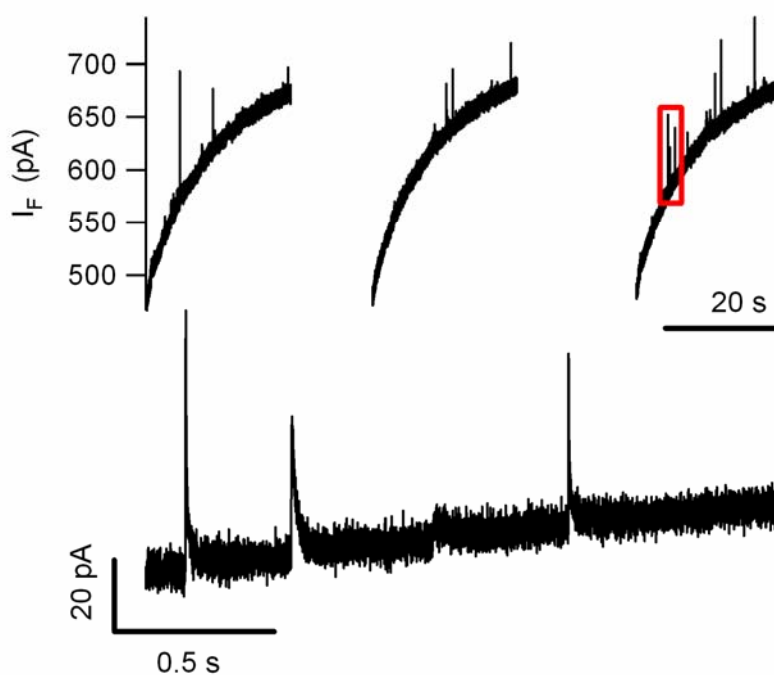
Fig. 5.12. An amperometric recording from digitonin-permeabilized chromaffin cells. Top: Typical amperometric spikes recorded from digitonin-permeabilized chromaffin cells sitting on top of ITO electrodes. The sloping baseline is a current artifact that resulted from cage photolysis. Bottom: Expanded view of the interval outlined by the red box in the top panel.

Surprisingly, we also detected a large background current that continued for tens of seconds even when the excitation light was terminated (Fig. 5.12). This slowly varying current occurred whether cells were present or not and resulted from photolysis of caged Ca^{2+} in the bath solution because it was absent when cage was removed (Fig. 5.13).

90

A

B
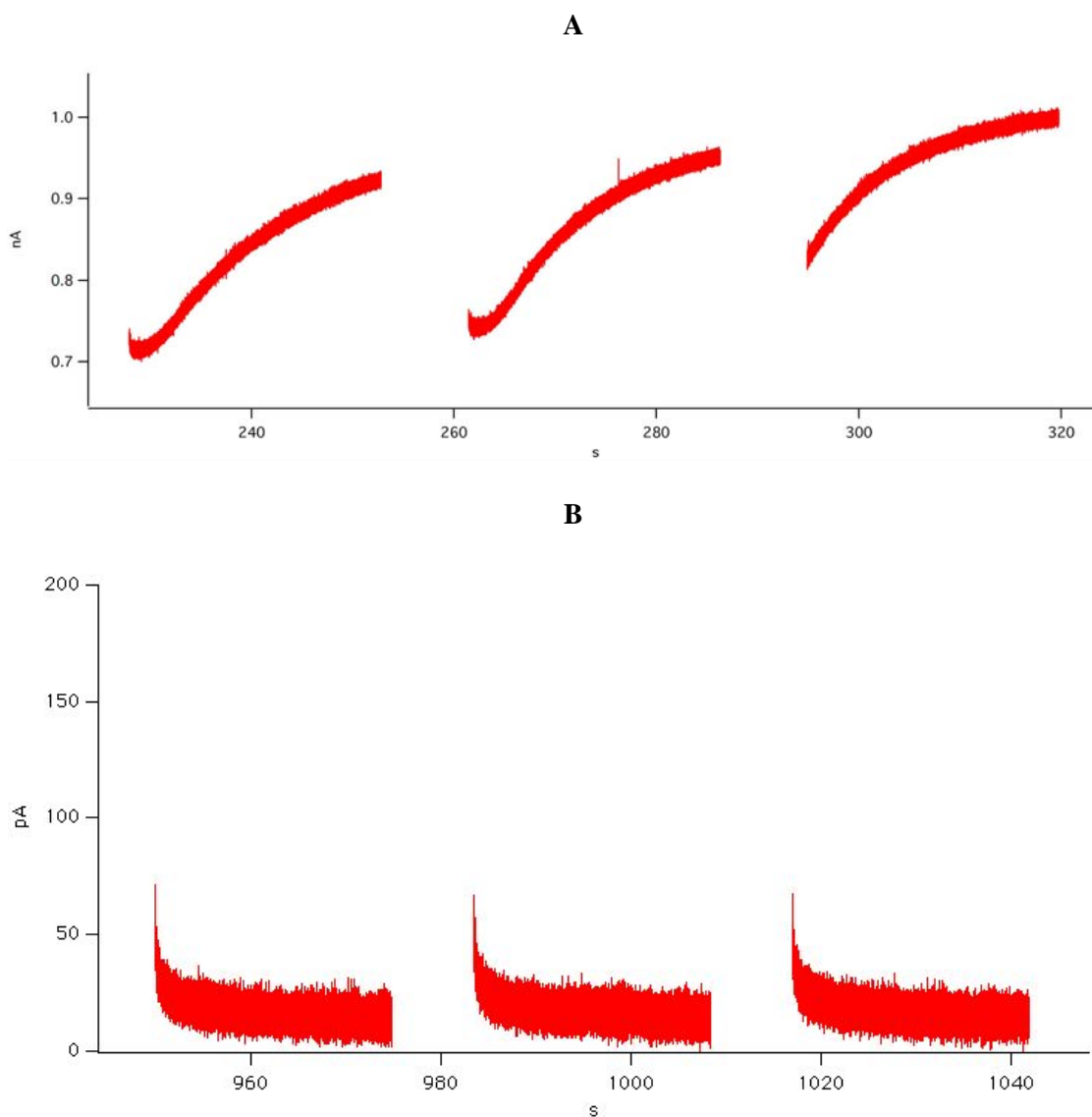
Fig. 5.13. Current artifact induced by photolysis of Ca^{2+} cage in the absence of chromaffin cells. A. The amperometric current recorded at an ITO electrode in the intracellular mimicking solution with 5 mM Ca^{2+} cage NP-EGTA. There is a time-dependent sloping current artifact. B. The current recorded at an ITO electrode in the intracellular mimicking solution without Ca^{2+} cage. The sloping caged Ca^{2+} current artifact disappeared when the Ca^{2+} cage is removed from the solution.

5.7   Conclusion and discussion

The experiments of ITO amperometry with digitonin-permeabilized cells demonstrate that it is feasible to do controlled on-chip stimulation and detection of quantal catecholamine release using photolysis of caged Ca^{2+} in permeabilized cells on ITO microelectrodes.

Somewhat surprisingly, we have encountered two kinds of light-induced artifacts that compromise the amperometric signal. One is due to the UV-light effect on the ITO electrodes, the other is the presence of Ca^{2+} cage in the bath solution. To avoid the current transients accompanying the ratiometric recordings from Ca^{2+} indicator dyes, we turned off the monochromator while recording the amperometric spikes. This introduced the problem of not knowing the exact $[Ca^{2+}]_i$ during amperometric recordings. Another problem came from the sloping baseline current due to the presence of Ca^{2+} cage in the bath solution. These two kinds of light-induced current artifacts made us pursue better methods to introduce caged Ca^{2+} into cells. As shown in next chapter, we employed the AM derivatives of Ca^{2+} cage and Ca^{2+} indicator dye to remove the artifact from the presence of caged Ca^{2+} in the bath solution. In experiments of ITO amperometry on digitionin permeabilized cells, we used the monochromator to photorelease caged Ca^{2+}, which took longer time and generated UV-light induced current transients. Using this method, we can only roughly control $[Ca^{2+}]_i$ after UV photolysis by adjusting the on-time of the monochromator. To photorelease caged Ca^{2+} faster and better control $[Ca^{2+}]_i$ after

UV photolysis, we pursued using a UV flash lamp and a feedback control system to maintain $[Ca^{2+}]_i$ for longer time after UV photolysis in the next chapter.

CHAPTER 6

CONTROLLED ON-CHIP STIMULATION AND DETECTION OF QUANTAL CATECHOLAMINE RELEASE USING PHOTOLYSIS OF CAGED CA^{2+} IN CELLS WITH AM ESTER LOADING AND ITO AMPEROMETRY

6.1   AM ester loading of chromaffin cells to remove current artifact generated from photolysis of cage-containing bath solution

As outlined in the last chapter, our original approach was to introduce caged Ca^{2+} into cells by using digitonin to permeabilize the cell membrane. However, this approach requires cage to be present in the extracellular solution throughout the experiment and photolysis of cage on the electrode surface leads to an undesirable background current as depicted in Fig. 5.12.   The large current artifact due to photolysis of cage-containing solution over the electrochemical electrode led us to pursue an alternative approach whereby we used membrane-permeant acetoxymethyl (AM) ester derivatives of the Ca^{2+} cage (NP-EGTA) and the Ca^{2+} indicator (fura-4F) so that the cage can be washed out of the extracellular solution before commencing the experiment. Fig. 6.1 and Fig. 6.2 show the structure of salt form and AM form of NP-EGTA and fura-4F.

(a)
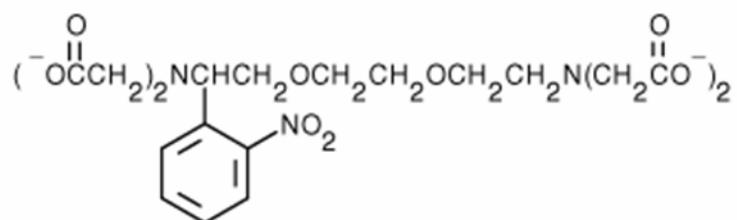
(b)
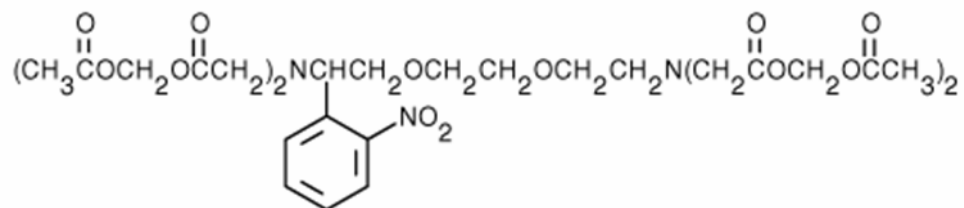
Fig. 6.1. Chemical structure of the salt and AM derivative of the Ca^{2+} cage. (a) Structure of tetrapotassium salt NP-EGTA; (b) Structure of NP-EGTA (AM)

(a)
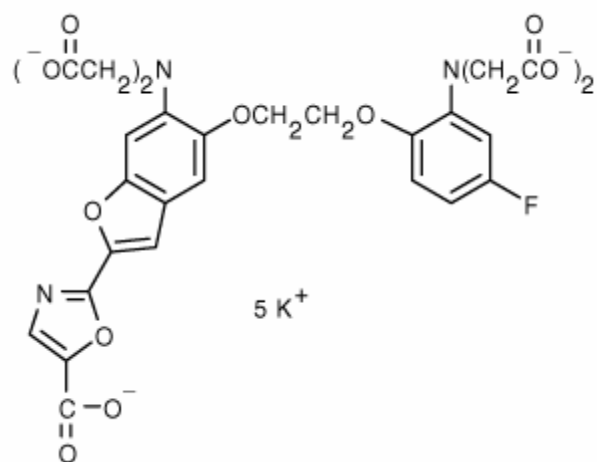
(b)
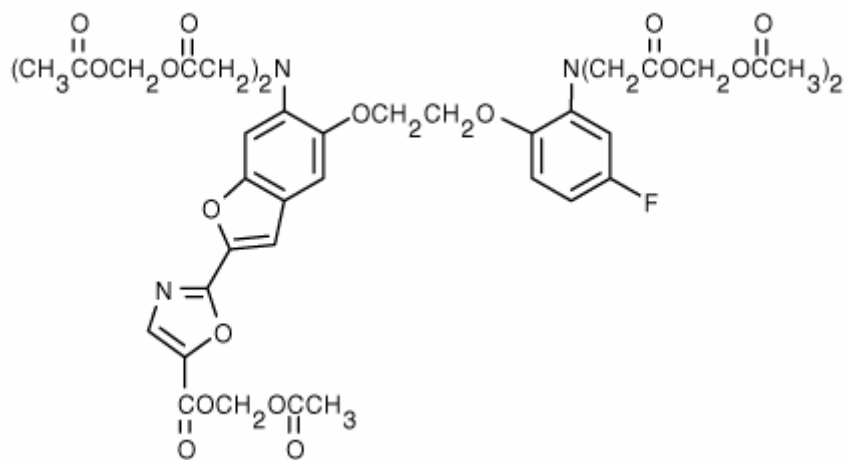
Fig. 6.2. Chemical structure of the salt and AM derivative of the Ca^{2+} indicator dye. (a) Structure of pentapotassium salt fura-4F; (b) Structure of fura-4F (AM)

Modification of carboxylic acids with AM ester groups creates an uncharged molecule that can permeate cell membranes. Once inside the cell, the lipophilic blocking groups are cleaved by nonspecific esterases within the cell, resulting in a charged form that leaks out of cells much more slowly than its parent compound (Invitrogen, http://probes.invitrogen.com/media/pis/g002.pdf). Taking advantage of this unique property, we first loaded our cell suspension with Ca^{2+} cage and Ca^{2+} indicator dye by incubating them with cell bath solution containing NP-EGTA (AM) and fura-4F (AM) for 45 min. We then removed NP-EGTA (AM) and fura-4F (AM) from extracellular solution by replacing it with cage-free and dye-free cell bath solution. Loaded cells were then transferred to the ITO electrodes for amperometric recordings. Our results showed that the light-induced artifact from photolysis of cage-containing solution over ITO electrodes was successfully eliminated using AM ester forms of Ca^{2+} cage and Ca^{2+} indicator dye (Fig. 6.3).

6.2 Using a monochromator to photorelease caged Ca^{2+} for stimulation of exocytosis

Since we were using 360 nm/380 nm to excite the Ca^{2+} indicator dye, we could as well use the same UV wavelengths to photorelease caged Ca^{2+}. Under the original configuration of the setup (Fig. 5.9), 90% of the UV light from the UV lamp passes through the combining condenser to reach the objective lens, while only 10% of the light from the monochromator is reflected from the combining condenser to the lens. We tried

97

to use this configuration to photorelease caged Ca^{2+} but were unsuccessful because the intensity of the monochromator was insufficient. To get higher intensity of UV light from the monochromator, we moved the optical fiber of the monochromator from the reflection pathway to the straight-through pathway so that the intensity of light coming from the monochromator was ~9 times stronger.

Chromaffin cells were incubated with NP-EGTA (AM) and Fura-4F (AM) and then washed with a dye-free and cage-free bath solution. Then the cells were transferred to the microchip device (See Chapter 2 for more details). Upon UV photolysis of caged Ca^{2+} inside a cell sitting right above one ITO electrode, fura-4F reported a rapid increase of $[Ca^{2+}]_i$ from 1.2 μM to 12.5 μM (Fig. 6.3A black trace). Simultaneously the ITO electrode detected a burst of quantal vesicle fusion events (Fig. 6.3A red trace). In contrast, without UV photolysis of caged Ca^{2+}, the frequency of spontaneous amperometric spikes was very low (Fig. 6.3B), which indicates that the burst of oxidative current spikes is triggered by the photolysis of caged Ca^{2+}.
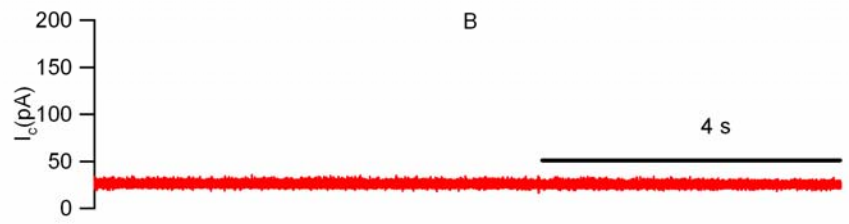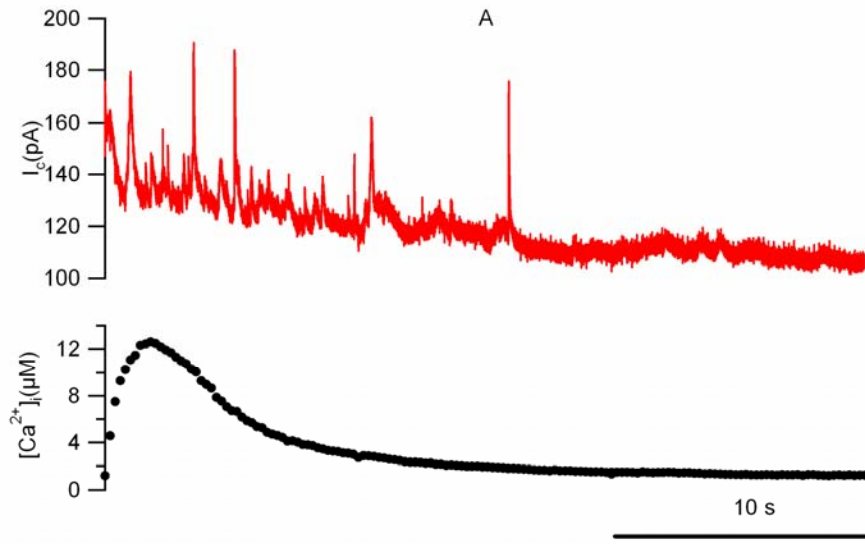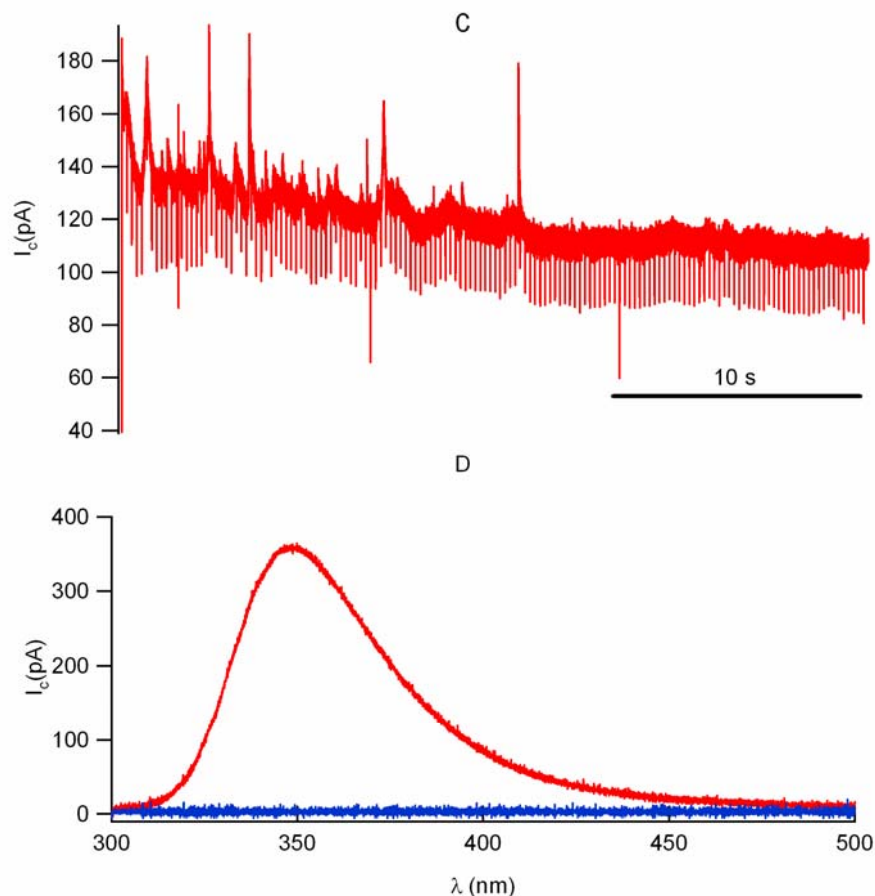
Fig. 6.3. Using AM ester derivatives of NP-EGTA and Fura-4F, it is possible to stimulate Ca^{2+}-dependent exocytosis in chromaffin cells. **A.** Upon UV photolysis of NP-EGTA inside the cells, $[Ca^{2+}]_i$ increased from 1.2μM to 12.6μM. Concurrently, a burst of amperometric spikes of catecholamine release was detected by ITO microelectrodes right beneath the cells. In addition, we got rid of the Ca^{2+} cage photolysis artifact by using the AM ester derivatives. **B.** Without UV photolysis of caged Ca^{2+}, no vesicle fusion events were detected by the ITO microelectrode (control trace), basal $[Ca^{2+}]_i$ was 1.2 μM. **C.** The raw data for Fig. 6.3B with UV-induced artifact at the working ITO microelectrode. The exponential transient at the very beginning of the trace and all the negative transients below the baseline are UV-induced artifacts recorded simultaneously with the amperometric recording. **D.** Oxidative current spectrum for the UV-induced artifact. Only Kreb-HEPES solution was added on top of the ITO electrodes. Blue trace is the spectrum without with the illumination aperture closed, the red trace is the spectrum scanning from 300 nm to 500 nm.

We noticed that UV illumination creates a background current even in the absence of cage in the bath solution (Fig. 6.3C, original recording without removal of background current artifacts. Fig. 6.3A red trace is a cleaner trace after removing the artifacts). A similar background current is induced by UV illumination when using carbon fiber electrodes. We used a monochromator to obtain the wavelength-dependence (spectrum) of the background current (Fig. 6.3D). Since we alternate between two excitation wavelengths (360nm and 380nm) to excite Fura-4F, the background contains current transients as shown in Fig. 6.3C. In addition, the background current for constant illumination is time dependent, and accounts for the transient current at the beginning of Fig. 6.3C.

Three more examples of photo-induced Ca^{2+} uncaging are shown in Fig. 6.4 to Fig. 6.6. There seems to be more exocytotic events when the initial (basal) $[Ca^{2+}]_i$ is elevated as shown in Fig. 6.6. In next chapter, we systematically studied the relationship between different basal $[Ca^{2+}]_i$ and cell secretion using Ca^{2+} clamping with a flash lamp illumination. In some experiments as shown in Fig. 6.5 and Fig. 6.6, the current consists of a "wave" of oxidation rather than discrete spikes. This loss of resolution of quantal exocytosis is also commonly seen in carbon fiber electrodes upon photolysis of caged Ca^{2+} that elevates $[Ca^{2+}]_i > \sim 5 \mu M$ (Haller and others, 1998).
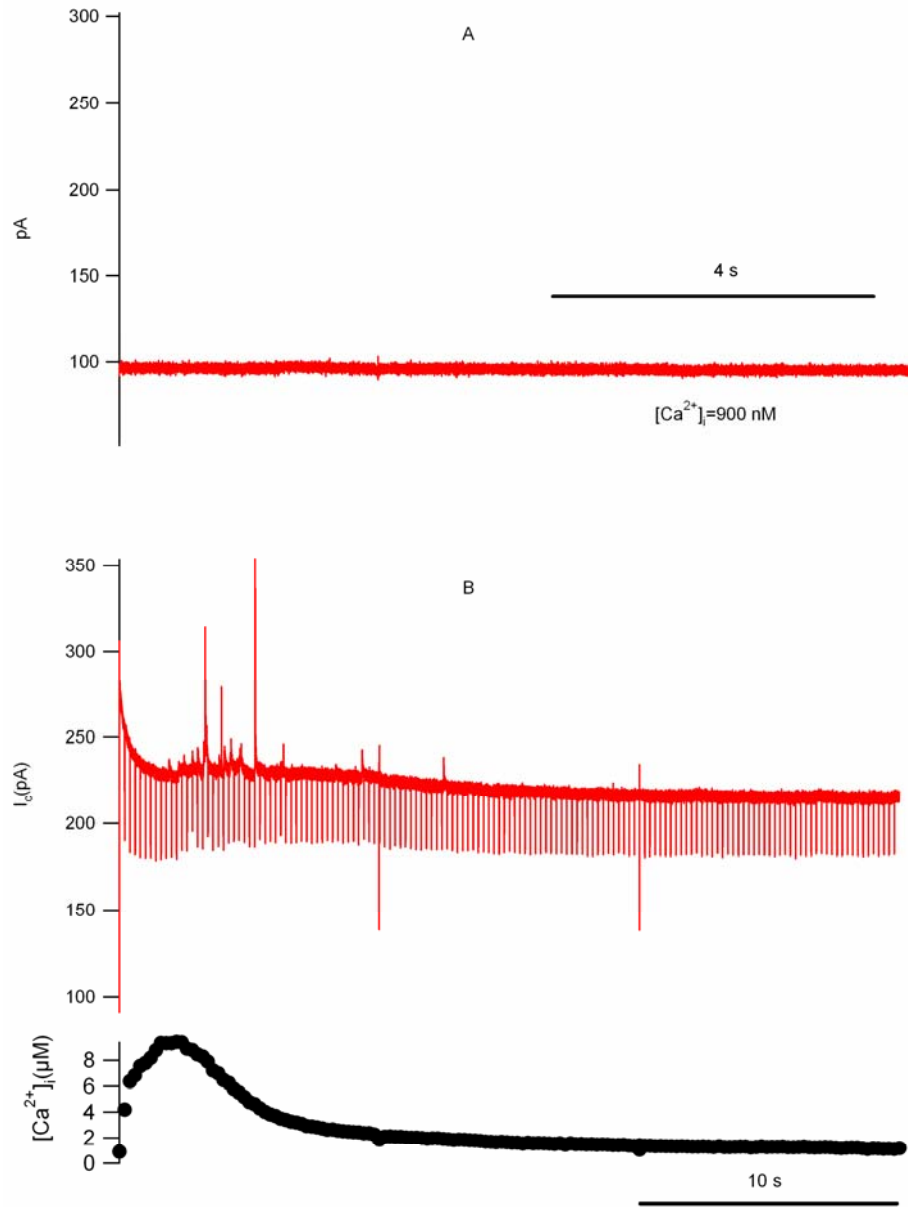
Fig. 6.4. Example 2 of catecholamine release from chromaffin cells stimulated by photolyzing caged Ca^{2+} NP-EGTA (AM) to increase $[Ca^{2+}]_i$. **A.** At basal $[Ca^{2+}]_i$ = 900 nM, there was no vesicle fusion event without photoreleasing caged Ca^{2+}. **B.** Upon photorelease of caged Ca^{2+}, there was a burst of spikes detected from the chromaffin cell on top of the ITO microelectrode. Fura-4F reported an increase of $[Ca^{2+}]_i$ from 900 nM to 9.4 µM.
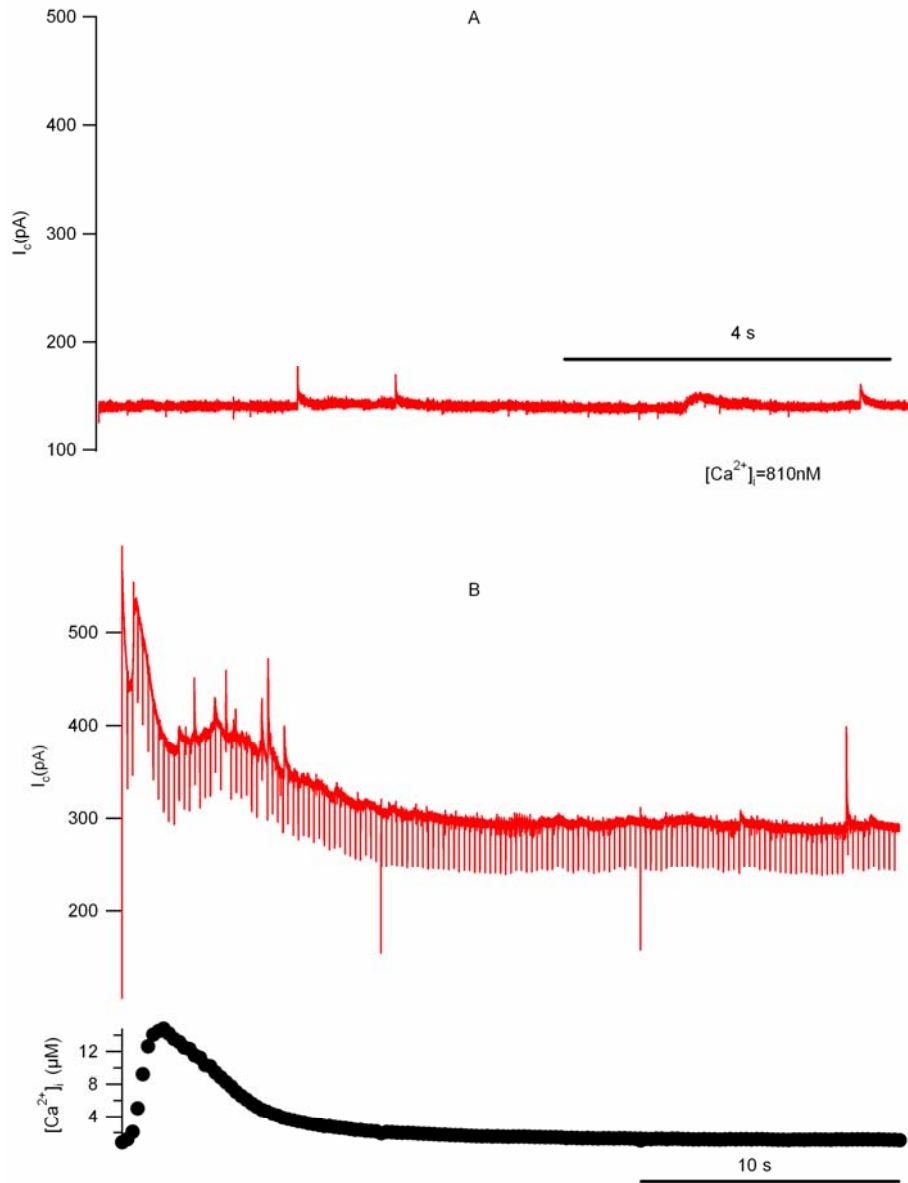
Fig. 6.5. Example 3 of catecholamine release from chromaffin cells stimulated by photolyzing caged Ca^{2+} NP-EGTA (AM) to increase $[Ca^{2+}]_i$. It shows that **A.** Spontaneous catecholamine release with very low frequency can be detected in the baseline trace ($[Ca^{2+}]_i = 810$ nM). **B.** Sometimes the accumulation of massive catecholamine release can give a wavy current with spikes on top of it.
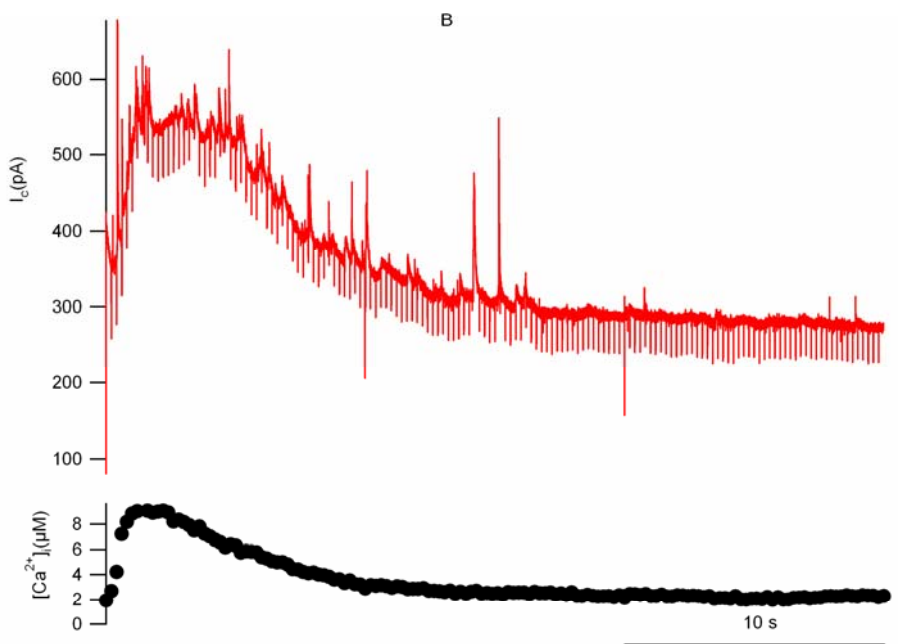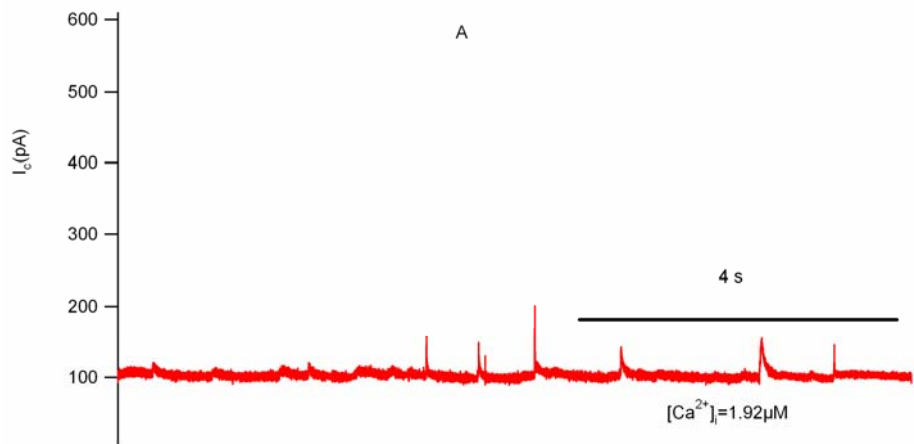
Fig. 6.6. Example 4 of catecholamine release from chromaffin cells stimulated by photolyzing caged Ca^{2+} NP-EGTA (AM) to increase $[Ca^{2+}]_i$. It shows that **A.** at a higher basal $[Ca^{2+}]_i$ (1.92 µM), the frequency of spontaneous events is higher. **B.** Photoelevation leads to massive release with a wave of oxidative current.

104

6.3   Ca^{2+} clamping to better manipulate [Ca^{2+}]$_i$ for stimulation of exocytosis

While using the monochromator to photorelease caged Ca^{2+} for stimuation of exocytosis, we noticed that [Ca^{2+}]$_i$ was typically elevated to above 10 μM after monochromator photolysis of caged Ca^{2+}. Intracellular sequestration of Ca^{2+} and membrane pumps brought [Ca^{2+}]$_i$ back to basal level within 10 to 20 s. In order to better control [Ca^{2+}]$_i$, we implemented a feed-back system to adjust the firing frequency of the UV lamp for "clamping" [Ca^{2+}]$_i$ at a desired level of several μM for up to 3 min (See Chapter 2 for more detailed information).

Fig. 6.7 presents a photomicrograph of cells that settled randomly on the microdevice.
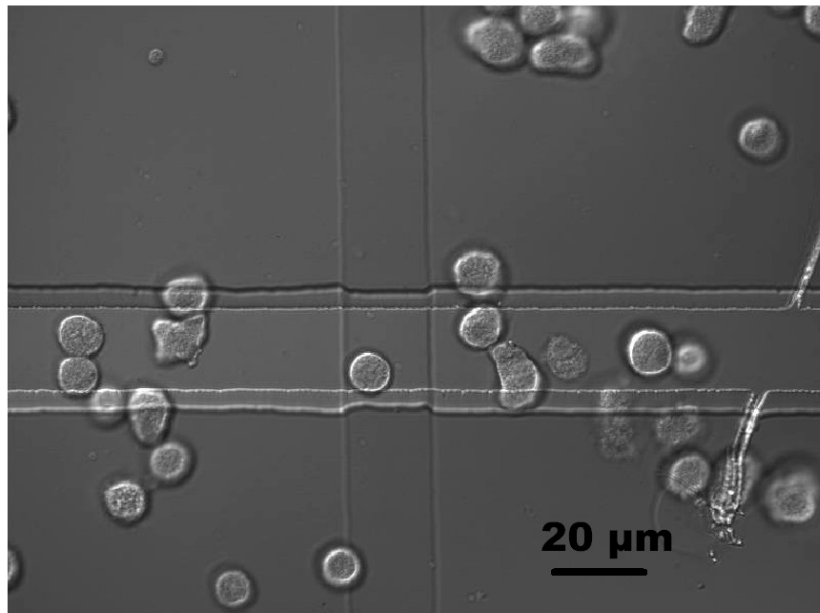
Fig. 6.7. A DIC picture of an individual chromaffin cell sitting on top of an ITO working electrode (20 μm by 20 μm).

In this example an individual chromaffin cell settled onto the working electrochemical electrode, which is at the intersection of the horizontal and vertical stripes in the center of the photo. We were able to verify the loading of fura-4F AM by measuring the green cell fluorescence in response to 360 nm/380 nm excitation (Fig. 6.8, picture taken from a different experiment).
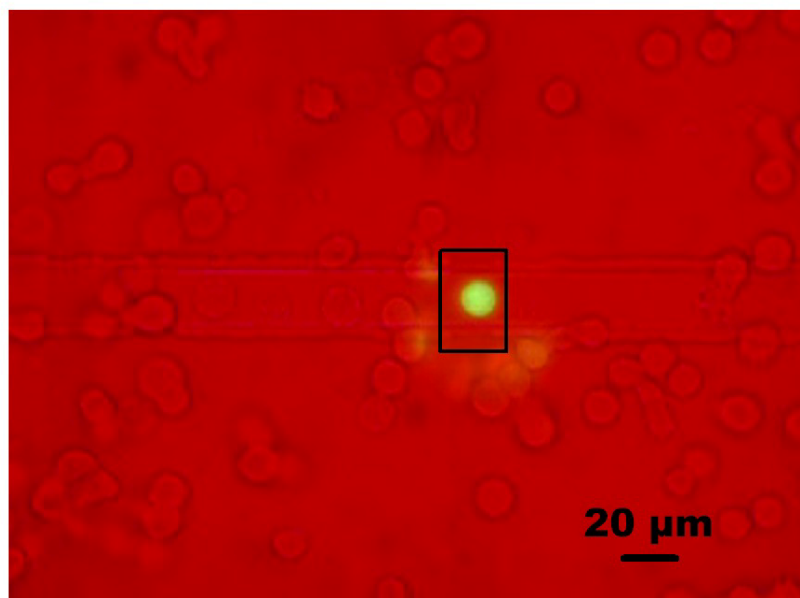
Fig. 6.8. A chromaffin cell loaded with Fura-4F (AM) sitting on top of a working ITO electrode (black square) fluoresces in response to UV excitation alternating between 360 nm and 380 nm.

We set the aperture defining the illuminated area and the aperture defining the area of collected fluorescent light equal to the location of the working electrode. This ensures that only the cell on the working electrode is stimulated upon photolysis of the cage and that the measured fluorescent light is reporting the $[Ca^{2+}]_i$ of the cell under study.

Upon flash photolysis of caged Ca^{2+} inside a cell sitting immediately above an ITO microelectrode, fura-4F reported a step-like increase of $[Ca^{2+}]_i$ to ~ 3.5 μM (Fig. 6.9(d)). Simultaneously the ITO microelectrode detected a wave of oxidative current consistent with a burst of catecholamine release from the cell (Fig. 6.9(a)) (Haller et al., 1998). By subtracting the light-induced artifact (Fig. 6.9(b)), we obtained the cleaned amperometric recording (Fig. 6.9(c)).

107
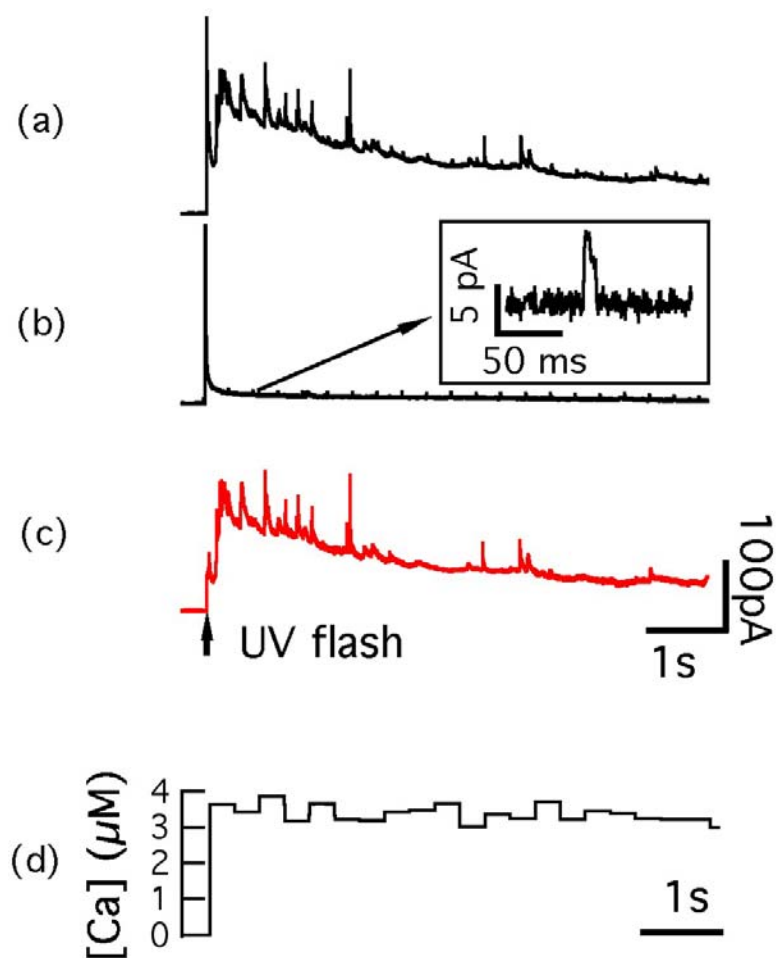
Fig. 6.9. Quantal catecholamine release from a chromaffin cell induced by Ca^{2+} uncaging with a flash lamp. **(a).** A sample amperometric response to flash photolysis of caged Ca^{2+} from a cell sitting on an ITO electrode. **(b).** Light-induced current artifact from an ITO electrochemical electrode measured in absence of cells. Discharge of the flash lamp produces a large, rapidly decaying current artifact. Illumination from the monochromator alternating between 360 nm and 380 nm to measure $[Ca^{2+}]_i$ with a fluorescent indicator produces small pulse-like current transients (inset). **(c).** Faradaic current due to oxidation of catecholamines released from the cell obtained by subtracting the light-induced artifacts (b) from the recorded current (a). **(d).** Fluorescent measurement of $[Ca^{2+}]_i$ using fura-4F (AM) reports rapid $[Ca^{2+}]_i$ elevation from 281 nM to 3.6 μM upon UV photolysis of caged Ca^{2+}.

Note that current spikes are evident, which likely represent quantal release from individual vesicles fusing to the bottom surface of the cell immediately adjacent to the electrode. Note that the amperometric current diminishes despite the continuous elevation of $[Ca^{2+}]_i$. This is thought to be due to depletion of a readily releasable pool of vesicles that are docked to the plasma membrane and primed for release (Sorensen, 2004).

6.4   On-chip detection of the enhancing effect of phorbol ester PMA on cell secretion

It has been shown that phorbol ester PMA increases the readily releasable pool of secretory vesicles through activation of protein kinase C (PKC), which leads to increased cell secretion (Gillis and others, 1996). To verify if our microchip device can quantify the difference between PMA induced exocytosis and control, we added 1μM PMA into the final cell suspension for ITO amperometry. We demonstrate that our microchip device can detect the enhancing effect of PMA on Ca^{2+}-dependent exocytosis (Fig. 6.10).
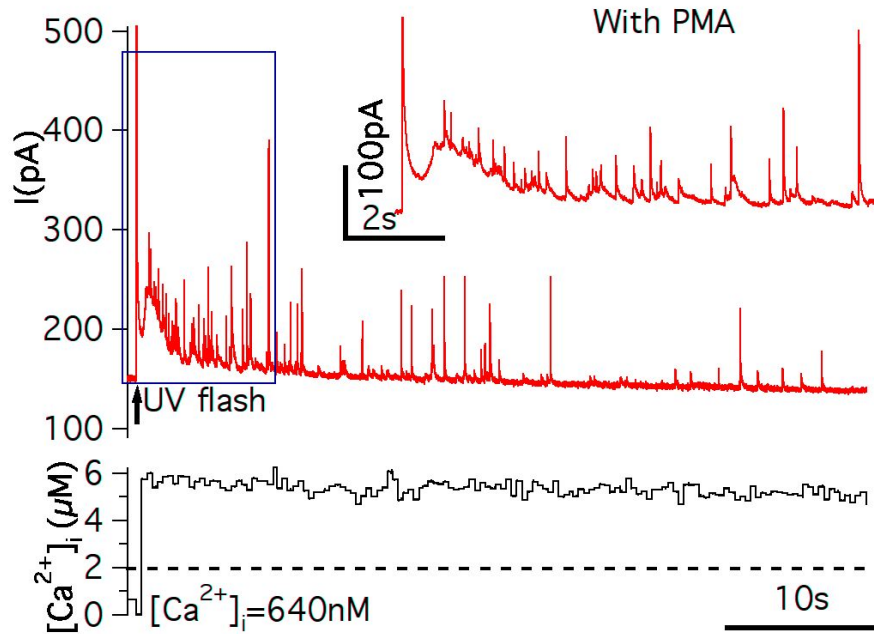
Fig. 6.10. The microchip device detects the PMA enhancing effect on cell secretion. Top: Cell exposed to 1 mM PMA has obvious enhanced secretion shown by the increase of frequency of amperometric events compared to Fig.6.10. (Inset: a close-up on the blue box); Bottom: Upon photolysis from the UV lamp, [Ca^{2+}]$_i$ was elevated from 640 nM to ~6 μM and was clamped at that level for more than 1 min.

Compared to cells in normal Ringer solution (Fig. 6.9, control), cells with PMA treatment demonstrated significantly enhanced response to elevated [Ca^{2+}]$_i$ (Fig. 6.10, with PMA). Integration of amperometric currents indicates the number of catecholamine molecules released from the cell captured by the working ITO electrode. Indeed, our biochip devices detect a significant increase both in the amplitude and frequency of oxidative spikes from chromaffin cells treated with PMA. The application of PMA leads to a nearly 2-fold increase of the total number of released catecholamine molecules oxidized on the surface of ITO microelectrodes (Fig. 6.11), consistent with previous report using

the capacitance measurement method (Gillis et al., 1996). Since we had a very small sample size for these two sets of experiments (n = 5) and significant cell-to-cell variability, we were unable to statistically differentiate the two populations. Nevertheless it still proved the suitability of using our microchip device for this kind of physiological experiments since we observed similar results as previous report.
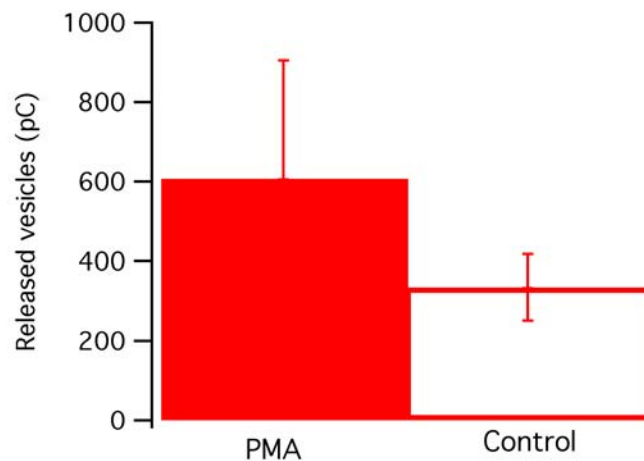
Fig. 6.11. Our microchip device detected increase of catecholamine release from PMA treated cell. Integration of oxidative currents from PMA treated cells (solid bar, n=5) indicates a 1.8-fold increase of released catecholamine molecules detected by ITO electrodes (control, open bar, n=5).

6.5 "Priming" effect of sub-stimulatory $[Ca^{2+}]_i$ on catecholamine release reported by microchip devices

A rise in $[Ca^{2+}]_i$ is not only the immediate trigger for exocytosis in most neuron and neuroendocrine cells but $[Ca^{2+}]_i$ also is believed to act on earlier steps of preparing vesicles for release such as translocation, docking and priming (Sudhof, 2004). Although the exact role of Ca^{2+} in every step of this vesicle cycle is not completely understood, experimental evidence suggests that a moderate increase in basal $[Ca^{2+}]_i$ facilitates priming vesicles to become fusion-competent (Bittner and Holz, 1992; von Ruden and Neher, 1993; Voets, 2000).

We performed a set of experiments using the ITO microdevices to correlate the response to flash photoelevation of $[Ca^{2+}]_i$ with the basal $[Ca^{2+}]_i$ level before the flash. In order to obtain a larger range of basal $[Ca^{2+}]_i$ we incubated cells in a bath solution containing either 1 mM or 2 mM Ca^{2+}. Fig.6.12B depicts a typical robust response to photoelevation of $[Ca^{2+}]_i$ when basal $[Ca^{2+}]_i$ is relatively high (680 nM) whereas Fig. 6.12A depicts a much smaller response from a cell with a low initial $[Ca^{2+}]_i$ (243 nM). Note that, whereas the basal, pre-flash $[Ca^{2+}]_i$ varies ~3-fold between the 2 cells, the post-flash $[Ca^{2+}]_i$ that triggers release is similar (3.29 μM versus 3.95 μM). Therefore the difference in response is likely due to Ca^{2+}-dependent "priming" of exocytosis.

112

(A)

Basal $[Ca^{2+}]_i$=243 nM

50 pA | 1 s | UV flash

$[Ca]/\mu M$

(B)

Basal $[Ca^{2+}]_i$=680 nM

50 pA | 1 s | UV flash

$[Ca]/\mu M$
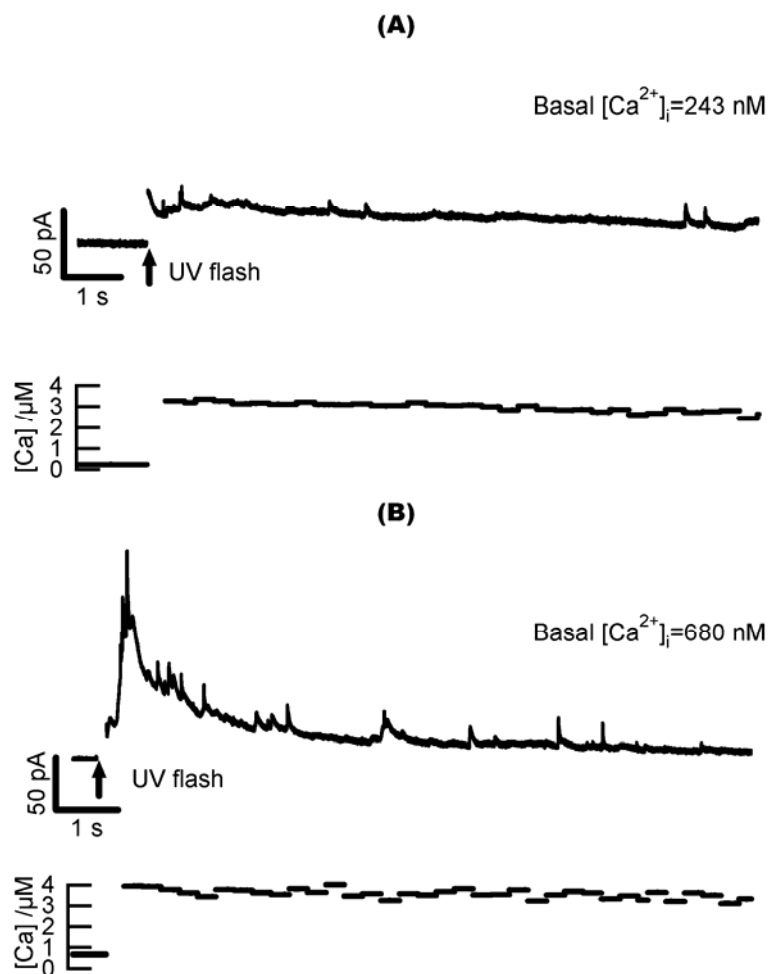
Fig. 6.12. Elevation of "basal" (pre-flash) $[Ca^{2+}]_i$ results in more catecholamine release in response to flash photoelevation of $[Ca^{2+}]_i$. **(A)** Sample response of a cell with lower initial $[Ca^{2+}]_i$ (243 nM), to photo-elevation of $[Ca^{2+}]_i$ to several μM. **(B)** Sample response of a different cell with higher initial $[Ca^{2+}]_i$ (680 nM).

We found that out of 37 cells with basal $[Ca^{2+}]_i$ lower than 600 nM (mean $[Ca^{2+}]_i$ = 267 nM), only 9 cells showed detectable catecholamine release (defined as one or more amperometric spikes with an amplitude greater than 10 pA) in response to flash

113

photoelevation of $[Ca^{2+}]_i$ (mean post-flash $[Ca^{2+}]_i$ = 3.11 μM). In contrast, 17 out of 34 cells with basal $[Ca^{2+}]_i$ above 600 nM (mean basal $[Ca^{2+}]_i$ = 976 nM) respond with a burst of amperometric spikes to photoelevation of $[Ca^{2+}]_i$ (mean post-flash $[Ca^{2+}]_i$ = 3.21 μM).

6.6   Conclusion and discussion

We describe here a novel biochip device to perform on-chip optical stimulation and electrochemical detection of Ca^{2+}-dependent exocytosis at the single-vesicle level. Use of transparent ITO electrodes on a glass coverslip substrate allows us to use an inverted microscope with a high numerical aperture objective lens for high efficiency fluorescence measurement of cell $[Ca^{2+}]_i$ and on-chip photolysis of caged Ca^{2+}. Previous work in our lab has shown that transparent ITO microelectrodes have a similar electrochemical performance as carbon fiber electrodes (Sun and Gillis, 2006). Using the acetoxymethyl ester derivative of the Ca^{2+} cage NP-EGTA and the Ca^{2+} indicator dye fura-4F, we are able to deliver caged Ca^{2+} and Ca^{2+} indicator dye into a cell population in a much faster and less invasive manner than delivery through a patch-clamp pipette. Since we can restrict the light excitation aperture to cell-size, we can confine photorelease of caged Ca^{2+} and measurement of $[Ca^{2+}]_i$ to an individual cell (Fig. 6.8). With 24 parallel cell-sized ITO electrodes, we can sequentially record from up to 24 cells on one microchip, which potentially provides a higher-throughput method to study Ca^{2+}-dependent exocytosis than sequentially positioning a carbon-fiber electrode.

114

Somewhat unexpectedly, we encountered 2 different light-induced current artifacts in our recordings. A large light-induced current was produced only when the Ca^{2+} cage was in the bath solution and decayed for tens of seconds after illumination was discontinued (Fig. 6.9B). Possible sources for this current are acidification of the solution upon cage photolysis or electrochemical activity of one or more byproducts of NP-EGTA photolysis. This artifact was eliminated by preloading cells with the membrane-permeant AM form of NP-EGTA. The other light-induced artifact was smaller, decayed rapidly following a light pulse, and was prominent for wavelengths in the blue to UV range (Fig. 6.9. A and B). Unfortunately, this artifact is difficult to avoid in ratiometric measurement of $[Ca^{2+}]_i$ because fluorescent indicators in the fura-2 family are excited over this same range of wavelengths. The use of fluorescent Ca^{2+} indicators excited by longer wavelengths could minimize this problem, but the available indicators are not ratiometric so accurate calibration is problematic. Nevertheless, we were able to eliminate this artifact by subtracting the current elicited by illumination of the electrode in the absence of a cell (Fig. 6.9C)

Our on-chip experiments show that this ITO biochip device is suitable for study of exocytosis. We observed a burst of amperometric spikes upon rapid elevation of $[Ca^{2+}]_i$ as shown in Figs. 6.9, 6.11 and 6.12. A wave of oxidative current with superimposed spikes was observed following flash photolysis of caged Ca^{2+}, which is likely due to a burst of catecholamine release from the cell, similar to previous reports using carbon fiber electrodes (Haller et al., 1998). Using our biochip device, we have also observed that the response to step elevation of $[Ca^{2+}]_i$ depends on the basal $[Ca^{2+}]_i$ level before the

flash (Fig.6.12). Higher basal $[Ca^{2+}]_i$ ($> \sim 600$ nM) appears to "prime" vesicles for exocytosis, similar to previous reports using different techniques (Bittner and Holz, 1992; von Ruden and Neher, 1993). Our microchip device should facilitate further study of this effect. For example, it would be straightforward to use a feed-back control system to control UV illumination to elevate $[Ca^{2+}]_i$ to different sub-stimulatory levels and study the dose response of the "priming" effect on a subsequent secretory response triggered by a higher $[Ca^{2+}]_i$ level.

Our approach allows very powerful control of the Ca^{2+} stimulus and measurement of quantal exocytosis. An area for future improvement to enable higher throughput would be to integrate approaches to automatically target cells to the electrochemical electrodes. Another opportunity for improvement would be to integrate on-chip amplifier arrays and a sensitive CCD camera to allow parallel stimulation and recording from many cells simultaneously in an electrode array.

CHAPTER 7

CONCLUSION AND FUTURE DIRECTIONS

7.1   Conclusion

The theme of this study is to develop novel technology and refine established technology to study Ca^{2+}-triggered exocytosis.

To elucidate how exocytosis is triggered by Ca^{2+} at a molecular level, we first used a combination of the patch-clamp technique and carbon fiber amperometry to study Ca^{2+}-regulated exocytosis. Previous work from our laboratory has revealed a highly Ca^{2+} sensitive pool (HCSP) of vesicles in chromaffin cells that respond to lower $[Ca^{2+}]_i$ (below 10 μM) more rapidly than the readily releasable pool (RRP) of vesicles (Yang et al., 2002). Protein Kinase C (PKC) tends to shift vesicles to a highly Ca^{2+} sensitive state by increasing the size of HCSP (Yang et al., 2002). A question that arises from dissection of vesicles into multiple functional pools is whether the size or content of vesicles are different. To answer this question, I performed combined patch clamp whole-cell recording and carbon fiber amperometry to simultaneously measure capacitance change and amperometric spikes from both pools upon stimulation of exocytosis in single chromaffin cells. Our results show that the content and transmitter release kinetics of

vesicles from both pools are similar. We speculate that the HCSP enables catecholamine release upon mild elevation of $[Ca^{2+}]_i$ such as following release of Ca^{2+} from internal stores following agonist stimulation.

There is no doubt that conventional techniques like patch clamp technique and carbon fiber amperometry have brought unprecedented revolution to the research of understanding exocytosis on a molecular level. However the intrinsic low-throughput characteristic of these conventional techniques has hindered their popularity in basic and clinical research. To sharpen our tools for high-throughput research of exocytosis, we have borrowed technology derived from the semiconductor industry to develop high-throughput bioassays for studying exocytosis. In this study, we have successfully designed and microfabricated a novel biochip device to integrate caged Ca^{2+} technique, ITO amperometry and fluorescence photometry together for higher-throughput on-chip stimulation and detection of Ca^{2+}-dependent exocytosis. A 100 nm – thick transparent Indium-Tin-Oxide (ITO) film was sputter-deposited onto glass coverslips, which were then patterned into 24 cell-sized working electrodes (~20 μm by 20 μm). We loaded bovine chromaffin cells with acetoxymethyl (AM) ester derivatives of the Ca^{2+} cage NP-EGTA and Ca^{2+} indicator dye Fura-4F, then transferred these cells onto the working ITO electrodes for amperometric recordings. Upon flash photorelease of caged Ca^{2+}, a uniform rise of $[Ca^{2+}]_i$ within the target cell leads to quantal release of oxidizable catecholamines measured amperometrically by the underlying ITO electrode. We observed a burst of amperometric spikes upon rapid elevation of $[Ca^{2+}]_i$ and a "priming" effect of sub-stimulatory $[Ca^{2+}]_i$ on the response of cells to subsequent $[Ca^{2+}]_i$ elevation,

118

similar to previous reports using different techniques. We conclude that UV photolysis of caged Ca^{2+} is a suitable stimulation technique for higher-throughput studies of Ca^{2+}-dependent exocytosis on transparent electrochemical microelectrode arrays. This biochip device has potential applications for higher-throughput screening of drugs and toxins that target exocytosis. In addition, studies of exocytosis which use Green Fluorescent Protein as a reporter of gene expression could benefit from the transparent device.

7.2   Future directions

The main part of this dissertation is part of a NIH Bioengineering Research Partnership (BRP) project that aims at developing microdevice for high-throughput electrochemical measurement of quantal exocytosis from neurons and neuroendocrine cells. There are four main specific aims in this project including targeting individual cells to microelectrodes on microfabricated devices, developing approaches to stimulate exocytosis from single cells on microdevices, integrating new electrode materials into microdevices to increase sensitivity and performance, and developing electronic instrumentation to allow simultaneous recording of many channels of electrochemical or electrophysiological data. This dissertation has focused on the second aim, which is to develop novel approaches to stimulate exocytosis from single cells on microdevices. Our results showed that both electrical stimulation and optical stimulation can trigger exocytosis from single cells. Applying a voltage pulse to a carbon fiber electrode adjacent to an individual cell, we can trigger action potential through capacitive coupling and thus electrically induce Ca^{2+}-dependent exocytosis in the same cell. Using cell-

permeant AM ester derivatives of caged Ca^{2+} and Ca^{2+} indicator dye, we can deliver caged Ca^{2+} and Ca^{2+} indicator dye into the individual cells sitting on microelectrodes. Upon UV photolysis of caged Ca^{2+} within these cells, elevated $[Ca^{2+}]_i$ triggers transmitter release measured by the underlying electrochemical microelectrodes.

The advantage of using an extracellular electrode to electrically stimulate exocytosis is that this is a relatively non-invasive approach and triggers action potentials - the physiological stimuli for exocytosis. However, the reproducibility of triggering action potentials with the carbon fiber electrode was not satisfactory. If we plan to pursue this stimulation method further, I think it would be best to pattern an additional pair of biopolar electrodes near the recording (electrochemical) electrode. Electric field modeling and numerical simulation could be used to figure out the best geometry and position of the electrodes.

As for the optical stimulation of exocytosis using photolysis of caged Ca^{2+}, our results show that it is a very promising method with easy control and consistent performance. One concern regarding the wave of oxidative current with superimposed spikes observed following UV photolysis of caged Ca^{2+} is that the $[Ca^{2+}]_i$ after UV flash is still higher than the physiological condition. To get even finer control of $[Ca^{2+}]_i$, we may optimize our Ca^{2+} clamping program and readjust our UV lamp intensity by modifying the flash-lamp amplifier. By maintaining $[Ca^{2+}]_i$ to a lower level after UV photolysis, we may get more discreet spikes that are easier to analyze for quantal parameters.

To further study the "priming" effect of sub-stimulatory $[Ca^{2+}]_i$ on cell secretion systematically, we can control the $[Ca^{2+}]_i$ after flash photolysis to different levels and compare the corresponding cell secretion. Or we can control preflash $[Ca^{2+}]_i$ to different level by adjusting the ratio of Ca^{2+} cage and free Ca^{2+} in the incubation solution and then bring $[Ca^{2+}]_i$ to same level after UV flash and then compare the difference of cell secretion.

As pilot experiments, the "PMA effect" experiments confirm that our biochip device can detect the enhancement of exocytosis following PMA treatment. To further quantify the PMA effect on cell secretion, we can do a dose-response of PMA treatment and analyze the amperometric frequency.

When we first used digitonin to permeabilize the cell membrane for the cross-membrane delivery of the caged Ca^{2+} and Ca^{2+} indicator dyes, we unexpectedly encountered two kinds of light-induced current artifacts. One is a large current artifact originated from the UV flash on Ca^{2+} cage presented in the bath solution; the other pulse-like current artifacts are the UV-induced current transients from the ITO electrodes themselves. The first artifact is removed successfully by switching to the AM ester derivatives of the caged Ca^{2+} and Ca^{2+} indicator dye. Since we are using fura type dyes that are working at the UV wavelength, we can not experimentally remove this artifact yet. Hopefully a new ratiometric dye for Ca^{2+} labeling at infrared or visible light range can be commercially available soon, so that we can switch to those dyes and dramatically reduce current artifacts.

We found that one major rate limiting factor for real high-throughput biochip device is to target individual cells to microelectrodes, another aim in our NIH BRP project. For all the experiments in this dissertation, we basically used individual cells that randomly settled onto microelectrodes to do our experiments. To really achieve high-throughput measurements, effective cell targeting methods need to be integrated into the microdevice. The microvalve method to stop solution flow in microchannels that we tried can be one candidate for this application although more work needs to be done in the future. The fantasy for this potential application is that we can target one cell to an electrode and make measurements and release the cell while introducing another cell to another electrode for next measurement. An alternative way to realize cell targeting is to pattern the surface of microchip device so that only the area of working electrodes is cell adhesive whereas the rest is cell repulsive. We then hope that by flowing cells across the surface, only those sticking on the working electrodes will remain in place for electrochemical recordings.

To apply our biochip device to more physiological experiments and verify its suitability for single cell bioassays, we can do a broad spectrum of experiments. For example, we can use this biochip device to further study the effects of different second messengers, such as Protein Kinase C, on regulating exocytosis; we can apply different drugs, such as L-DOPA or Botulinum Toxins, to different cell lines or primary cells on the chip to do massive screening of the drug effect on neurotransmitter release, which can help elucidate the basic mechanism of cell-to-cell communication and potentially benefit the

health-related research. Our biochip device is a very promising prototype platform towards achieving these goals.

REFERENCES

1991. http://nobelprize.org/nobel_prizes/medicine/laureates/1991/press.html.

Albillos A, Dernick G, Horstmann H, Almers W, de Toledo GA & Lindau M. 1997. The exocytotic event in chromaffin cells revealed by patch amperometry. Nature 389(6650):509.

Amatore C, Arbault S, Chen Y, Crozatier C, Lemaitre F & Verchier Y. 2006. Coupling of electrochemistry and fluorescence microscopy at indium tin oxide microelectrodes for the analysis of single exocytotic events. Angewandte Chemie-International Edition 45(24):4000-4003.

Anderson JR, Chiu DT, Jackman RJ, Cherniavskaya O, McDonald JC, Wu H, Whitesides SH & Whitesides GM. 2000. Fabrication of topologically complex three-dimensional microfluidic systems in PDMS by rapid prototyping. Anal. Chem. 72(14):3158-3164.

Ashery U, Betz A, Xu T, Brose N & Rettig J. 1999. An efficient method for infection of adrenal chromaffin cells using the Semliki Forest virus gene expression system. Eur J Cell Biol 78(8):525-532.

Ashery U, Varoqueaux F, Voets T, Betz A, Thakur P, Koch H, Neher E, Brose N & Rettig J. 2000. Munc13-1 acts as a priming factor for large dense-core vesicles in bovine chromaffin cells. Embo Journal 19(14):3586-3596.

Bashir R. 2004. BioMEMS: state-of-the-art in detection, opportunities and prospects. Adv Drug Deliv Rev 56(11):1565-1586.

Bittner MA & Holz RW. 1992. Kinetic analysis of secretion from permeabilized adrenal chromaffin cells reveals distinct components. J Biol Chem 267(23):16219-16225.

Blazej RG, Kumaresan P & Mathies RA. 2006. Microfabricated bioprocessor for integrated nanoliter-scale Sanger DNA sequencing. Proc Natl Acad Sci U S A 103(19):7240-7245.

Blumenfeld AM, Dodick DW & Silberstein SD. 2004. Botulinum neurotoxin for the treatment of migraine and other primary headache disorders. Dermatol Clin 22(2):167-175.

Boghen DR. 1996. Disorders of facial motor function. Curr Opin Ophthalmol 7(6):48-52.

Chang C-Y, Niblack B, Walker B & Bayley H. 1995. A photogenerated pore-forming protein. Chem. Biol. 2(6):391.

Cheley S, Braha O, Lu X, Conlan S & Bayley H. 1999. A functional protein pore with a "retro" transmembrane domain. Protein Sci. 8(6):1257-1267.

Chen P, Xu B, Tokranova N, Feng X, Castracane J & Gillis KD. 2003. Amperometric detection of quantal catecholamine secretion from individual cells on micromachined silicon chips. Anal. Chem. 75(3):518-524.

Chow RH, von Ruden L & Neher E. 1992. Delay in vesicle fusion revealed by electrochemical monitoring of single secretory events in adrenal chromaffin cells. Nature 356(6364):60-63.

Connolly M & de Berker D. 2003. Management of primary hyperhidrosis: a summary of the different treatment modalities. Am J Clin Dermatol 4(10):681-697.

Cui HF, Ye JS, Chen Y, Chong SC, Liu X, Lim TM & Sheu FS. 2006. In situ temporal detection of dopamine exocytosis from L-dopa-incubated MN9D cells using microelectrode array-integrated biochip. Sensors and Actuators B-Chemical 115(2):634-641.

Del Castillo J & Katz B. 1954. Quantal components of the end-plate potential. J Physiol 124(3):560-573.

Deng WL, Ohgi T, Nejo H & Fujita D. 2001. Characteristics of indium tin oxide films deposited by DC and RF magnetron sputtering. Japanese Journal of Applied Physics Part 1-Regular Papers Short Notes & Review Papers 40(5A):3364-3369.

Di Carlo D & Lee LP. 2006. Dynamic single-cell analysis for quantitative biology. Anal. Chem. 78(23):7918-7925.

Dias AF, Dernick G, Valero V, Yong MG, James CD, Craighead HG & Lindau M. 2002. An electrochemical detector array to study cell biology on the nanoscale. Nanotechnology 13(3):285-289.

Elhamdani A, Zhou Z & Artalejo CR. 1998. Timing of dense-core vesicle exocytosis depends on the facilitation L-type Ca channel in adrenal chromaffin cells. J Neurosci 18(16):6230-6240.

Evanko D. 2005. Primer: spying on exocytosis with amperometry. Nat Meth 2(9):650.

Fatt P & Katz B. 1950a. Membrane potentials at the motor end-plate. J Physiol 111(1-2):46p-47p.

Fatt P & Katz B. 1950b. Some observations on biological noise. Nature 166(4223):597-598.

Fatt P & Katz B. 1952. Spontaneous subthreshold activity at motor nerve endings. J Physiol 117(1):109-128.

Frampton JE & Easthope SE. 2003. Botulinum toxin A (Botox Cosmetic): a review of its use in the treatment of glabellar frown lines. Am J Clin Dermatol 4(10):709-725.

Fromherz P & Stett A. 1995. Silicon-Neuron Junction: Capacitive Stimulation of an Individual Neuron on a Silicon Chip. Phys Rev Lett 75(8):1670-1673.

Gillis KD. 2000. Admittance-based measurement of membrane capacitance using the EPC-9 patch-clamp amplifier. Pflugers Archiv-European Journal of Physiology 439(5):655-664.

Gillis KD & Chow RH. 1997. Kinetics of exocytosis in adrenal chromaffin cells. Semin Cell Dev Biol 8(2):133-140.

Gillis KD, Mossner R & Neher E. 1996. Protein kinase C enhances exocytosis from chromaffin cells by increasing the size of the readily releasable pool of secretory granules. Neuron 16(6):1209-1220.

Gouaux E. 1998. alpha-hemolysin from Staphylococcus aureus: An archetype of beta-barrel, channel-forming toxins. J. Struct. Biol. 121(2):110-122.

Grell E, Lewitzki E, Ruf H, Bamberg E, Ellis-Davies GC, Kaplan JH & de Weer P. 1989. Caged-Ca^{2+}: a new agent allowing liberation of free Ca^{2+} in biological systems by photolysis. Cell Mol Biol 35(5):515-522.

Grynkiewicz G, Poenie M & Tsien RY. 1985. A new generation of Ca^{2+} indicators with greatly improved fluorescence properties. J. Biol. Chem. 260(6):3440-3450.

Guttman A, Khandurina J, Ronai Z & Sasvari-Szekely M. 2003. High-throughput genotyping by microchip electrophoresis. J. Capillary Electrophor. 8(3-4):77-80.

Hafez I, Kisler K, Berberian K, Dernick G, Valero V, Yong MG, Craighead HG & Lindau M. 2005. Electrochemical imaging of fusion pore openings by electrochemical detector arrays. Proc. Natl. Acad. Sci. U. S. A. 102(39):13879-13884.

Haller M, Heinemann C, Chow RH, Heidelberger R & Neher E. 1998. Comparison of Secretory Responses as Measured by Membrane Capacitance and by Amperometry. Biophys. J. 74(4):2100-2113.

Hamill OP, Marty A, Neher E, Sakmann B & Sigworth FJ. 1981. Improved patch-clamp techniques for high-resolution current recording from cells and cell-free membrane patches. Pflugers Arch 391(2):85-100.

126

Heinemann C, Chow RH, Neher E & Zucker RS. 1994. Kinetics of the secretory response in bovine chromaffin cells following flash photolysis of caged Ca^{2+}. Biophys J 67(6):2546-2557.

Ho CT, Lin RZ, Chang HY & Liu CH. 2005. Micromachined electrochemical T-switches for cell sorting applications. Lab Chip 5(11):1248-1258.

Hodgkin AL & Huxley AF. 1952. A quantitative description of membrane current and its application to conduction and excitation in nerve. J Physiol 117(4):500-544.

Holz RW, Bittner MA, Peppers SC, Senter RA & Eberhard DA. 1989. MgATP-independent and MgATP-dependent exocytosis. Evidence that MgATP primes adrenal chromaffin cells to undergo exocytosis. J Biol Chem 264(10):5412-5419.

Invitrogen. http://probes.invitrogen.com/handbook/images/g000270.gif.

Invitrogen. http://probes.invitrogen.com/media/pis/g002.pdf.

Jankowski JA, Schroeder TJ, Ciolkowski EL & Wightman RM. 1993. Temporal Characteristics of Quantal Secretion of Catecholamines from Adrenal-Medullary Cells. Journal of Biological Chemistry 268(20):14694-14700.

Kaplan JH & Ellis-Davies GC. 1988. Photolabile chelators for the rapid photorelease of divalent cations. Proc Natl Acad Sci U S A 85(17):6571-6575.

Kawagoe KT, Jankowski JA & Wightman RM. 1991. Etched carbon-fiber electrodes as amperometric detectors of catecholamine secretion from isolated biological cells. Anal. Chem. 63(15):1589-1594.

Kissinger PT, Hart JB & Adams RN. 1973. Voltammetry in brain tissue--a new neurophysiological measurement. Brain Res 55(1):209-213.

Kreyden OP & Burg G. 2000. [Toxin treatment of sweat pearls. A review of the treatment of hyperhidrosis with a special view of a new therapy option using botulinum toxin A]. Schweiz Med Wochenschr 130(29-30):1084-1090.

Leszczyszyn DJ, Jankowski JA, Viveros OH, Diliberto EJ, Jr., Near JA & Wightman RM. 1990. Nicotinic receptor-mediated catecholamine secretion from individual chromaffin cells. Chemical evidence for exocytosis. J Biol Chem 265(25):14736-14737.

Li C, Wang Y, Gao Y, Guo X & Gu Z. 2005. Magnetically actuated micromixing on an array-pattern microfluidic chip for immunoassay of human thyrotropin. J Nanosci Nanotechnol 5(8):1297-1300.

Li N, Tourovskaia A & Folch A. 2003. Biology on a chip: microfabrication for studying the behavior of cultured cells. Crit. Rev. Biomed. Eng. 31(5-6):423-488.

Mann HB & Whitney DR. 1947. On a Test of Whether one of Two Random Variables is Stochastically Larger than the Other. The Annals of Mathematical Statistics 18(1):50-60.

Marty A & Neher E. 1995. Tight-seal whole-cell recording. In: Sakmann, B. N., Erwin, editor). Single-Channel Recording. 2nd ed., p31-51

McCreery RL, Dreiling R & Adams RN. 1974. Voltammetry in brain tissue: the fate of injected 6-hydroxydopamine. Brain Res 73(1):15-21.

McNeer KW, Tucker MG & Spencer RF. 2000. Management of essential infantile esotropia with botulinum toxin A: review and recommendations. J Pediatr Ophthalmol Strabismus 37(2):63-67; quiz 101-102.

Mennerick S & Matthews G. 1996. Ultrafast exocytosis elicited by calcium current in synaptic terminals of retinal bipolar neurons. Neuron 17(6):1241-1249.

Mosharov EV & Sulzer D. 2005. Analysis of exocytotic events recorded by amperometry. Nat Methods 2(9):651-658.

Neher E. 1998. Vesicle pools and Ca^{2+} microdomains: new tools for understanding their roles in neurotransmitter release. Neuron 20(3):389-399.

Neher E & Marty A. 1982. Discrete changes of cell membrane capacitance observed under conditions of enhanced secretion in bovine adrenal chromaffin cells. Proc Natl Acad Sci U S A 79(21):6712-6716.

Neher E & Sakmann B. 1992. The patch clamp technique. Sci Am 266(3):44-51.

Obeid PJ, Christopoulos TK & Ioannou PC. 2004. Rapid analysis of genetically modified organisms by in-house developed capillary electrophoresis chip and laser-induced fluorescence system. Electrophoresis 25(6):922-930.

Palade G. 1975. Intracellular aspects of the process of protein synthesis. Science 189(4200):347-358.

Parpura V. 2005. Nanofabricated carbon-based detector. Anal Chem 77(2):681-686.

Pothos E, Desmond M & Sulzer D. 1996. L-3,4-dihydroxyphenylalanine increases the quantal size of exocytotic dopamine release in vitro. J Neurochem 66(2):629-636.

Pothos EN. 2002. Regulation of dopamine quantal size in midbrain and hippocampal neurons. Behav Brain Res 130(1-2):203-207.

Pothos EN, Davila V & Sulzer D. 1998. Presynaptic recording of quanta from midbrain dopamine neurons and modulation of the quantal size. J Neurosci 18(11):4106-4118.

Pusch M & Neher E. 1988. Rates of diffusional exchange between small cells and a measuring patch pipette. Pflugers Arch 411(2):204-211.

Said S, Meshkinpour A, Carruthers A & Carruthers J. 2003. Botulinum toxin A: its expanding role in dermatology and esthetics. Am J Clin Dermatol 4(9):609-616.

Sakmann B & Neher E. 1995. Single-Channel Recording,2nd ed., p263

Schmoranzer J, Goulian M, Axelrod D & Simon SM. 2000. Imaging constitutive exocytosis with total internal reflection fluorescence microscopy. J Cell Biol 149(1):23-32.

Segura F, Brioso MA, Gomez JF, Machado JD & Borges R. 2000. Automatic analysis for amperometrical recordings of exocytosis. J Neurosci Meth 103(2):151-156.

Smith C. 1999. A persistent activity-dependent facilitation in chromaffin cells is caused by Ca^{2+} activation of protein kinase C. J Neurosci 19(2):589-598.

Song KH. 1998. Botulinum toxin type A injection for the treatment of frown lines. Ann Pharmacother 32(12):1365-1367.

Sorensen JB. 2004. Formation, stabilisation and fusion of the readily releasable pool of secretory vesicles. Pflugers Arch 448(4):347-362.

Sudhof TC. 2004. The synaptic vesicle cycle. Annu Rev Neurosci 27:509-547.

Sulzer D & Pothos EN. 2000. Regulation of quantal size by presynaptic mechanisms. Rev Neurosci 11(2-3):159-212.

Sun XH & Gillis KD. 2006. On-chip amperometric measurement of quantal catecholamine release using transparent indium tin oxide electrodes. Anal. Chem. 78(8):2521-2525.

Tengholm A, Hellman B & Gylfe E. 2000. Mobilization of Ca^{2+} stores in individual pancreatic [beta] -cells permeabilized or not with digitonin or [alpha] -toxin. Cell Calcium 27(1):43.

TerBush DR, Bittner MA & Holz RW. 1988. Ca^{2+} influx causes rapid translocation of protein kinase C to membranes. Studies of the effects of secretagogues in adrenal chromaffin cells. J Biol Chem 263(35):18873-18879.

Travis ER & Wightman RM. 1999. Spatio-temporal resolution of exocytosis from individual cells (vol 27, pg 102, 1998). Annual Review Of Biophysics And Biomolecular Structure 28:VII-VIII.

Tsien RY & Zucker RS. 1986. Control of cytoplasmic calcium with photolabile tetracarboxylate 2-nitrobenzhydrol chelators. Biophys J 50(5):843-853.

Unger MA, Chou H-P, Thorsen T, Scherer A & Quake SR. 2000. Monolithic Microfabricated Valves and Pumps by Multilayer Soft Lithography. Science 288(5463):113-116.

Voets T. 2000. Dissection of three Ca^{2+}-dependent steps leading to secretion in chromaffin cells from mouse adrenal slices. Neuron 28(2):537-545.

Voets T, Neher E & Moser T. 1999. Mechanisms underlying phasic and sustained secretion in chromaffin cells from mouse adrenal slices. Neuron 23(3):607-615.

von Ruden L & Neher E. 1993. A Ca-dependent early step in the release of catecholamines from adrenal chromaffin cells. Science 262(5136):1061-1065.

Whitesides GM, Ostuni E, Takayama S, Jiang X & Ingber DE. 2001. Soft lithography in biology and biochemistry. Annu Rev Biomed Eng 3:335-373.

Wilke R & Buttgenbach S. 2003. A micromachined capillary electrophoresis chip with fully integrated electrodes for separation and electrochemical detection. Biosens. Bioelectron. 19(3):149-153.

Xu T, Naraghi M, Kang H & Neher E. 1997. Kinetic studies of Ca^{2+} binding and Ca^{2+} clearance in the cytosol of adrenal chromaffin cells. Biophys J 73(1):532-545.

Yang Y, Craig TJ, Chen X, Ciufo LF, Takahashi M, Morgan A & Gillis KD. 2007. Phosphomimetic Mutation of Ser-187 of SNAP-25 Increases both Syntaxin Binding and Highly Ca^{2+}-sensitive Exocytosis. J Gen Physiol 129(3):233-244.

Yang Y & Gillis KD. 2004. A highly Ca^{2+}-sensitive pool of granules is regulated by glucose and protein kinases in insulin-secreting INS-1 cells. J Gen Physiol 124(6):641-651.

Yang Y, Udayasankar S, Dunning J, Chen P & Gillis KD. 2002. A highly Ca^{2+}-sensitive pool of vesicles is regulated by protein kinase C in adrenal chromaffin cells.[see comment]. Proceedings of the National Academy of Sciences of the United States of America 99(26):17060-17065.

Zeck G & Fromherz P. 2001. Noninvasive neuroelectronic interfacing with synaptically connected snail neurons immobilized on a semiconductor chip. Proc Natl Acad Sci U S A 98(18):10457-10462.

Zhang C, Xu J, Ma W & Zheng W. 2006. PCR microfluidic devices for DNA amplification. Biotechnol Adv 24(3):243-284.

Zhou Z & Misler S. 1995. Action potential-induced quantal secretion of catecholamines from rat adrenal chromaffin cells. J Biol Chem 270(8):3498-3505.

VITA

Xiaohui Chen was born in Changsha, Hunan, China in August, 1973. She obtained her Bachelor of Science degree in Electrical Engineering from Xi'an Jiaotong University, Xi'an, China in 1995. After working as an engineer and science journalist for a couple of years, she came to United States to pursue her advanced degree in 2001. She obtained her Master of Science degree in Electrical Engineering in 2003 and her Doctor of Philosophy degree in Biological Engineering in 2007 from University of Missouri-Columbia. She will continue her biomedical research at GE Global Research Center in Niskayuna, NY, USA.